UNIVERSITÀ DEGLI STUDI DI NAPOLI FEDERICO II

DEPARTMENT OF CHEMICAL, MATERIALS AND PRODUCTION ENGINEERING (DICMAPI)

PhD in "INDUSTRIAL PRODUCTS AND PROCESSES ENGINEERING"
XXIX cycle

"DESIGN AND DEVELOPMENT OF A MICROFLUIDIC DEVICE FOR THE ASSESSMENT OF FIRST-PASS METABOLISM"

Supervisor
Prof. Paolo Antonio Netti
Advisor
Dr. Francesco Urciuolo
Dr. Giorgia Imparato
Dr. Vincenza De Gregorio
Coordinator
Prof. Giuseppe Mensitieri

PhD Student
Brunella Corrado

2014/2017

Contents

Introduction

Orally administration of drugs is one of the preferred methods because it is easy and the compliance of the patient is high. Once ingested, a drug is dissolved and metabolized into the gastrointestinal fluid (GI), then crosses the intestinal and liver barrier where it is subjected to the first-pass metabolism. First-pass metabolism consists into the sequential actions of intestinal and hepatic metabolism to which a drug is subjected that leads to a reduction of its concentration before it reaches the blood circulation. First-pass extraction is associated with poor bioavailability of a variety of drugs. One of the limitation to oral drug bioavailability is the pre-systemic extraction by both the liver and the gut wall. In order to avoid low bioavailability and poor therapeutic effects of the drugs, it is necessary to predict the elimination route of the new developed drugs. Conventional *in vivo* and *in vitro* test are not so predictive and correlated to a numerous disadvantages, such as high costs, elevated time for the screening, not ethical and difficulties for high-throughput screening. With the rapid progresses in the microfabrication technologies, new *in vitro* microfluidic platforms are developed. For this purpose, organs-on-a-chip show great promises in the field of predictive/personalized medicine and are gaining increasing attention especially for the development of new drugs. According to that, the scope of this thesis is to propose a microfluidic model to simulate and mimic the physiological mechanism of the first-pass metabolism of orally ingested drugs. In the first part of the thesis, there is an introduction about the *in vivo* mechanism involved in the in process of first-pass metabolism. In particular are explained the principal organs involved in the first-pass metabolism, that is the intestine, where a first metabolic process takes place, and the liver where the quote of drugs is metabolized again. New bioengineered *in vitro* models to assess first-pass metabolism are presented with a particular attention on 3D intestine and liver models. Furthermore, the first chapter is focused on the recent studies on organ-on-chip device that can recapitulate the *in vivo* physiology and microenvironment, with the relative steps of fabrications. In the chapter 2, we first focused on the production of an innovative hepatic three dimensional tissue and made a comparison with the spheroid model, as gold standard model. Then we designed and validated a microfluidic device for the culturing of 3D HepG2 microtissues, in order to have a dynamic perfusion culture. The chapter 3 is focused on the fabrication of an organotypic intestinal 3D tissues cultured in both static and dynamic conditions. This 3D intestinal tissues are obtained by bottom-up approach of intestinal stromal microtissues, moulded in a maturation chamber. A Caco-2 epithelium was seeded on the surface of the biohybrid tissue. Furthermore, a gut-on-chip

microfluidic device was fabricated in order to obtain an air-liquid interface culture. The microfluidic gut-on-chip device was also used to study the stroma assembly and modification in the two different culture conditions. The combination of the two hepatic and intestine model on chip, is addressed in chapter 4. In this forth chapter, indeed a microfluidic biochip can accommodate both hepatic microtissues and 3D human intestinal equivalent. By the selective communication of the two tissues recreated into the biochip, it is possible to reproduce *in vitro* the mechanisms of orally ingested drugs and xenobiotics compounds.

Chapter 1

State of the art

1.1 First-pass metabolism

The selection of drug administration route is based on the specific site of action, the clinical situation of the patients, and the rate of the drug absorption. It is widely accepted that prescription of orally formulated drugs is the preferred method of administration, because it is easy, and patient's compliance and comfort are high [1]. Once ingested, the drug is dissolved and metabolized into the gastrointestinal fluids (GI), then cross the intestinal and liver barrier where it is subjected to the first-pass metabolism. First-pass metabolism consists into the sequential actions of intestinal and hepatic metabolism to which a drug is subjected that lead to a reduction of its concentration before it reaches the blood circulation (Figure 1.1). Sometimes only a small amount of active drug emerges from the liver to the rest of the circulatory system. The fraction of oral dose, which reaches the target site as intact drug is refereed to oral bioavailability (F_{oral}).

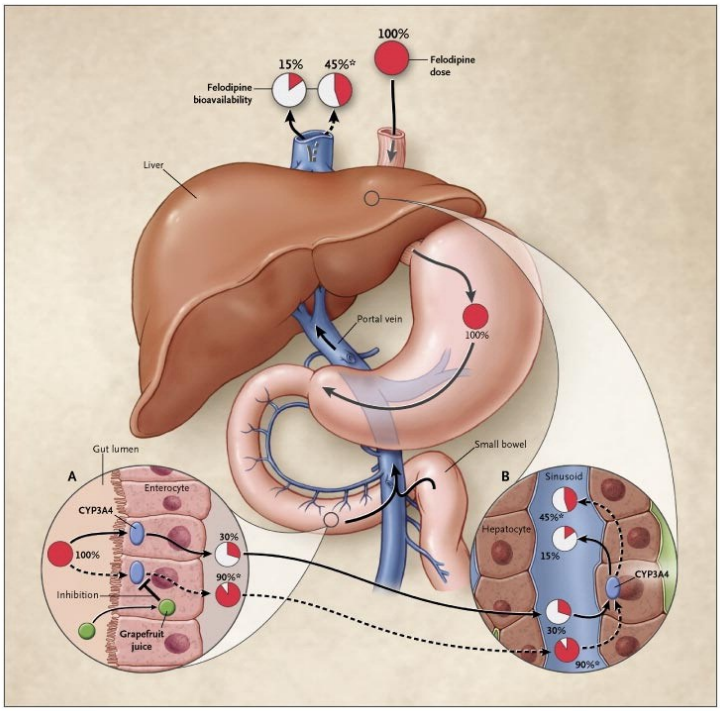

Figure 1.1: Schematic representation of first-pass metabolism. Once ingested a drug undergoes to a series of modifications that reduce its dose until it reaches the bloodstream [2].

The oral drug bioavailability is determined by the product of the fraction of dose absorbed from the GI tract (F_a), and the fraction of absorbed dose that escapes the metabolism at the intestine (F_G) and liver F_H. This is expressed mathematically in the Eq.(1) [3]:

$$F_{oral} = F_a + F_G + F_H \quad (1)$$

It is clear that first-pass metabolism reduces the bioavailability of the drugs. Poor oral bioavailability (F_{oral}) as been established as one of a reason for the failure of drug candidates in pre-clinical and clinical development. A lead compound should therefore have adequate F_{oral} to achieve the necessary drug plasma concentration time profile efficiently. F_{oral} also has to be predictable in order to prevent undesirable toxic side effects or sub-therapeutic drug plasma concentration [4].

As mentioned before, one of the limitation to oral drug bioavailability is the pre-systemic extraction by both the liver and the gut wall. First-pass extraction is associated with poor bioavailability of a variety of drugs [2]. Metabolism is the principal mechanism for the elimination of most of the drugs on the market and is a major component of pre-systemic extraction [5]. Metabolism can be divided into two phases, phase I and II. Phase I metabolism consists in the process of functionalization in which functional groups like hydroxyl, carboxylic, amino are introduced to the drug's structure via oxidation, reduction and hydrolysis. Phase II reactions involve conjugation between high polar moiety to either phase I metabolite or the parent drug to facilitate biliary or urinary excretion. Among the metabolic enzymes, cytochrome P450s (CYP) (phase I) and the UDP-glucuronosyltransferases (UGT) (phase II) are responsible for the majority of metabolic elimination. More than three quarters of the metabolic reactions of the 200 most prescribed are mediated by the CYP enzymes, whilst CYP3A4 is accountable for almost 46% of these reactions [6].

1.1.1 Hepatic first-pass metabolism and biliary excretions

The liver is one of the largest organ in our body whose functional unit is the haptic lobule. This organ has a wide range of functions like glycogen storage, plasma protein synthesis, production of bile and body detoxification from xenobiotic compounds (Figure 1.2-A). The liver is a highly vascularized organ with a stratified cellular structure [7]. Hepatocytes [parenchymal cells (PCs)]

are separated from non-parenchymal cells (NPCs) by a protein-enriched interface called the Space of Disse (SoD) (Figure 1.2-B).

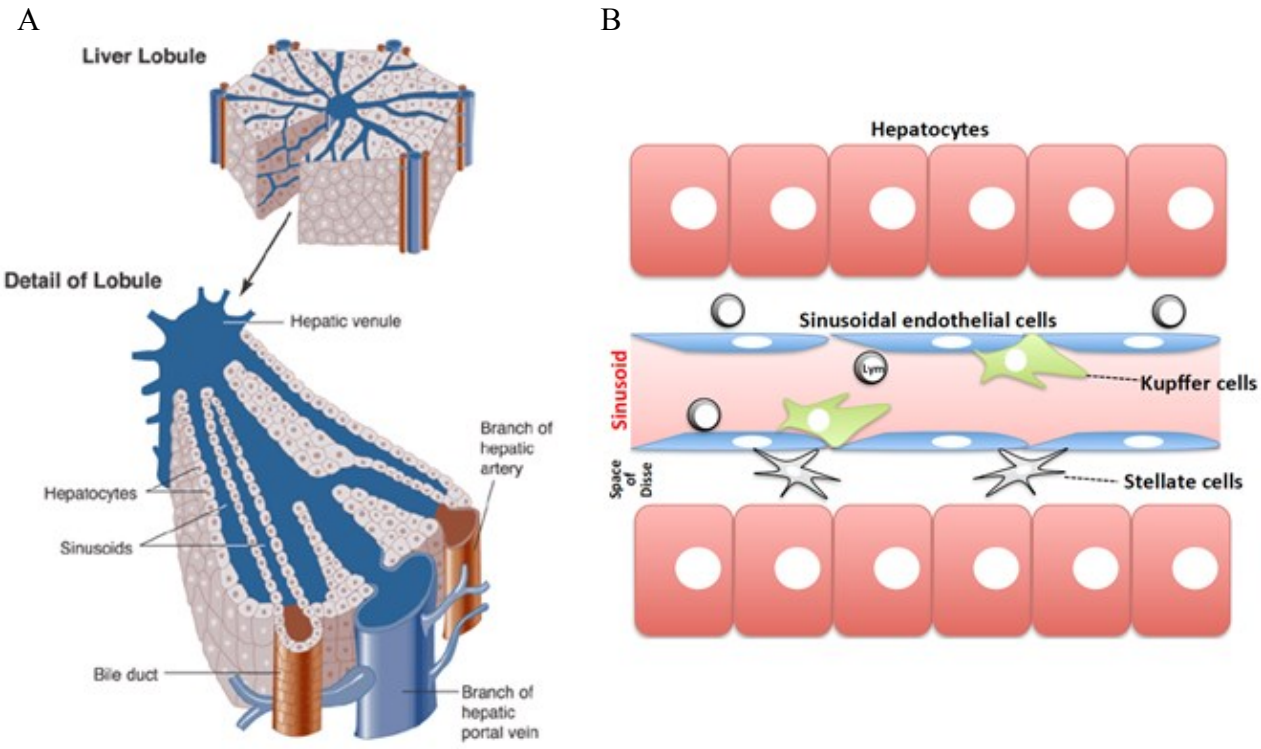

Figure 1.2: A) Schematic structure of the liver lobule. B) Hepatic sinusoids, where blood circulates, are characterized by sinusoidal endothelial and Kupffer cells. Hepatocytes, or liver parenchymal cells are localized to the space of Disse, distant from the sinusoid. Natural killer (NK) and invariant NK T (NKT) cells are abundant in the liver. Lym: lymphocytes, including NK cells, NKT cells, and other lymphocytes [8].

Hepatocytes account for approximately 70% of the volume of the liver, other cells are comprised of NPCs such as liver sinusoidal endothelial cells (LSECs), hepatic stellate cells (HSCs), and Kupffer cells (KCs). The SoD contains extracellular matrix (ECM) proteins, proteoglycans, and other molecules that enable hepatic cells to maintain their differentiated state. Hepatocytes abundantly express a large repertoire of enzymes for phase I and II metabolism. The contribution of the liver to pre-systemic extraction and therefore to F_H can occur by means of two mechanisms: first-pass metabolism and biliary excretion. The factors affecting the liver first-pass metabolism are the same factors governing the hepatic clearance: blood flow, unbound fraction of drug in the blood/plasma, enzyme abundance, the affinity and the capacity of the metabolic enzymes to bio-transform these drugs, expressed as hepatic intrinsic clearance (CL_{int}) [9]. About liver enzymes, the major ones involved in the hepatic first-pass metabolism include CYPs, UDP-glucuronosyltransferases (UGTs) and sulfotransferases (SULTs). Cytochrome P450 enzymes are the most important enzyme systems of phase I metabolism, a microsomal superfamily of

isoenzymes that catalyzes the oxidation of many drugs. CYPs are membrane proteins found in either the endoplasmic reticulum (ER) or mitochondrial membrane [2]. The electrons are supplied by NADPH–CYP450 reductase, a flavoprotein that transfers electrons from NADPH (the reduced form of nicotinamide adenine dinucleotide phosphate) to CYP450. There are 57 isoform of CYP enzymes that are categorized to 18 different families and 43 subfamilies. CYP450 enzymes are commonly expressed in the liver, but also found in the intestine, skin kidney and brain. CYP3A is the most important and abundant isoform of these enzymes. CYPs can be induced or inhibited by many drugs and substances resulting in drug interactions in which one drug enhances the toxicity or reduces the therapeutic effect of another drug. As the liver contains the greatest abundance of drug-metabolizing CYPs, CYP substrates are susceptible to efficient first-pass metabolism, which leads to low bioavailability. UDP-glucuronosyltransferases (UGTs) are the second main enzymes involved in the first-pass drug metabolism. The reaction catalysed by the UGT enzymes involves the addition of a glucuronic acid moiety to xenobiotics and is the most important pathway for the human body's elimination of the most frequently prescribed drugs. It is also the major pathway for foreign chemicals (dietary, environmental, pharmaceutical), removal for most drugs, dietary substances, toxins and endogenous substances. UGT is present in humans, other animals, plants, and bacteria. Sulfonate conjugation is an important pathway in the biotransformation of numerous xeno- and endo-biotics such as drugs, chemical carcinogens, hormones, bile acids, neurotransmitters, peptides, and lipids. The universal sulfonate donor for these reactions is 3′-phosphoadenosine 5′-phosphosulfate (PAPS), and the transfer of sulfonate to a hydroxyl or amino-group is catalysed by a super gene family of enzymes called sulfotransferases (SULTs). In the case of most xenobiotics and small endogenous substrates, sulfonation has generally been considered a detoxification pathway leading to more water-soluble products and thereby aiding their excretion via the kidneys or bile. For a drug like acetaminophen or a neurotransmitter such as dopamine, this is certainly the case. The abundance of the metabolic enzymes in the liver is higher than in any other organ in the human body [2]. In Caucasians the total abundance of CYP enzymes in the liver has been reported to be 0.43 nmol/mg of microsomal protein, where the most abundant phase I enzymes is CYP3A, followed by CYP2C, CYP1A2, CYP2E1, CYP2A6 and CYP2D6 [10]-[11]. Biliary excretion, on the other hand, is affected by the drug efflux to the canalicular space between hepatocytes and it is believed to occur mainly through active transport [12]-[13]. Transporters located in the canalicular membrane include P-gp, MRP2 and BCRP, therefore the substrate affinity for these transporters is an important factor for biliary excretion [14]. There are a number of drug-specific physicochemical factors that can influence biliary excretion, such as molecular weight, polarity and lipophilicity. The impact of biliary excretion in

drug bioavailability has been demonstrated for several drugs such as cardiovascular, anticancer, anti-infective and biologically active peptides. However, determination of the extent of biliary excretion in humans is very difficult, and therefore is mostly estimated by employing animal models, *in vitro* cell cultures or in silico models [12],[14].

1.1.2 Intestinal first-pass metabolism

Besides liver, it is important to know how intestine attend the first-pass metabolism. In order to understand the permeation of a drug through the gastrointestinal (GI) tract membrane it is important to have a general understanding of the anatomical and physiological factors affecting drug absorption in the human GI tract. The GI is an organ system which digests food, absorb energy and nutrients, and excretes the waste products as feci and urine. It can be divided into different segments: mouth cavity, esophagus, stomach, small intestine, and large intestine. The absorption of the drug can occur in all the segments of the GI but in particular in the stomach, small intestine and colon [15]-[16]. The small intestine is the major portion of the GI tract accounting for around 81% of the total intestinal length and is the major site for digestion and absorption of nutrients and xenobiotics. It consists of three major parts: duodenum, jejunum and ileum whose lengths are approximately 8%, 37% and 55% of the total length of the small intestine, respectively. The mucosa is the membrane that covers the luminal portion of the intestine and consists of a single layer of epithelial cells over a vascularized *lamina propria*. To maximize the efficiency of absorption and digestion, the human small intestine possesses highly complex 3D microenvironment. In particular, it forms circular folds on whose surface possesses finger like protrusions called intestinal *villi*. Each *villus* is about 0.5-1.0 mm high, and there are 20-40 *villi* per mm^2 [18].

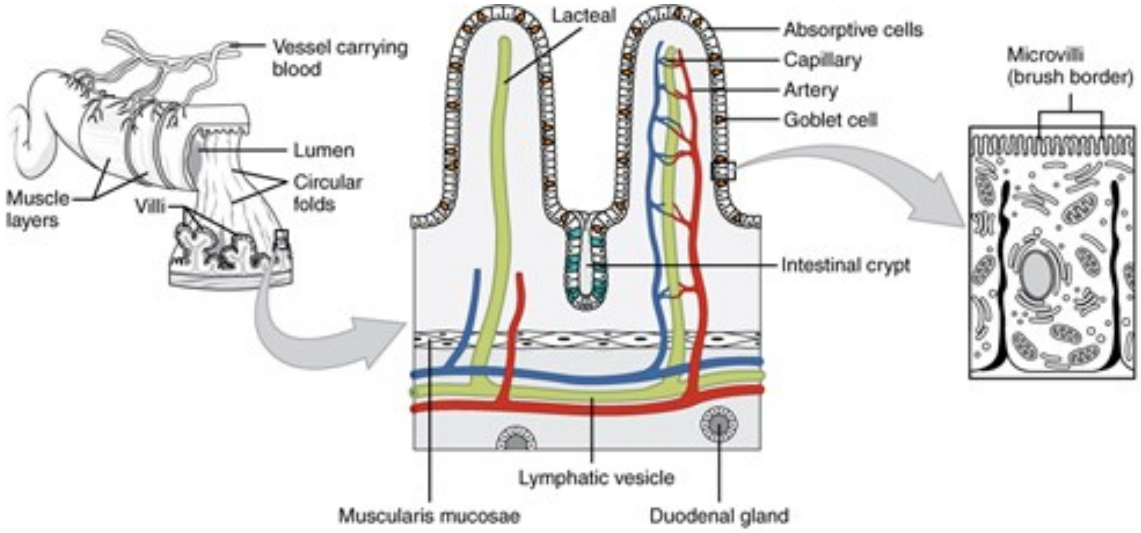

Figure 1.3: Structure of the small intestinal membrane. In the *villi*, the absorptive cells (enterocytes) rest over the vessel rich mucosa where the absorbed nutrients, drugs and xenobiotics are transported to the portal circulation. The enterocytes display a brush border structure in the apical side formed by micro*villi*.

The intestinal contribution to first-pass metabolism has been subject to increasing interest during the last decades and it is believed to play a major role for determining oral bioavailability [18-20]. As in the liver, CYP3A enzymes are the most abundant enzymes in the human intestinal wall, accounting for almost 80% of the small intestine CYP content [10]. CYP enzymes are strategically located at the villous part of enterocytes and their presence varies along the small intestine. Quantification studies showed that CYP3A4 abundance decreases from the proximal duodenum towards the distal ileum, being highly expressed in the jejunal segment [21]. This distribution pattern can have an impact on the bioavailability of CYP3A4 substrates administered as controlled release formulations [22]. Even though the CYP3A4 abundance is about 1% of that in the human liver [23], it plays an important role in the intestinal pre-systemic extraction for several drugs [24]. In addition, it has been hypothesized that both CYP3A4 and P-gp might act together as barriers for the absorption of drugs and xenobiotics. This hypothesis is supported by their location within the enterocytes, overlapping affinity for several substrates and suggestions of coordinated regulation between them [24-25]. The factors influencing first-pass gut wall metabolism and therefore affecting the F_G are similar to those governing the hepatic clearance: intestinal blood flow, intestinal fraction unbound and intestinal intrinsic clearance [27]. However, there is a complex interplay between drug absorption and intestinal first-pass metabolism, where the factors affecting drug absorption might have an impact on the rate and extent of intestinal first-pass extraction (i.e., the solubility, permeability, residence time, and inter individual variability) [28].

1.2 Prediction of first-pass metabolism

In order to predict the oral bioavailability of new developed drugs, several models for the prediction of first-pass metabolism have been developed. These includes both *in vitro* and *in vivo* approaches during drug discovery process. About drug discovery process, the first step is to identify and select a "target", such as a gene or protein, which can potentially be affected by a drug or a molecule. Once the target is established, a promising molecule, or a "lead" is identified that can interact with the target. The lead is optimized by screening many similar compounds. The first pre-clinically screening is developed with *in vitro* 2D culture model as well as animal models. *In vitro* methods are widely used to investigate kinetic, metabolic, and toxicity (ADME-Tox) of new lead compounds early in the drug discovery process. However, *in vitro* cell-based assay do not provide a realistic model of the environment to which the cells are exposed in the body, for example the extracellular matrix environment which provide mechanical support and dynamic signalling cues, the exchange of metabolites from one cell type to another and the physiological shear stresses from the fluid flow are all missed. This assay also do not takes into account of the complexity of multiple organs and their interaction.

Anyway, if the drug is evaluated positively with cell-based assays, more advanced tests with animal models are conducted. Unfortunately, animal models do not always predict the actions of drugs accurately, because human metabolism and animal metabolism can differ considerably. Because of these differences, it is possible that drug candidates are eliminated even though they might be effective in humans. As a result, using an extensive number of animals to study the actions of drugs gives rise to ethical concerns, especially because animal model are not so predictive. Indeed, only about 10% of compounds that promised potential in animal models, were allowed to enter clinical trials. Anyway, many drugs fail during full clinical development in Phases II and III [29], the most expensive phases of drug development, because they have poor bioavailability or are considered not clinically safe because of toxic side effects. Since this models are not so predictive, there is the need to develop better *in vitro* models of human and animal metabolisms in order to reduce drug development times and costs.

1.2.1 *In vivo* model

During pre-clinical drug discovery, research teams use animal models to test the pharmacokinetic characteristics of new drug candidates. The most commonly animal species used in such clinical studies are mouse, rats, dogs and non-human primates (NHP) [30]. For intravenous administration, human pharmacokinetic parameters such as clearance, half-life and volume of

distribution have been predicted empirically from pre-clinical species data by means of allometric scaling techniques [31]. Allometric scaling requires the investigation of the desired pharmacokinetic parameters in one or more pre-clinical species, where the parameters of interest are regressed against a species body size descriptor (usually body weight) and the resulting regression equation can be used to predict the value of the parameters in humans [32]. However, one of the major drawbacks of allometric scaling is its empirical nature, which does not necessarily allows the understanding of the underlying mechanisms that can explain the species differences in the pharmacokinetic parameters, such as metabolic clearance [22]. Moreover, the usefulness of allometric scaling for the prediction of human pharmacokinetic parameters has been questioned due to large prediction errors that can arise from the allometric relationship and the use of arbitrary constants with little or no physiological meaning [33]. As a part of the drug development process oral bioavailability is usually investigated in pre-clinical species and the resulting data is subsequently employed as a part of the lead selection/optimization process. In some research teams, thresholds have been set up for oral bioavailability, for instance 20-30% in rats, as an indicator of acceptable human oral bioavailability for the new drug candidate [34]. Preclinical species seem to provide a good indication of the human oral absorption for certain drug candidates. Several groups have demonstrated acceptable correlations levels between the F_a and intestinal permeability between humans and pre-clinical species, particularly for rat and monkeys, though this correlation was found to be poor in dogs [35,36]. When it comes to oral bioavailability, however, a similar relationship remains unclear. One of the first attempts to summarize the relationship between human and animal bioavailability was done by Sietsema in 1989 where he collected bioavailability data for several drugs in humans, rodents, dogs and primates, showing a poor interspecies correlation [37], while in 2000 Mahmood also highlighted that allometric scaling was not an adequate tool for the direct prediction of human bioavailability [38]. From the analysis of the previous datasets it can be noticed that the bioavailability data obtained from preclinical species seems to underestimate the value in humans [37], [39]. While the reason for this underprediction might not be necessarily clear, as mentioned before, the factors governing oral bioavailability are numerous and depend both on the drug-related properties and physiological, environmental and population characteristics. Therefore one can speculate that interspecies differences in physiological aspects, such as body size, blood flows, plasma proteins, GI tract morphology and physiology, enzymatic abundance in the GI tract and liver are probably the main contributors for the differences observed in bioavailability. Most of the aforementioned comparisons and datasets were based on a limited number of compounds (< 50 compounds) [38] [39] [40] whereas the largest dataset is from 1989 and does not differentiate between preclinical

species such as rats, mouse and/or rabbits nor include enough data points, especially for the analysis of the correlations between monkeys and humans [37]. Interestingly, one of the most cited articles when it comes to the comparison between animal and human oral bioavailability is based on Sietsema's review on interspecies bioavailability data [41]. Therefore there is the need for an updated, wider and specific dataset that can be employed for the comparison between human and animal oral bioavailability, in order to definitely elucidate whether animal data can be used for the prediction of human oral bioavailability *per se*. This dataset can be also used for the development of quantitative and qualitative models for the extrapolation of bioavailability values from pre-clinical species to human, which can be of value in drug development.

1.2.2 *In vitro* liver model

To understand liver physiology, researchers have relied primarily on hepatocytes cultured as monolayers. Primary human hepatocytes are considered the gold standard of *in vitro* liver models in drug development. In the late 1960s Berry et al. [42] extracted viable rat hepatocytes using collagenase method. In the 1980s, extraction of human hepatocytes became a more common culture assay for drug screening [43]. However, primary hepatocytes have well-known disadvantages, such as limited availability of the liver tissue for cell harvesting, high functional variability between hepatocytes from different donors, and difficulty maintaining differentiated phenotype and functions in cell cultures. Since primary hepatocytes are not so easy to handle, perpetual cell lines represents a potential alternative in drug metabolism and hepatotoxicity studies[44]. Some example include HepG2, Hep3B, Huh7, and HepaRG. Anyway these cell lines may lack many features of the hepatocytes but sure they have a lot of advantages: good availability, unlimited growth, are easy to handle and there isn't the donor variability. The most frequently used liver cell line, HepG2, was derived from the liver tissue of a male patient with hepatocellular carcinoma [45]. HepG2 are equal to primary hepatocytes in assessing parent compound toxicity, but they have low metabolic activity when cultured on plastic or glass surfaces[46].

Fortunately, improvements in the culture environment have shown to induce both drug metabolizing enzymes and transporters in HepG2 cells [47],[48].

A recent hepatoma cell line, HepaRG, was derived from a liver tumor of a female patient who suffered from the hepatitis C virus and hepatocarcinoma [49]. HepaRG is a superior cell line compared to the other immortal hepatic cell lines. It expresses the metabolizing enzymes at a level comparable to the primary human hepatocytes [50],[51]. This cell line also expresses several active drug transporters [52]. Other advantages of HepaRG are the stability of the phenotype,

extends to several weeks in duration [53], and its suitability for toxicity studies [51], [52], [54]. HepaRG cells are commercially available as a fully differentiated form that is suitable for drug metabolism studies, whereas the original HepaRG hepatic progenitor cell line is a proprietary cell line that is provided only to a few research laboratories. The versatile HepaRG progenitor cell line expresses bipotent differentiation. At low density, the HepaRG resembles liver progenitors, and in the confluent state, the culture is composed of hepatocyte-like and cholangiocytes-like cells [50],[55]. Furthermore, the differentiated cells show reverse differentiation to the progenitor phenotype while seeded at low density. The xenobiotic metabolism of the HepaRG progenitor is initially low, but is induced after several weeks of treatment with dimethyl sulfoxide (DMSO) [50]. Because cells on monolayer rapidly loss hepatic phenotype, multicellular cultures have gained attention for the promotion of heterotypic interactions [46].

The heterotypic co-culture between hepatocytes and non-parenchymal cells allows the increase of the phenotype and of the functions of the hepatocytes compared to monoculture for several weeks [56]. This effects is due to the direct heterotypic cell-cell contacts, and partially to the paracrine influences of cytokines secreted by the surrounding cells [57].

Co-culture with fibroblasts, hepatic stellate cells, Kupffer cells, or liver sinusoidal endothelial cells have improved at least some of the hepatic functions [58].

From another point of view, co-culture with NP cells is necessary to recreate hepatotoxicity mechanism which require collaboration with different cell type of the liver. Thus, to predict liver toxicity from *in vitro* data, hepatocytes have been co-cultured with immune system cells, such as Kupffer cells, a promising type of co-culture. This kind of co-culture seems promising since it enhances cytotoxicity to the hepatotoxic chemicals [59],[60]. Several experimental approaches to perform this co-culture includes direct co-culturing on standard culture plastic [61], co-culturing with collagen layer [62], or culturing in membrane inserts, where different cell types are separated by a membrane, but soluble mediators can migrate between the compartments [63]. Moreover, co-culturing has been performed with cell sheet technology where confluent cell monolayers of hepatocytes and non-parenchymal cells are stacked on top of each other [64]. Two dimensional co-cultures of PCs and one or more NPCs, such as LSECs [65], fibroblasts [66], or other cell types, showed stable hepatic markers for several weeks. Despite co-cultures are clearly advantageous in term of cost and time, they do not recapitulate the cellular composition or the 3D liver architecture *in vivo*. Indeed, 3D culture model enable the maintenance of NPC phenotypes for longer culture periods and recapitulate more the physiological hepatic microenvironment[67]. Despite these advances, closely recreating the hepatic microenvironment remains a challenge.

Hepatocytes in our body have a polygonal shape but they lose this characteristic when cultured in 2D culture, appearing flattened. The flattened cell morphology limits cell-cell interactions, and leads to reduce polarization, limiting signaling pathway and liver functions. Hence, research groups have been working on the retaining the physiological cell-cell and cell-ECM contact by various 3D cell-culture techniques. Hepatic spheroids are simple 3D systems which are formed by the natural tendency of the cells to aggregate. Spherical multicellular aggregates, spheroids, are formed when the cells self-assemble and re-establish the cell-cell contacts in three dimensions. Spheroids culture shows many advantages such as prolonged survival [68],[69], *in vivo*-like characteristics like polarity, enhanced secretion of albumin and urea and formation of bile acids [70],[71]. These effects may are obtained from the retention of the 3D architecture, the presence of ECM and the high number of cell-cell contacts [68],[72],[73].

Spheroids formation can be induced by a variety of different techniques including hanging drop method, liquid overlay cultures and dynamic bioreactors. In the hanging drop method, cells are arranged in small droplets in a plastic slide. Due to the surface tension, liquid can maintain droplets when the lid is inverted and cells settled at the bottom of the droplet. A simple method for spheroid production involves liquid overlay of a cell suspension over a non-adherent surface, such as agar-coated plates. Spheroids can also be formed by culturing in spinner flasks or bioreactors, which can provide dynamic conditions preventing cell-substrate contact and promoting cells to form aggregates by either stirring or rotating bioreactors. This system can produce large numbers of relatively consistent spheroids, but they both require specialized equipment and additional processing steps when used for drug testing. One of the major uses of human spheroids has been as a preclinical screening tool for drug candidates because they remain viable and maintain liver functions. However, a drawback associated with spheroids is the lack of cell–ECM contacts or nutrients for cells that are located in the necrotic core. Cellulose hydrogels, which exhibit diffusion coefficients comparable to ECM-derived gels proteins, supported the growth and differentiation of HepaRG (hepatic progenitor cells) and HepG2 spheroids with minimal cytotoxicity [74]. Encapsulation of HepG2 spheroids in alginate hydrogels led to an increased induction of CYP1A1 and CYP3A4 [44]. Recognizing the importance of heterotypic interactions, recent studies have encapsulated more than one cell type within spheroids, for example endothelial cell cords were formed using a co-culture of human umbilical vein endothelial cells (HUVECs) and mouse mesenchymal cells encapsulated in type I collagen [75]. These cords resulted in patent blood vessels and albumin promoter activity in hepatocytes. Induced pluripotent stem cells (iPSCs), HUVECs, and human mesenchymal stem cells (hMSCs) were cultured together to form iPSC derived liver buds (IPSC-LBs), which on transplantation resulted in

successful anastomosis to the host vasculature and formation of blood vessels [76]. Hepatic cord-like structures were also observed, suggesting the maturation of hepatocytes. These major developments open new avenues to enhance the complexity and physiological relevance of engineered tissues through the inclusion of vasculature in spheroids. Spheroids are convenient and relatively simple techniques to simulate *in vivo* liver microarchitecture. In spite of these advantages, the lack of interstitial fluid dynamics, which is highly relevant to drug transport within the tissue, is one of the major limitations.

Scaffold-based systems are a comparable 3D *in vitro* model for testing novel drugs. In this kind of culture, cells are grown in a semi-solid matrix that allows to study the influences of external physical factor on micro spheroids growth and signalling. Biomaterials scaffold have been produced as synthetic ECM to enable the 3D organization of liver cells. Scaffolds are designed to be porous and their mechanical properties should be viscoelastic like natural tissue. The cells are seeded on prefabricated scaffolds where they grow on the surface of the pores and may form 3D cell assemblies. 3D scaffolds mimic ECM of connective tissues and provide architectural support for tissue engineering and regeneration with select cell types. In particular, biodegradable scaffolds have been widely used since they may be further suitable for tissue engineering purposes [77]. In general, scaffolds can be classified in two groups: natural and synthetic scaffold. Based on the nature of the scaffolding materials, they are either biodegradable or non-biodegradable and biocompatible or non-biocompatible. Biomaterials, either natural or synthetic, that are biodegradable and biocompatible are highly demanded in tissue engineering. The most successful synthetic polymers include poly(lactic acid) (PLA), poly(glycolic acid) (PGA), and poly(lactic-co-glycolic acid) (PLGA). The PLA, PGA, and their derivatives have supported 3D hepatocyte growth for up to two weeks [78]. More recently, a cross-linked polystyrene scaffold, Alvetex $_{TM}$, has been shown to support hepatocytes morphology and upregulation of CYP enzymes better than the conventional 2D polystyrene plastic ware [79].

About natural scaffolds, the most used are the hydrogels. They exhibit low mechanical properties but they provide a biomimetic environment that supports cell proliferation and differentiation. Most of the hydrogels used are made up of naturally occurring materials or proteins found in the ECM, one of the many examples is collagen type I. The scaffold based on the natural alginate polymer, has shown to increase the aggregation of primary hepatocytes [80], to maintain albumin synthesis of primary hepatocytes [81], and to increase CYP and UGT enzyme activity of hepatocyte cells. Selection of the ideal biomaterial scaffold for a given cell type is problematic and has been accomplished to date mostly by trial and error. Even if the right biomaterial is available, achieving a high enough cell density and the homogeneous cell distribution necessary to construct

a viable tissue is extremely time consuming. Furthermore, pre-shaping the scaffold may present further difficulties. In order to get over these limitations, efforts have been focused on scaffold-less tissue engineering and bottom-up approaches which aimed to generate larger tissue by assembly small building blocks. This approach try to mimic the *in vivo* structure of tissues and organs which are constituted in repeating small functional units.

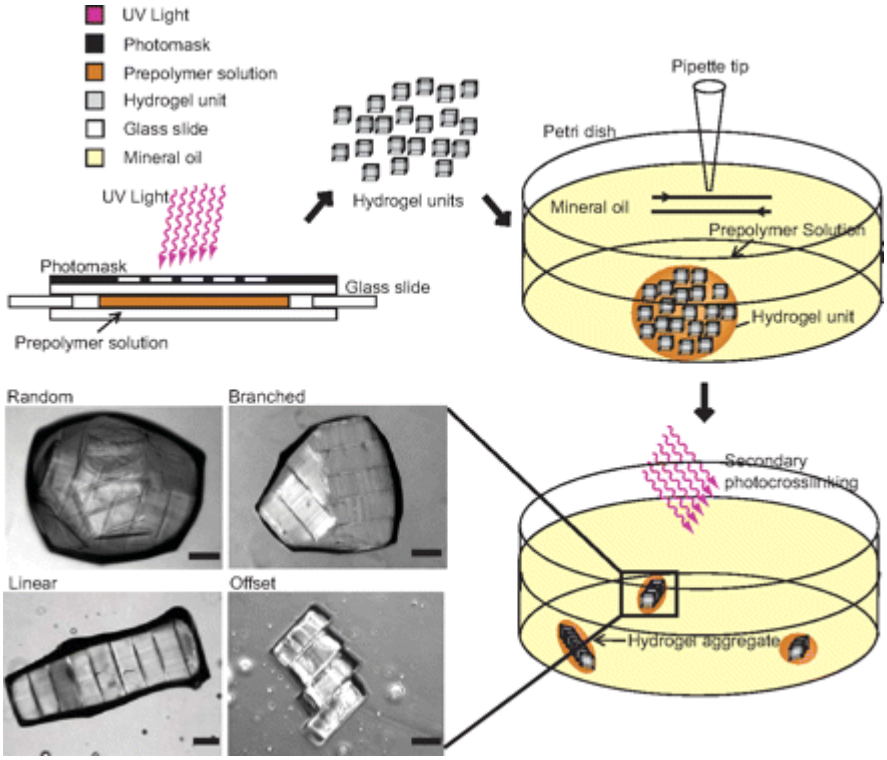

Figure 1.4: Schematic diagram of microgel assembly process. Microgel units were synthesized by photolithography, transferred into a dish containing mineral oil, and subjected to mechanical agitation applied by manually manipulating a pipette-tip in a back-and-forth manner[82].

An example of a bottom-up approach was used by Du et al. [82], to direct the assembly of cell-laden microgels to generate 3D tissue with tunable microarchitecture and complexity (Figure 1.4). McGuigan and Sefton (2006), proposed another interesting use of modular components for generating tissue. In their approach, rod-shaped collagen microgels that were seeded with HepG2 hepatocytes on the inside and endothelial cells on the surface were "packed" together within a bioreactor and perfused with medium [83]. 3D bioprinting has been applied to the development of several types of tissues and organs by using different cell types. The bioprinting of functional perfusable hepatic constructs is still in its first phase. However, 3D bioprinting techniques have been explored to reproduce hepatic constructs with limited function. Metabolically active 3D hepatic tissue has been printed using the NovoGen MMX Bioprinter (Organovo Holdings, Inc., San Diego, CA, USA). An increased liver-specific function of the tissue (for up to 135 h) compared with matched 2D cell cultures was demonstrated. Furthermore, compartment-specific

organization was shown for hepatocytes, hepatic stellate cells, and ECs by rudimentary microanatomy. The extrusion-based bioprinting technique was used to print alginate-encapsulated HepG2 cells, growth factors, and scaffolding materials in an organized 3D architecture [84]. These microlivers were dynamically microperfused to mimic an in vivo condition to study drug metabolism. Furthermore, this system was also utilized to perform as a model for a radioprotection study on liver cells. Netti and co-workers (2010), produced a new microtissue precursor assembly strategy (μTP) to produce pieces of viable 3D tissue equivalent in order to capture the feature of the native tissue. μTPs were produced by means of dynamic cells seeding of bovine fibroblasts on porous gelatin using spinner flask bioreactor [85]. In this culture condition the porous structure of microcarriers created a suitable environment for the development of fibroblasts and other cells type, as the cells within the porous carrier will experience lower shear stress than those encountered with non-porous carriers.

Ultimately, 3D cultures, both spheroids and scaffold based-models, can contribute to the reduction in animal testing and allow for economical savings as well as become a powerful model to optimize drug candidates for enhanced tissue distribution and efficacy.

1.2.3 *In vitro* gut model

Currently, modelling of the GI tract has focused on the small intestine because it is responsible for a large portion of digestion and secretion (Figure 1.5).

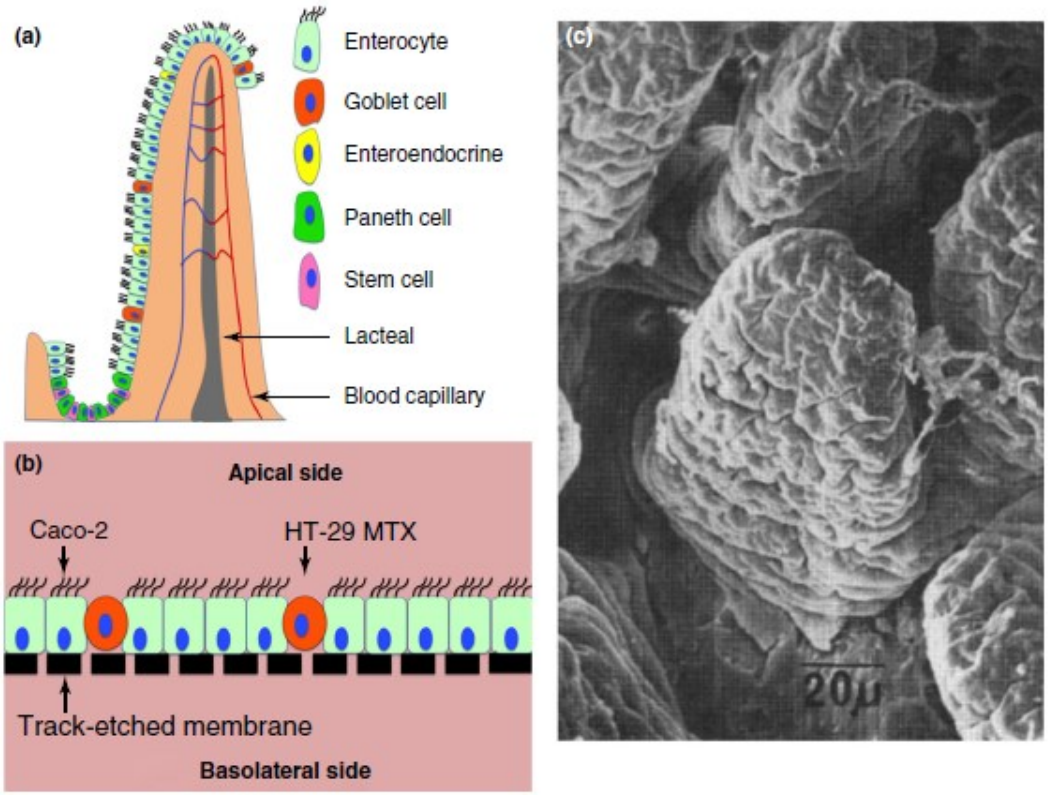

Figure 1.5: (a) Illustration of human small intestine epithelium on crypt–*villus* axis. (b) A schematic of conventional 2D small intestine model. Caco-2 and HT-29 MTX are cultured on the track-etched membrane. (c) A scanning electron microscope image of human small intestine *villi*.

Typical *in vitro* GI model are characterized by the culture of epithelial monolayer under static condition. The cell line commonly used are immortalized or cancerous intestine-like cells, [86] such as Caco-2, HT-29, T84, TC-7, and SW620. Among these cell types, Caco-2 and HT-29 cells are used extensively as substitutes for enterocytes and goblet cells, respectively [87]. Caco-2 cells are derived from human colon carcinoma and have been shown to form a polarized enterocyte-like monolayer after 21 days in culture on Transwell inserts where they become fully differentiated (Figure 1.3). Polarized Caco-2 monolayers are characterized by the presence of *villi*, brush border enzymes, and drug transporters. Caco-2 cells can be cultured on a variety of biomaterials including alginate, collagen, polycarbonate, polystyrene, and Biocoat. This cell line is very versatile and it is extremely appealing for use in engineered *in vitro* models. Unfortunately, in terms of xenobiotic transport modelling, such culture models have low permeability because Caco-2 monolayer is eight-times smaller than that of human small intestine epithelium, which is considered as one of the reasons for poor drug paracellular permeability correlation between conventional *in vitro* models and human small intestine. Additionally, the expression of critical phase I and phase II biotransformation enzymes is significantly lower in such cells as compared to

in vivo [86]. The P-glycoprotein (P-gp) efflux pump is overexpressed in Caco-2 cells compared to the level measured *in vivo* with primary small intestinal enterocytes, which to some extent enhances the transport activity of the epithelium significantly during drug absorption. HT-29 cells are also derived from human colon carcinoma and can express mature mucin proteins. Caco-2 monocultures or co-cultures with HT-29 cells are frequently cultured on the apical side of a Transwell insert to mimic the intestinal barrier [88]. Transwell systems have been commonly used to assess the effect of environmental chemicals and pharmaceuticals. The permeability of a drug or chemical is measured by determining the rate of transport across the monolayer. The viability of the cultures has been assessed by tight junction degradation through trans-epithelial electrical resistance (TEER) measurements, changes in mitochondrial metabolism and cell viability, production of ROS, and changes in protein synthesis.

However, it should be noted that these stationary 2D cell cultures recapitulate neither the tissue architecture of the mucus layer nor the interactions between the epithelium and the stroma in intestinal mucosa. This is most important because such interactions involved in tissue microenvironment play a dominant role in determining the phenotype and functionality of enterocytes, and consequently affecting the process of drug absorption.

By using three-dimensional culture models for intestinal mucosa tissues it is possible to better mimic the *in vivo* tissue microenvironment. Tissue engineering techniques allowed to develop 3D cell culture system for studies of drug toxicity evaluation and replacement therapy.

With the development of microfabrication and other biomaterial fabrication techniques, biomimetic topography has been integrated into *in vitro* intestinal models to represent human small intestine 3D features. One example of 3D intestinal model obtained by microfabrication techniques is an human small intestine crypt-like topography fabricated using photolithography and transferred to poly(dimethylsiloxane) (PDMS) and collagen membrane substrates [89]. Compared with 2D flat substrates, Caco-2 cultured on PDMS substrates with crypt-like topography exhibited higher mitochondrial activity and lower alkaline phosphatase activity, similar to the cell phenotype in human intestinal crypts [89]. Transepithelial electrical resistance (TEER) values were found to be slightly lower for Caco-2 monolayers cultured on topographically modified collagen membranes relative to flat collagen controls, suggesting that crypt-like topography might affect tight junctions of the Caco-2 monolayer.

Human small intestine *villus* structures have also been fabricated by combining different microfabrication techniques. 3D printing (3DP) was used to construct porous poly(lactic-coglycolic acid) (PLGA) villous scaffolds [90]. However, take into account the resolution limitation of this technique, porous PLGA villous structures had considerably bigger basal areas

than human small intestine *villi* and hence could not reproduce the dimension and density of the *villi* relevantly. Recently, by combining laser techniques, a collagen villous scaffold was fabricated with 0.5 mm villous height and 25 *villi* per mm^2 density, with striking similarity to the human jejunal *villi* [91] (Figure 1.5 c,d). By using a custom-made cell culture insert kit, the collagen villous scaffold was integrated with a six-well cell culture plate to study drug absorption [92]. When cultured on collagen villous scaffold, Caco-2 exhibited differentiation gradients along the villous axis, on the top of the villous cells were more columnar and polarized than cells near the bottom of the *villus*, according to the *in vivo* observation that enterocytes become more differentiated when migrating from the crypt to the top of the *villus* [92]. About TEER measurements, Caco-2 monolayers cultured on collagen villous scaffolds showed to be significantly lower than 2D controls, and similar to *in vivo* intestinal values. The apparent permeability coefficient (Papp) of the slowly absorbed drug atenolol measured on the collagen villous scaffold was 13 times higher than that measured using conventional 2D models, and much closer to the average permeability value from perfused human small intestines, suggesting that the 3D villous model could improve the poor permeability correlation of paracellularly transported drugs between *in vitro* models and native human small intestine.

Recently, Schweinlin et al. engineered small intestinal organoids using a decellularized small intestinal submucosa as a scaffold [93]. CYP3A4 and P-glycoprotein levels were measured and compared between organoids cultured alone or on the scaffolds [93]. Both CYP3A4 and P-glycoprotein levels were more than 3-fold higher in organoids cultured on scaffolds in a bioreactor than organoids in a static system.

1.3 Microfluidics technologies

1.3.1 General principles of microfluidics

Microfluidic is the science of manipulation of small amounts of fluids ($10^{-9} - 10^{-18} L$) in micro hollow channel. It involves the development of miniaturized devices (microchip) and to control, manipulate, and analyze flows in submillimeter dimensions. It is a microsystem technology that has been used to generate and precisely tune dynamic fluid flown fluid flows and spatio-temporal gradients, as well as deliver nutrients and other chemical cues to cells in a controlled manner [94]. Thanks to the small size, fluid flow in the microsystem is laminar and there isn't the mixing of different fluids. Typically, microfluidic systems have a geometry with characteristic dimension length on the order of tens to hundred microns. Advantages of this microsystems are easiness of

fabrication, low reagent consumption, parallel and rapid processing ability and large-scale integration. Microfluidic chips have been developed for various purposes, like real-time PCR, immunoassays, whole blood sample preparations, two-dimensional chromatographic separations, and to culture cells under flow conditions. It is the creation of networks of interconnecting channels that makes the field of microfluidics so powerful.

1.3.2 Materials

Firstly, the development of microfluidic devices was focused on micro-machining and electronic application but the emergence of BioMEMS fabrication techniques such as replica moulding has opened the development of microfluidic cell culture models in an array of materials platforms including synthetic and natural materials as well as bioresorbable systems.

For the selection of substrate materials for microfluidic device, it is important to take into account about some particular characteristics such as optical transparency for cell imaging, the desired degree of mechanical rigidity or flexibility, surface chemistry and reactivity and biocompatible. Synthetic polymers such as PolyDiMethylSiloxane (PDMS) are the most common platforms for microfluidic systems and have been applied to cell culture models based on their high oxygen permeability, optical transparency, and easiness of fabrication [95]. In particular, the typical characteristic of the PDMS are the high gas permeability that allows sufficient oxygen supply to the cells in the microchannels, transparency from ultraviolet to the near infrared wavelength. However, the tendency of PDMS to absorb, retain and release other chemicals and some organic solvents in an unpredictable fashion has been a problem for different applications. Other used materials are, poly(methyl methacrylate) (PMMA), polycarbonate (PC), and polystyrene (PS).

1.3.3 Fabrication

There is a wide range of microfabrication techniques for constructing microfluidic device. The basis for the fabrication processes of most microfluidic devices is photolithography, a set of techniques originally developed to integrate semiconductor structures on microelectronic chips. Photolithography exploits a photosensitive polymer, so-called photoresist, to pattern chip surfaces. Two types of photoresist exist, positive and negative photoresist. When positive photoresist is exposed to UV light, the exposed region becomes soluble and the unexposed region is polymerized. In the case of negative photoresist, it is the other way around: the exposed region

becomes polymerized and the unexposed area is soluble in appropriate solution. Commonly, glass or silicon wafers are coated with a thin layer of photoresist. Subsequently, a latent image is formed in the resist by exposing it to ultraviolet light through a photomask with opaque and transparent regions containing the channel layout of the microchip. After patterning, the unpolymerized photoresist is removed by rinsing with an appropriate solvent, leaving the desired pattern behind on the wafer. Subsequently, the glass or silicon can be selectively dissolved with an appropriate etching solution like hydrofluoric acid (wet-etching) or with e.g. reactive ion etching (dry etching), to form the structures in the substrate. However, silicon and glass are rather expensive, and silicon is opaque, which means it cannot be used for optical measurements in the UV or visible range.

Another approach is to fabricate chips in polymers, using a process known as soft lithography. Instead of using the wafer material to fabricate the chip, the wafer is now used as mold with a positive relief of the channel structure. This mold can be re-used multiple times. In this procedure thermosetting elastomer like PDMS is poured over the mold, and allowed to polymerize. In this case, the thickness of the original photosensitive layer determines the depth of the channel. After polymerization, the elastomer with structure can be gently peeled off the wafer (Figure 1.6). The open channel structure in the elastomer can be closed by placing another piece of elastomer or glass on top of it, to obtain a closed microchip. The bonding of these two pieces occurs by chemical interaction without the need of glue. In general, microfluidic devices offer many advantages over conventional systems. The biochip are very minute so only small amounts of the tested substrates are needed, a fundamental consideration during early drug development screening that usually require large amount of compounds. Other advantages are less waste and lower reagents costs compared to conventional system. Due to the small dimension, it is possible to conduct high-throughput screening analysis in a compact device. The analysis and response times are also much faster compared to conventional systems, due in part to the short diffusion distances. With microfluidic technology, many new devices and applications have been and continue to be developed for various applications, in order to improve on conventional systems or to open up new applications.

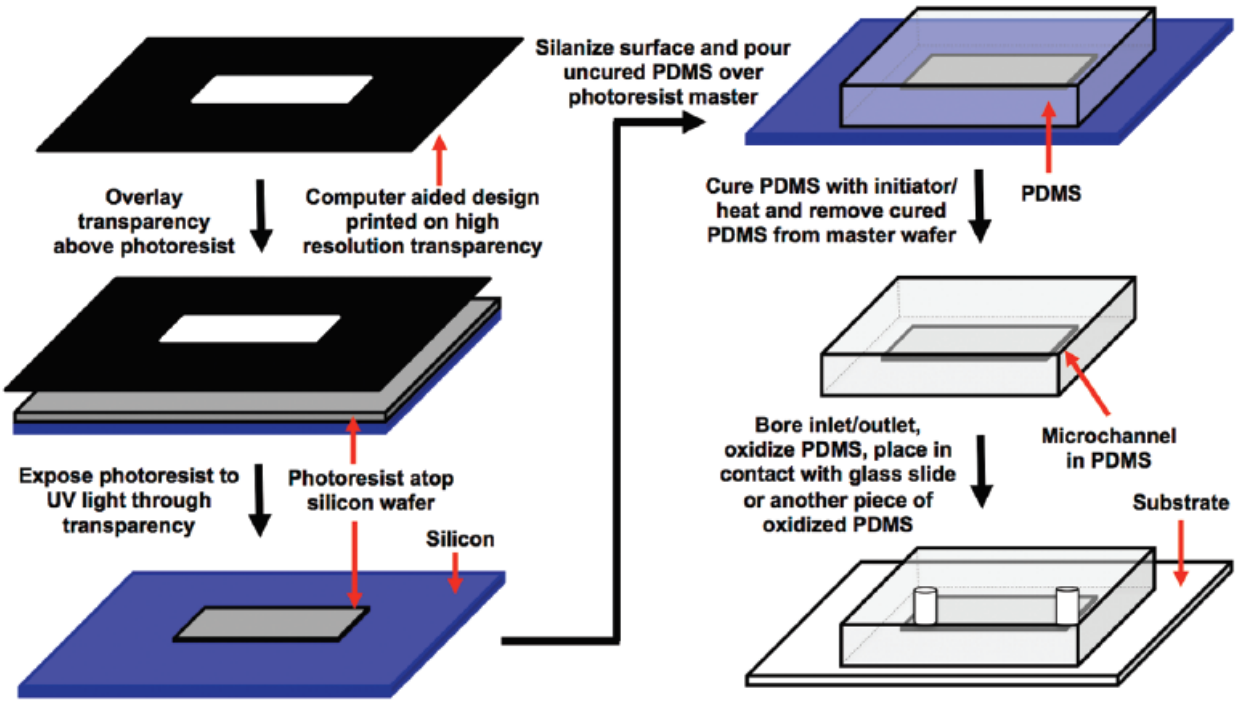

Figure 1.6: Creation of microfluidic devices. A photolithographic process is used to first create a pattern of a photoresist on a silicon wafer. Then, soft polymers such as polydimethylsiloxane (PDMS) are cast on the wafer to generate a stamp. This stamp can then be irreversibly bonded to a basement substrate (i.e., glass, PDMS, or acrylic) to create microfluidic channels for perfusion of cultures [96]

1.4 Liver-on-chip

The liver has proven to be one of the most difficult organs for drug approval, due to the strong interactions it has with other organs, as well as its sensitivity to the metabolism of certain drugs. This takes to a high percentage that are removed from the market due to hepatotoxicity. By improve the method and the technology to test for toxicity, it will be more easy, fast and safe develop new drugs and reach the market [97]. In last years, considerable amount of research has been done in the toxicity test area using accurate microfluidic system mimicking the liver functions. Incorporating flow into the culture system has been shown to increase and maintain a higher level of metabolic functions. Physiologic oxygen gradients can be established in these microfluidic systems which can assist in elucidating the physiological mechanisms involved in hepatotoxicity [98]. According to the literature there are a lot of valid microfluidic liver models that can provide a dynamic, tunable environment emulating *in vivo* conditions.

The microscale design of the biochips allow for microscopic imaging, oxygen sensing, physiologically relevant ratios of chamber sizes and liquid residence times in each compartment, physiological hydrodynamic shear stress, physiological liquid to cell ratios, and requires less media and cells.

One of the first developed liver microfluidic device was introduced by Lee et al. in 2007. They designed microfluidic devices that mimic the hepatic sinusoid. An endothelial cell-like barrier was incorporated to separate different cell types resulting in the preservation of hepatocyte viabilities and functionalities [99]. In terms of high throughput screening, Toh et al. [100] created a system with separate independent cell culture, so that different drugs concentrations can be simultaneously increased. The "3D HepaTox Chip," is designed to support parallel channels containing separate cell cultures, in order to test different level of drug concentration to each channel, in particular the hepatotoxicity testing was performed using five model drugs: acetaminophen (20mM), diclofenac (1000μM), quinidine (1000μM), rifampin (2000μM) and ketoconazole (420μM). Albumin production and various metabolic activities were measured to assess liver functionality. Results showed that this microfluidic model was equally capable of the functional maintenance of the hepatocytes as a multi-well plate model. Results showed that the cells were more sensitive to the drug-mediated hepatotoxicity than the multi-well plate cultures. The toxicity data also showed a positive correlation with comparable *in vivo* toxicity data. Nakao et al. [101] focused on functionality of liver cells by developing a microfluidic cell culture device that mimics the microscopic structure of the hepatic cords. Liver specific functions of freshly isolated primary hepatocytes decline rapidly due to the lost if their membrane polarity so a new technique for maintaining the cells was proposed, in which hepatic activity was prolonged by suctioning the cells into the cord-like compartment of the device, creating a "collagen sandwich culture". In this way the aligned hepatocytes were able to self-organize themselves and form bile canaliculi along the hepatic cord-like structure as shown by MRP2 and CD147 marker protein.

Lee et al [102] designed a microfluidic device that contained polyethyleneglycol (PEG) pillars within a weaving channel, with each pillar containing rat liver microsomes enclosed within a 3D hydrogel matrix (Figure 1.7). The concentrations of seven different substrates were used to test the P450 reaction in a microsome solution within a standard well plate system, ranging from 2μM to 80μM. Data was extrapolated and a mathematical model of the system based on Michaelis-Menten kinetics was produced, showing a high level of agreement between the two. The chip was then analyzed and a model was created.

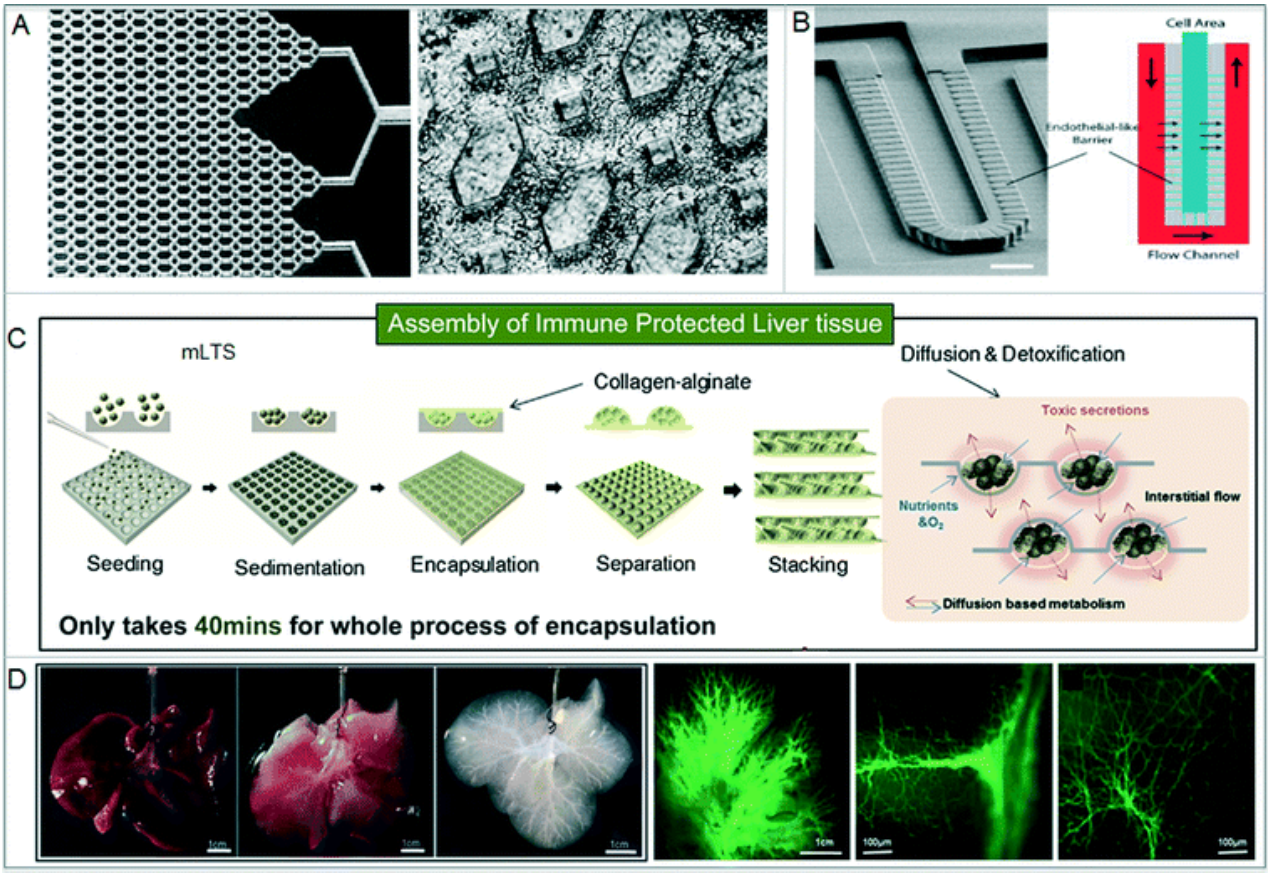

Figure 1.7: Engineering methods for the development of liver ultrastructures [103]: A) branched vascular channels developed by the silicon micromachining technique. B) An artificial liver sinusoid with an endothelial-like barrier using microfluidic devices [99]. C) Development of an in vivo-mimetic microliver tissue using concave microwells and the tri-culture method of three types of primary liver cells encapsulated in collagen–alginate composites. D) The decellularization method for obtaining an ultrastructure-embedded liver scaffold.

Chao et al.[104] published an evaluation of a novel microfluidic device, the HμREL® biochip. Four biochips are enclosed in a polycarbonate housing connected, by tubing lines, to a fluid reservoir and peristaltic pump. Each biochip has one or more separate compartments in which different cells can be housed. The compartments are microfluidically connected, in a linear path, to allow for interaction between the cell types. Evaluation of the system using primary human hepatocytes indicated the system preserved cell viability and metabolic competency at least as high as, and sometimes higher than, the traditional static culture conditions.

The use of a single cell culture has shown to bring to successful results, but at the same time using multiple cells in a liver-on-a-chip model, has the potential for even more realistic *in vitro* results, since liver has a complex structure composed of multiple cells in interaction with each other.

An example of co-culture on a chip was developed by Schütte et al. [105], where a co-culture of primary human hepatocytes and endothelial cells was used to recreate a 3D sinusoidal-like structure by dielectrophoresis (DEP).

Lee at al. [106] employed a spheroid-based microfluidic chip, for the development of the 3D *in vitro* model of ALD progression (Figure 1.8 B). They co-cultured rat primary hepatocytes and hepatic stellate cells (HSCs) in a fluidic chip to investigate the role of HSCs in the recovery of liver with ALD. An interstitial level of flow derived by an osmotic pump was applied to the chip to provide *in vivo* mimicking of fluid activity. Using this *in vitro* tool, it was observed structural changes and decreased hepatic functions with the increase in ethanol concentration. The recovery process of liver injured by alcohol was observed by providing fresh culture medium to the damaged 3D liver tissue for few days. A reversibly- and irreversibly-injured ALD model was established. Other example of co-culture on chip is represented by the fabrication of spheroids of HSCs and hepatocytes maintained in microfluidic systems, [107] exhibited improved albumin secretion and stained positive for CYP450 reductase, in contrast to their monocellular controls.

Also, to investigate and consider the mutual effects of various organs on their drug toxicity, co-cultured organ models on a chip have also been introduced.

Multi-organ device was created by Wagner et al. [108], which combined a microfluidic channels system with separated tissue compartments, liver microtissues (HepaRG and HHSteC) and skin biopsies. This system allowed the crosstalk between the different organs in order to assess the metabolic state of the cells during culture time. It also can facilitate the effective drug screening considering diverse pharmacodynamic parameters through organ–organ interaction.

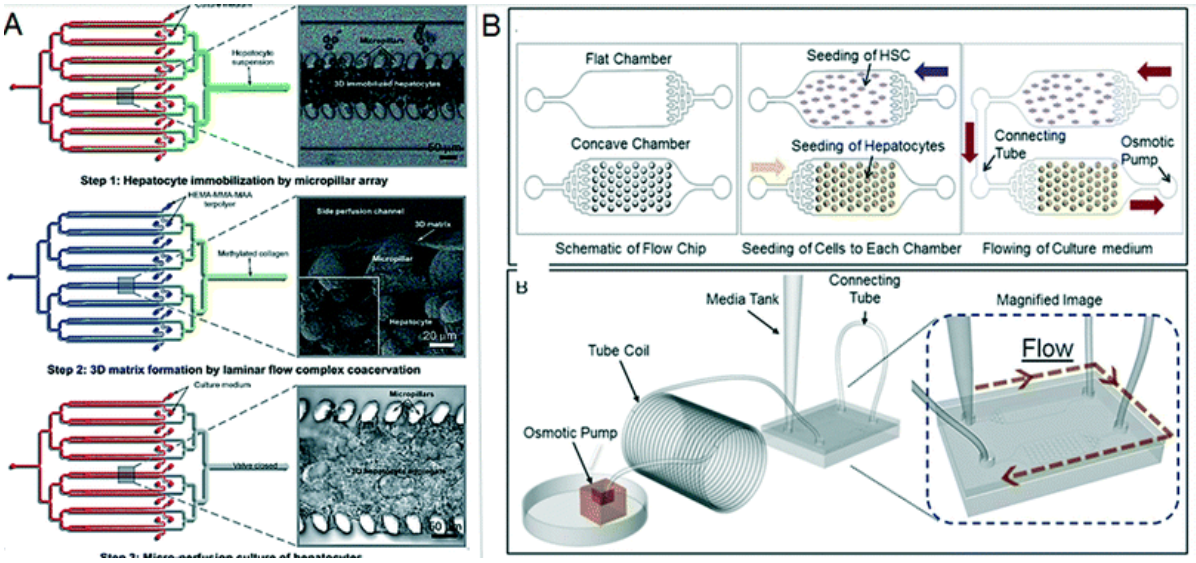

Figure 1.8: The application of microtechnology-based liver systems in drug screening and toxicity testing [103]: A) the 3D HepaTox Chip with microchannels in 2D and 3D co-culture systems for in vitro toxicity test. B) A 3D-based liver-on-a-chip system of hepatic microtissues and hepatic stellate cells with interstitial flow [107].

1.5 Gut-on chip

Microfluidic systems can be used to reproduce the dynamic microenvironment in the intestine which is characterized by peristaltic motions and intraluminal fluid flow. Recently, microporous SU-8 membranes were fabricated with 3D *villus*-like features, with the goal of incorporating a more relevant 3D intestinal microenvironment into the mCCA system [109] (Figure 1.9A).

Long-term perfusion culture of Caco-2 cells on track etched membranes was demonstrated in a microfluidic device with integrated micro-pumps and on-chip optical fibre sensors [110].

Kim et al reported a human gut-on-a-chip device that include peristalsis, fluid flow, and microbial flora [111] (Figure 1.9). Compared to static culture, cells cultured on the device exhibited accelerated intestinal epithelial cell differentiation, formation of *villi*-like structures and increased intestinal barrier functions. This finding challenged the traditional understanding that Caco-2 cells only differentiate into enterocyte cell types under normal culture conditions. Mucus production and CYP3A4 enzyme activity, which are usually missing in Caco-2 monolayers, were also detected under the dynamic culture condition without any drug inductions. However, the level of CYP3A4 activity was about three orders of magnitude lower than that reported for human small intestine. The aforementioned models are mostly characterized 2D culture over a porous membrane which can be organized in a 3D fashion. Integration of 3D tissues in a microfluidic device could be better reproduce the *in vivo* interaction with ECM under dynamic conditions.

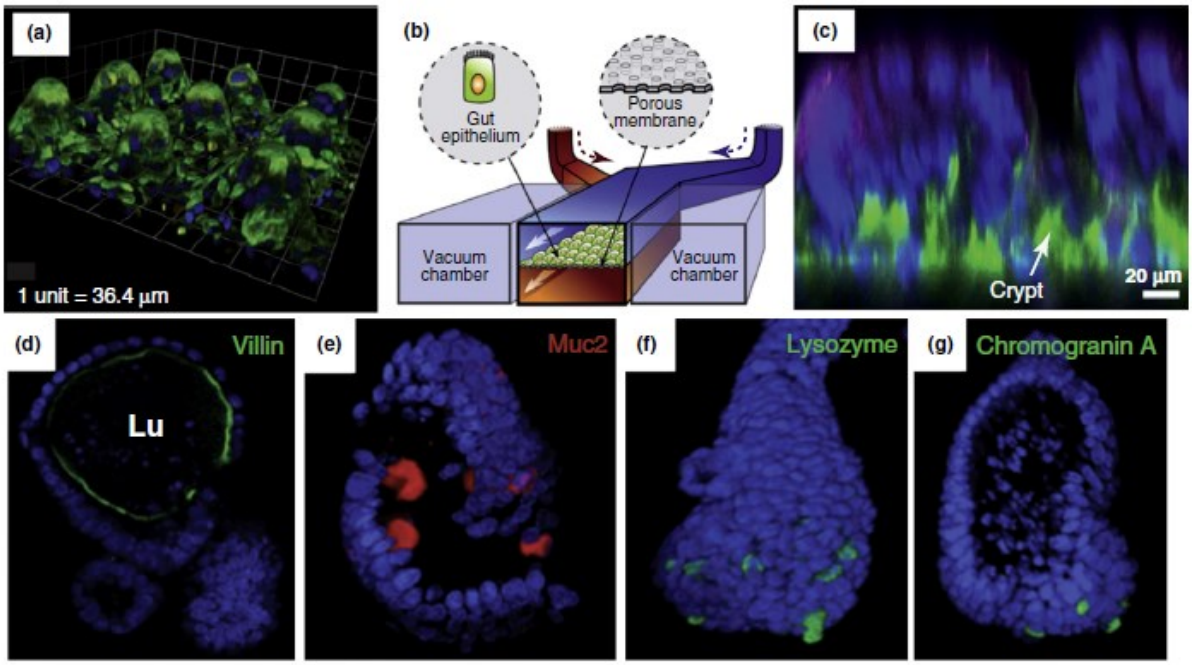

Figure 1.9: a) Caco-2 cells grown on microporous SU-8 membranes [109] Cells were stained for actin (green) and nucleic acid (blue). (b) A schematic of the gut-on-a-chip device [111]. (c) Vertical cross section of villous-like structures [60]. Cells were stained for actin (green), nucleic acid (blue) and Muc2 (magenta). (d–g) Single Lgr5+ stem-cell-derived organoids were stained for

*villi*n [(d): green, enterocytes), Muc2 (e): red, goblet cells], lysozyme (f): green, Paneth cells], chromogranin A [(g): green, enteroendocrine cells] and nucleic acid (blue) [112].

1.6 First-pass metabolism *in vitro* model

To predict the drug bioavailability and toxicity *in vivo* in an accurate and predictive manner, it is essential to model the enterohepatic circulation and first-pass metabolism. *In vitro* models of the liver and GI have been developed individually, but the single-organ systems lack the complex intercellular and inter-organ communication that occurs *in vivo* and therefore are unable to properly model first-pass metabolism and bile acid regulation that has been shown to be critical for assessing drug metabolism. In an attempt to recapitulate the integration of the GI tract and the liver, several *in vitro* models have been established. About static integrated model, Choi et al. first [113] developed a static integrated Caco-2/HepG2 system to study toxicity. In this model a transwell insert was used to seed Caco-2 on the apical side and HepG2 on the basal side of the polycarbonate membrane, in order to mimic the sequence of oral absorption and metabolism of xenobiotics *in vivo*. This type of co-culture enhance the CYP1A2 activity and increase sensitivity when a drug was used to treat the system. Similar models have been used to investigate first-pass metabolism, bioavailability, and toxicity of pharmaceuticals undergoing clinical trials.

1.7 Microfluidic model of first-pass metabolism

First-pass elimination takes place when a drug is metabolized between its site of administration and the site of sampling for measurement of drug concentration. Clinically, first-pass metabolism is important when the fraction of the dose administered that escapes metabolism is small and variable. In an attempt to model the dynamic nature of first-pass metabolism, several models have been developed incorporating intestinal and hepatic models in fluidic systems to monitor drug transport, metabolism and toxicity. In a microfluidic model in which fluid flow is present, metabolites are transported from the GI-tract cells to the liver cells located downstream. Mahler et al. developed a microfluidic biochip in which HT-29 goblet-like cells are included in the GI-tract compartment so that the Caco-2 cell layer was covered with mucous. The model responded to a challenge involving acetaminophen with liver cell toxicity in a dose-dependent manner, and acetaminophen metabolites were detected in the medium. Acetaminophen is a widely used analgesic and antipyretic drug that can cause hepatotoxicity when taken at an overdose. It is a small, non-ionized molecule that passively diffuses across the GI-tract epithelium. The presence

of the GI-tract barrier in the micro cell culture model reduced liver cell death because acetaminophen diffused slowly across the mucous-covered Caco-2/HT-29 cell layer, and, in addition, intestinal cells also converted some of the drug into nontoxic metabolites [114]. The result obtained with the first-pass metabolism model was consistent with those obtained with acetaminophen challenges in mice [115]. Prot et al. developed instead a polycarbonate bioreactor where the Caco-2 cells were cultivated on a conventional cell culture insert. The insert was then incorporated into a dedicated fluidic platform that could be coupled with a microfluidic biochip which is cultivated with HepG2/C3a, freshly isolated rat primary hepatocytes and human cryopreserved hepatocytes, for comparative purposes. First-pass intestinal absorption and liver metabolism were studied using phenacetin. In addition, a mathematical model was built based on the experimental data. The corresponding PK model was used to estimate the kinetic parameters describing the transfer of the molecule across the intestinal barrier, as well as intestinal and hepatic clearances. Finally organ mathematical models were used to predict situations in humans [116]. Midwoud et al. designed a microfluidic system for the purpose of investigating inter-organ effects, made by coupling two microchambers, one containing an intestinal tissue slice, the other a liver slice, which can be sequentially perfused. In this way, metabolites formed by the intestine in the first chamber can be directed to the liver in the second chamber for further metabolism, thereby mimicking *in vivo*, first-pass metabolism. In addition, the possible influence of metabolites or other mediators formed by the intestine on the liver can be studied, providing insight into interorgan effects [117].

Chapter 2

A novel three dimensional hepatic model on chip: functionality study and xenobiotic toxicity assessment

2.1 Introduction

During the last 20 years, progress in pharmaceutical industry has revolutionized the field of drug discovery, producing an elevated number of new compounds. *In vivo* animal tests provide complete data sets on the absorption, distribution, metabolism, and excretion (ADME) parameters for a given molecule. Nevertheless, *in vivo* studies performed with laboratory animals do not predict human responses exactly. They are also expensive, time-consuming, and can be considered as unethical. On the other hand, *in vitro* experiments cannot easily reproduce the organ to organ interactions and thus poorly mimic the ADME process. For these reasons, the actual drug development process is affected by a high rate of failure during clinical trials, which is due to the lack of an appropriate *in vivo* and *in vitro* model to predict the effect of a drug. There is the need to develop more predictive platforms that can better reproduce the human *in vivo* environment and can complement the existing models. Liver plays a fundamental role in drug metabolism and body detoxification from xenobiotics compounds. Xenobiotics induced hepatotoxicity is one of the main reasons for drug withdrawal thus imply the need of the development of robust *in vitro* model for evaluate hepatotoxicity. Conventional hepatic model are based on 2D mono- and co-cultures of primary hepatocytes. These model cannot reproduce the complex 3D microenvironment and extracellular matrix support. For these reason, primary hepatocytes shows rapid loss of their phenotype, resulting in downregulation of their metabolic biomarker. To overcome this limitations, efforts are focused on the developing of new 3D models that can mimic the cell-cell and cell-ECM interactions. Among various 3D liver culture models, hepatic spheroids which formed by aggregation of cells, have been the focus of a number of studies. However, spheroids involve in the formation of a necrotic core as spheroids size increase limiting their use for long-term culture [118]. Recently, Matsunaga et al. seeded HepG2 cells onto collagen gel microbeads, assembled them in a construct with a doll-like shape, which however was only several millimeters in size. Moreover, these authors illustrated the co-culture of HepG2 cells with NIH 3T3 cells in

this system, conferring the possibility of engineering complex tissues [119]. Other important studies based on cell and microcarrier approach was develop by Brancato et al. where it was carry out a comparison between two different kind of 3D cancer model, spheroids and microtissues, in order to evaluate the best micromodules type that reproduce tumor microenvironment [120]. However, since the *in vivo* microenvironment is dynamic, it is fundamental for drug toxicity studies to use dynamic models, which provide appropriate mass-transport for gas and metabolite waste. With the rapid advancements in microfabrication technologies it have been possible to create new platforms that mimic the *in vivo* dynamic conditions. For this purpose, Ho et al. developed a microfluidic device seeded with a co-culture of hepatocytes and endothelial cells to recreate the *in vivo* physiology of liver lobule [121]. Giobbe et al. have derived functional tissue-specific cells via hPSC differentiation directly on a chip through a robust multistage microfluidic technology, and demonstrate the derivation of functional hepatocyte-like cells that may prove suitable for high-throughput drug testing [122]. However, hepatic models based on 2D mono- or co-culture of human cells are not suitable to reproduce the 3D architecture and extracellular matrix, leading to a poor predictive platform for drug screening process. For this purpose, the combination of 3D tissue model and microfluidic systems can improve the tissue specific functions mimicking the *in vivo* environment with blood flow suppling oxygen and nutrients. One example of this approach is represented by the microfluidic culture of liver tissue slice developed by van Midwoud et al. [123]. Using tissue slice may represents a valid 3D model but it is difficult to obtain healthy hepatic biopsies not to mention that they lost viability in few days *in vitro* and are not suitable for high-throughput studies. For this purpose, in our recent studies we design a perfusion bioreactor for on-line investigation of ECM remodeling. Coupling engineered 3D dermal engineered tissue in a microfluidic it have been possible to evaluate the cellular and extracellular behavior [124]. The same approach, a microfluidic platform was presented to study the interactions between normal and cancer cells [125].

In this study we describe the design and fabrication of a 3D liver-on-chip system that enables cell culture under continuous fluid flow and mimic the liver sinusoid. *In vivo*, the hepatic sinusoid is a microfluidic system that carries blood from the hepatic artery and portal vein, exposing the liver to oxygen and nutrients; this blood supply can also expose the liver to toxins and infectious agents. To achieve this, we first compare two different 3D hepatic tissue, HepG2- μTPs and HepG2-spheroids in terms of morphology and functionality and then develop a microfluidic device that could resemble the hepatic sinusoid. With the aim to produce a model for predictive drug toxicity comparable with *in vivo* conditions, three-dimensional liver HepG2- μTPs were selected to be cultured into the biochip with different ethanol concentration to tests alcoholic effects. Viability

assessment through cell auto-fluorescence coupled with two-photon microscopy allows on-line monitoring of ethanol toxicity without using dyes in a non-invasive manner.

2.2 Materials and Methods

2.2.1 Cell type

HepG2 were provided by American Type Culture Collection (ATCC). Cells were sub-cultured onto 150 mm Petri dishes in Minimum Essential Medium Earle's Salt (Microtech) containing 10% fetal bovine serum, 100 μg mL^{-1} L-glutamine, 100 U mL−1 penicillin/streptomycin, 0.1 mM Non Essential Amino Acid and 0.1 mM Sodium pyruvate. Cells were maintained at 37 °C in a humidified atmosphere containing 5% CO2.

2.2.2 Microscaffold production

Gelatin porous microbeads (GPMs) have been prepared according to a modified double emulsion protocol (O/W/O). Gelatin (type B, Sigma Aldrich Chemical Company, Bloom 225, Mw = l76 654 Dalton) was dissolved into 10 ml of water containing TWEEN 85 (6% w/v) (Sigma Aldrich Chemical Company). Toluene containing SPAN 85 (3% w/v) (Sigma Aldrich Chemical Company) was continuously added to the aqueous gelatin solution (8% w/v) to obtain primary oil in water emulsion. Gelatin's beads containing droplets of toluene were made through the addition of excess toluene in order to have a double emulsion (O/W/O). The resulting microspheres were dried at room temperature and selected in the range of 75–150 μm in diameter by using commercial sieves (Sieves IG/3-EXP, Retsch). GPMs have been stabilized by crosslink reaction with glyceraldehydes (GAL), in order to make them stable in aqueous environment at 37 °C, as previously described. GAL at 4% w/w of the microbeads has been used to perform all the experiments. Before their use, dry GPM were sterilized with ethanol 100% for 24h then washed three times in PBS. Before cell seeding PBS was removed and replaced with culture medium [126].

2.2.3 HepG2-Microtissues production

All cell cultures on microscaffolds were performed in spinner flask (Integra). Briefly, 35 mg of GPMs were loaded with $5{,}25 \times 10^6$cells (30 cell/GMP ratio). To promote cell seeding on GMPs an intermittent stirring regime (30 min at 0 rpm, 5 min at 30 rpm) for 24 h. After seeding, the stirring speed was kept at a continuous 30 rpm for up to 14 days. Culture medium were changed every two days. All cultures were maintained at 37 °C in a humidified 5% CO_2 incubator. The

HepG2 microtissues precursors obtained (HepG2-µTPs) samples were taken for further investigations at days 3, 5, 7, 10 and 14 and fixed for further investigations.

2.2.4 HepG2-Spheroid formation

Cells grown as a monolayer were trypsinized to generate a single-cell suspension. The cell suspension was diluted to $1{,}5 \times 10^4$ cells per milliliter in EMEM supplemented with 20% of 0.24% methyl cellulose and seeded onto round bottom non-tissue culture treated 96 well-plates (Falcon, BD NJ,USA) in order to have 3000 cells/well. For preparation of methylcellulose stock solution 3 g of methylcellulose powder (M0512, Sigma-Aldrich) was autoclaved in a 250 ml bottle containing a magnetic stirrer. The autoclaved methylcellulose was dissolved in preheated 125 ml EMEM at 60 °C for 20 min by using the magnetic stirrer. Thereafter, 125 ml medium (RT) containing double amount of FBS (20%) was added to a final volume of 250 ml and the whole solution mixed overnight at 4 °C. The final stock solution was aliquoted and cleared by centrifugation (5000 g, 2 h, RT). Only the clear highly viscous supernatant was used for the spheroid assay (about 90 - 95% of the stock solution). Spheroids were grown under standard culture conditions (5% CO_2 at 37 °C) and fixed at days 3, 5, 7, 10 and 14 for further investigations.

2.2.5 Cell viability

At the day 3, 5, 7,10 and 14 of culture, 200 µL aliquots were collected from the spinner flask to assess the viability of the µTPs. Then aliquots were transferred to a cell culture dish (w/2 mm grid Nunc) for microcarriers counting, then the microcarriers suspension was placed in a new 2 ml tube and washed twice with PBS. To detach cells from microcarriers, µTPs were incubated with trypsin for 5 min. The detached cells were stained with Trypan Blue to assess viability of the cells over the microbeads. For Trypan blue staining, 200 µL of cells suspension was transferred to a 1,5-mL clear Eppendorf tube and incubated for 3 min at RT with 300 µL of PBS and 500 µL of 0,4% Trypan Blue solution (Sigma-Aldrich). Cells were counted using dual chamber hemocytometer and a light microscope. Viable and non-viable cells were recorded separately, and the means of three independent cells counts were pooled to obtain a percentage of viability. In the same way, a 96-well plate of HepG2-spheroids were trypsin digested for each time point in order to evaluate cell viability.

2.2.6 Histological and immunohistochemical analysis

1 mL aliquots of HepG2-μTPs or HepG2-spheroids at day 3, 5, 7,10 and 14 were fixed in a solution of 10% neutral buffered formalin for 1 h, rinsed in PBS, dehydrated in an incremental series of alcohol (75%,85%, 95% and 100% twice, each step 30 min at RT), then treated with xylene (30 min twice) and embedded in paraffin. Tissue sections, 5 μm thick, were stained with hematoxylin and eosin (H&E), mounted with Histomount mounting solution (Bioptica) on coverslips and the morphological features of 3D tissues were observed with a light microscope. For immunohistochemical staining (IHC) of anti-human Caspase-3, A mouse and rabbit specific HRP/DAB (ABC) detection kit (Abcam, UK) was used according to the manufacturer's protocol.

2.2.7 Diameter evaluation of micromodules

To evaluate the diameter variation of HepG2-μTPs or HepG2-spheroids, 1 mL aliquots were collected at different time point (3, 5, 7,10 and 14 days) and placed under microscope (Olympus CK X41) in order to obtain at least 100 images of spheroids and μTPs for each time point. The acquired images were processed using Image J software. After binary transformation and thresholding of the initial images, the areas distribution of both HepG2-μTPs and HepG2-spheroids was evaluated by using the tool "Analyze Particles". From the areas distribution, we estimate the diameter for all samples at each time point. Values were reported as mean ± standard deviation.

2.2.8 Immunofluorescence analysis

For immunofluorescence staining of HepG2-μTPs or HepG2-spheroids, deparaffinized and reyhdrated 5 μm thick tissue sections were heat-induced epitope retrieval in sodium citrate buffer at pH 6.0 for 5 min at 97 °C followed by 10 min at 70 °C in uncloaking chamber, washed with PBS containing 0.2% Triton X-100, blocked with 6% BSA, 5% FBS solution for 1h at RT, and incubated with rabbit anti-human P-gp (dilution 1/100) (Abcam UK) overnight at 4 °C. Then, secondary antibody incubation (Alexa Fluor 488) was performed, cell nuclei were detected by DAPI staining (5 μm/mL, Sigma Aldrich).

2.2.9 Albumin and Urea measurement

At each time point (3, 5, 7, 10 and 14 days) HepG2-μTPs or HepG2-spheroids' supernatants were collected from the spinner flask and from 96 well-plates respectively, in order to measure albumin and urea released by HepG2 cells. Once collected, the supernatants were centrifuged at 2000 g for

10 min in order to remove the cell debris. The supernatants were stored at -20 °C before being analysed. Albumin secretion in cell culture supernatants quantified by a sandwich enzyme-linked immunosorbent assay (ELISA) kit (Abcam ab179887) according to the manufacturer's protocol. Briefly, albumin specific antibody has been pre-coated onto 96-well plates and blocked. 50 µL of samples were added to the wells and subsequently albumin specific biotinylated detection antibody was added and then followed by washing with wash buffer. Streptavidin Peroxidase Complex was added and unbound conjugates were washed away with wash buffer. TMB was then used to visualize Streptavidin Peroxidase enzymatic reaction. TMB was catalysed by Streptavidin Peroxidase to produce a blue colour product that changes into yellow after adding acidic stop solution. Then the absorbance of individual well was measured at 450 nm by a microplate reader (Enspire Multimode Plate Reader PerkinElmer). All experiments were done in triplicates. The density of yellow colouration was directly proportional to the amount of albumin captured in plate. Urea levels of cell supernatants were determined by Quanti Chrom TM Urea Assay Kit (DIUR-500) according to the manufacturer's instruction. Briefly, 50 µL of samples are added to the wells and then 200 µL of working reagent, incubate for 50 min. The intensity of the colour, measured at 430nm using a microplate reader, was directly proportional to the urea concentration in the sample. The concentration of these biomarker was used to calculate the secretion rates (pg/h) of the four biomarkers during the 24 h period normalized for viable cells.

2.2.10 Microdevice fabrication

The microfluidic Liver-on-chip device used in this work, was fabricated by a rapid prototyping procedure. The microfluidic device was prepared by demolding polydimethylsiloxane (PDMS) (Sylgard 184, Mascherpa), from a Poly(methyl methacrylate) (PMMA, Goodfellow) slab. The PMMA master mold was designed by AutoCAD and carved with micromilling machine (Minithech CNC Mini-Mill) making a relief positive geometry in order to avoid silanization process of PDMS. The central microchannel (0.5 mm wide, 0.3 mm high) was separated from three parallels tissue chamber (0.5 mm wide, 0.3 mm high, 1 mm long) by small pillars (0.100 mm diameter, 0.09 mm pillar interspace). The ratio of PDMS pre-polymer and curing agent was 10:1 (w/w), then the mixture was degassed under vacuum for 20 min to remove air bubbles and then poured on PMMA masters. The set-up was incubated at 80 °C for 60 min, then peeled off from master moulds. Inlet and outlet holes were punched with a 2.5 mm biopsy punch (DifaCooper). The device was bonded to a glass coverslips (24 mm wide × 60 mm long) by oxygen plasma treatment for 1 min at 50 W in an oxygen plasma oven (Plasma Femto, Diener). Subsequently, the whole setup was incubated at 80 ºC overnight to achieve irreversible bonding of the PDMS

and the glass. Before tissue culture, liver-on-chip microdevice, tubes and connectors were sterilized by autoclaving. Tygon tubes were inserted into the inlets and outlets of the central channel using male luer lock connectors (Harvard Apparatus), then, the microtissues were placed into the liver chambers by pipetting. Furthermore, the whole setup was connected to syringe pump (Harvard Apparatus) in order to obtain a flow rate of 5 $\mu l\, min^{-1}$. Finally, the liver-on-chip microdevice was placed at 37 ºC in a humidified incubator under 5% CO_2 in air.

2.2.11 Perfusion culture and ethanol injury

The HepG2-µTPs were collected from the spinner flask, in a time range from day 5 to day 7, and were inoculated into the three chambers of the liver-on-chip device through the inlet µTPs by pipetting. During the filling steps, all the inlet and outlet channels were left open to allow fluid escape. For the creation of the ethanol injury, medium containing different concentrations of ethanol was applied to HepG2-µTPs and they were cultured for 2 and 4 days. In each experiment three different devices were perfused, one for the control group and two with different ethanol concentrations, 100mM and 300mM. The culture media supernatants from each devices were collected for the evaluation of albumin, urea and LDH release at each time point. Culture media supernatants accumulated in the reservoir was collected and stored at -20 °C before being analyzed. Then albumin and urea measurement were performed as reported in Par. 2.2.9. LDH activity was performed, using Lactate Dehydrogenase Activity Assay Kit (Sigma Aldrich) according to the manufacturer's protocol. Briefly, 50 µL of sample or NADH standard were added to a well of a 96-well microtiter. Then reaction mix was added to each well and after 2-5 min the absorbance at 450 nm was measured using a microplate reader, in this way a $T_{initial}$ was fixed. Subsequent measurement were lead every 5 min until the value of the most active sample is greater than the value of the highest standard, the time of the penultimate reading is T_{final}. The LDH activity was evaluated by the following equation:

$$LDH = \frac{B \times Sample\ diluition\ factor}{Reaction\ time\ \times V}$$

Where B is the amount (nmole) of NADH generated between $T_{initial}$ and T_{final}, reaction time is the difference between T_{final} and $T_{initial}$, and V is the sample volume.

2.2.12 On line cell viability: Cell auto-fluorescence

Live and dead cells emission spectra were obtained by the following procedure [127]. Firstly we used 2D cells culture as a proof of the technique. To prepare live cells, HepG2 were seeded onto a Fluorodish and placed in a at 37 ºC in a humidified incubator under 5% CO_2 in air. To prepare

dead cells, HepG2 were detached using trypsin and suspended in PBS then 1 mL of HCl 1N was added to 9 mL of cell suspension for 10 min at RT. Then by mixing known amounts of living cells, we obtained different fraction of living cells (α): 100%, 75%, 50%, 25% and 0%. Cells and HepG2-µTPs images were acquired on a Leica TCS SP5 coupled with a Multiphoton Microscope stage (Chamaleon Compact OPO-Vis Coherent) with a 25X/1.25 NA objective. The excitation light source was tuned to an excitation wavelength λ_{ex} = 730 nm. Spectral images were obtained by separation of the emitted auto-fluorescence into 19 wavelength bands from 400 to 608 nm with a step of 10 nm. Then, by using microscope internal software, characteristic emission spectra of 100% and 0% live cells were generated from spectral images. In order to evaluate the cell viability of the HepG2-µTPs into the liver-on-chip device, two-photon images of the biochips were acquired by placing the device chamber on the multiphoton stage. HepG2-µTPs viability was measured for control and treated samples at days 2 and 4. In order to exclude the signal rising from the microbeads, specific ROI were chosen to obtain emission spectra on the spectral images. Analysis were performed on 100 images, and the resultant spectra were normalized to the highest intensity value. Emission spectra data was post-processed to obtain means and standard deviation of the collected spectral curves, in particular the emission spectra corresponding to 100% and 0% live cells, were fitted with a 3th order polynomial function (P) bringing to P_{100} e P_0. To get viability information from liver-on-chip devices (control and treated groups), the polynomial (Px) corresponding to an emission spectra from an unknown cell fraction (α_x), was considered as a linear function of P_{100} and P_0 as reported in Eq 1.

$$P_x = \alpha_x P_{100} + (1 - \alpha_x) P_0 \quad (1)$$

Where P_x is the polynomial function of the unknown cell fraction spectrum, P_{100} and P_0 are the polynomial functions of the spectra of known cell fractions α = 100% and at α = 0, α_x is the unknown cell fraction. This operation was performed by means of a custom-written MATLAB. In order to validate the effectiveness of this procedure, we inserted in the equation 1 the spectra obtained by known cell fraction, 25%, 50% and 75%.

2.2.13 Analysis of oxidative stress

Oxidative stress was measured by assessing intracellular ROS levels generated after exposure for 2 days and 4 days with ethanol, through the green-fluorescent ROS detection reagent 6-carboxy-2′,7′-dichlorodihydrofluorescein diacetate, di(acetoxymethyl ester) (carboxy-H2DCFDA, Thermo Fisher Scientific), according to the manufacturer's instructions. Briefly, liver-on-chip devices were rinsed in PBS and loaded with 10 µM of the cell-permeant probe carboxy-H2DCFDA for 30 min at 37°C in PBS solution to exclude hydrogen peroxide generation in phenol red containing

medium, before fluorescence analysis. Incubation with 400 μM H_2O_2 (Sigma-Aldrich) was used as a positive control for ROS. FITC images were acquired on a Leica TCS SP5 coupled with a Multiphoton Microscope stage (Chamaleon Compact OPO-Vis Coherent) with a 25X/1.25 NA objective.

2.2.14 Statistical analysis

Data are expressed, as mean ± standard deviation and show the results from three independent experiments. The differences between two or more groups were evaluated (p value < 0.05) using one-way analysis of variance (ANOVA). A Gaussian distribution for each population was assumed. For pair-wise comparisons within each experimental group, Tukey's post-test was used.

2.3 Results

2.3.1 Time evolution of viability and morphology of μTPs and spheroid model

Two types of 3D tissue models were fabricated and compared, HepG2-μTPs and HepG2-spheroids. Viability of both samples was evaluated by Trypan Blue assay during 14 days of culture. In Figure 2.1 was reported the cell viability for HepG2-μTPs and HepG2-spheroids at day 3, 5, 7, 10 and 14. The HepG2-μTPs exhibited a cell viability maintained between 95% and 85% till day 10, with a little decrease to 73% ± 7.085% at day 14. As reported in the graph (Figure 2.1), from day 5 μTPs shows higher viability then spheroids for all the time of the culture. In particular at day 7 the viability of the HepG2-spheroid (70% ± 15,631%) corresponded to the viability of HepG2-μTPs at day 14, indicating a rapid decrease of HepG2-spheroids viability already at day 7.

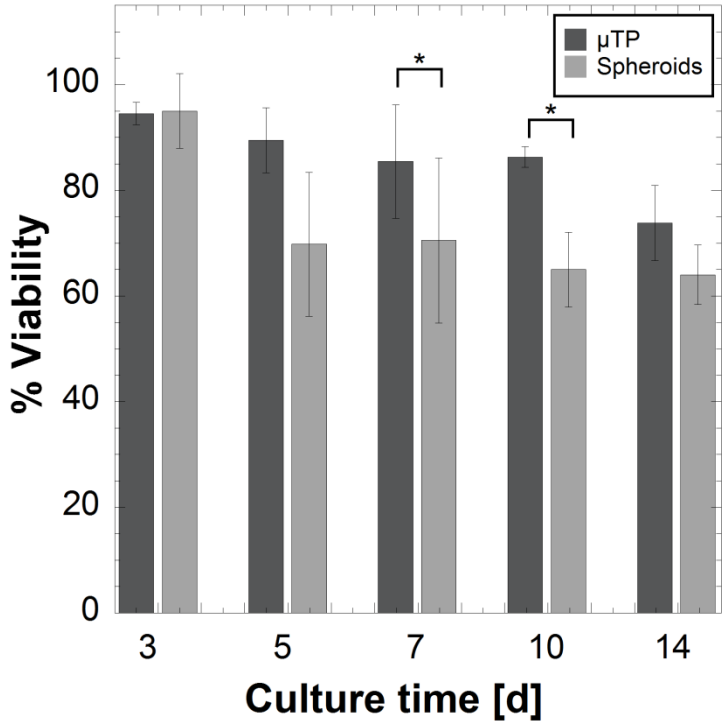

Figure 2.1: Cell viability assessment of µTPs and spheroids at day 3, 5, 7, 10, 14. Asterisks indicates statistical difference $p < 0.05$

The bright field images of the HepG2-µTPs (Figure 2.2 A-E) highlighted that during the spinner culture time, the HepG2-µTPs from day 5 increased their size starting to aggregate in more large constructs. Instead, the HepG2-spheroids started already from a larger size, then they exhibited only a little increment of their size (Figure 2.2 F-J).

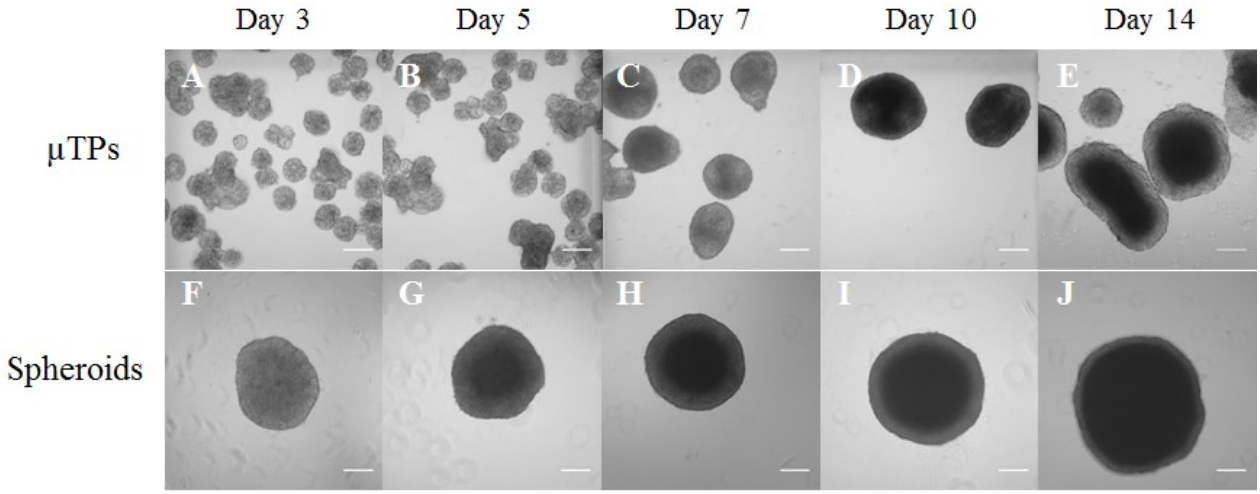

Figure 2.2: Bright field images of HepG2 µTPs (A-E) and HepG2 spheroids (F-J) at day 3, 5, 7, 10 and 14. Scale bar is 200 µm

In Figure 2.3 was reported the diameter variation during culture time for both HepG2-µTPs (A) and HepG2-spheroids (B) models. Starting from day 3, the diameter variation was evaluated by Image J software using "Analyze Particles" tool. As reported in the graph (Figure 2.3), the µTPs

showed a progressive increasing of the diameter corresponding to the fusion capability of the micromodules, the spheroids'size instead was almost the same during all culture time. To evaluate the morphological features of the HepG2-µTPs and HepG2-spheroids, histological analysis were performed. The HepG2-µTPs and HepG2-spheroids were stained with Hematoxylin and Eosin at day 3, 5, 7, 10, 14, as shown in Figure 2.4 . The H&E staining of HepG2-µTPs showed the cells distribution over the microbeads surface (Figure 2.4 A-E) demonstrating typical liver histotypic features such as a cuboidal hepatocyte cell shape with tight cell-cell contacts. These features were preserved over the tested culture period. For the HepG2-spheroid model, the latter features were also expressed but there was the presence of a necrotic core started from day 7 (Figure 2.4 F-J) which suggests that the quantity of oxygen and other nutrients transported into the inner regions of the spheroids, was not sufficient. This was confirmed by immunohistochemistry of Caspase-3 (Figure 2.5) of HepG2-µTPs (Figure 2.5 A-C) and HepG2-spheroids (Figure 2.5 D-F). The images shows that spheroids are in apoptotic phase since only low signal is present in µTPs.

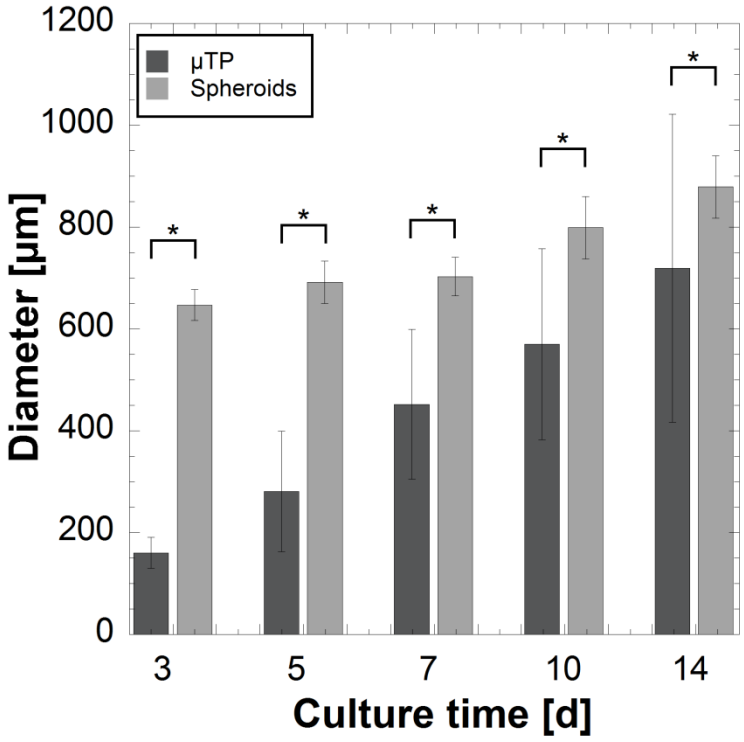

Figure 2.3: Diameter variation of HepG2-µTPs and HepG2-spheroids during culture time. Asterisks indicate statistical difference with $p<0.05$

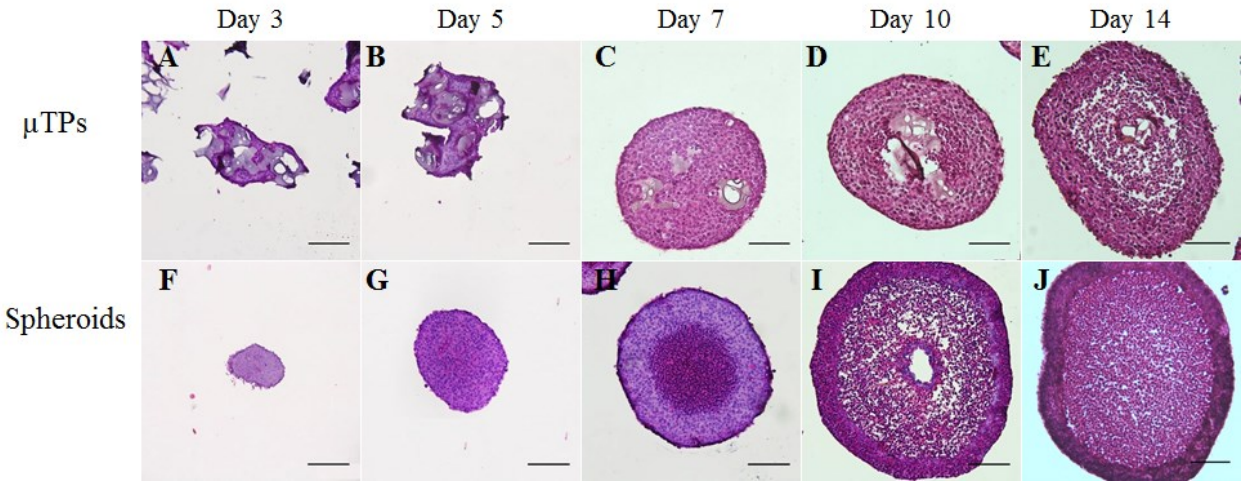

Figure 2.4: Hematoxylin and eosin images of HepG2-µTPs(A-E) and HepG2-spheroids (F-J) at Day 3,5,7,10 and 14. Scale bar 100 µm.

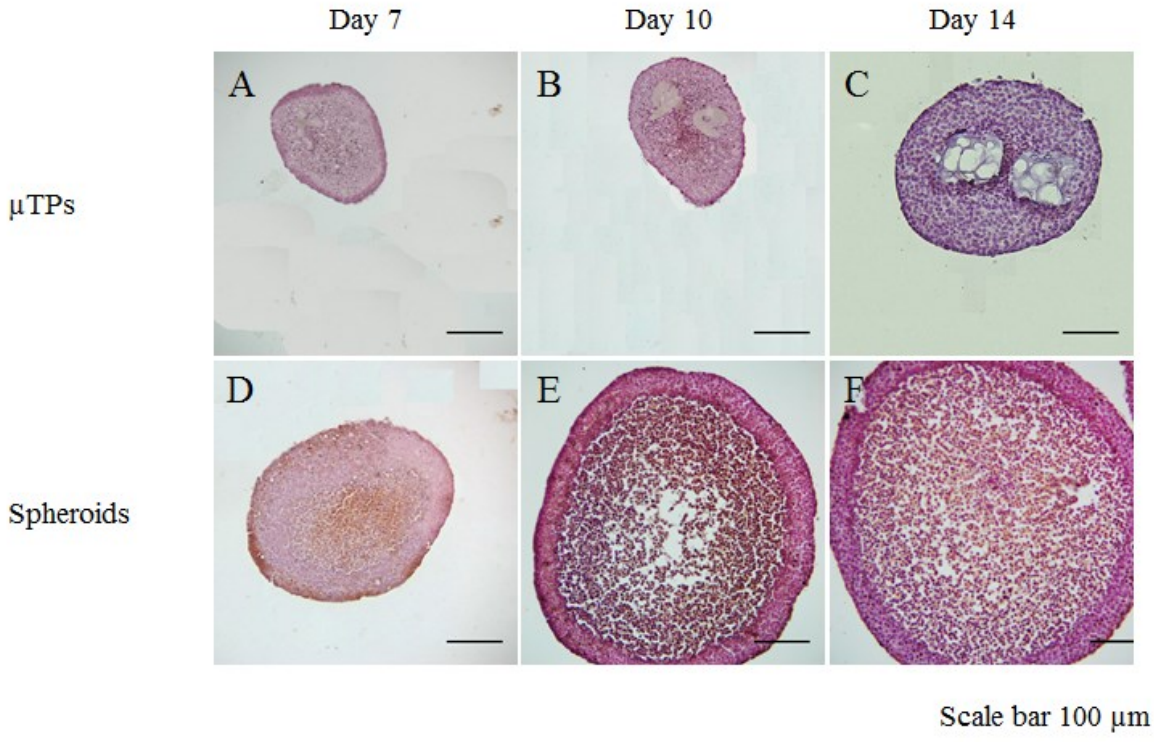

Figure 2.5: Immunohistochemical analysis of Caspase 3 for HepG2-µTPs(A-C) and HepG2-spheroids (D-F) at Day 3,5,7,10 and 14. Scale bar 100 µm.

2.3.2 Functional assessment of HepG2-µTPs and HepG2-spheroids

The functions of HepG2-µTPs and HepG2-spheroids were evaluated by measuring albumin and urea synthesis which are typical functions of liver cells, at different time point: day 3, 5, 7, 10, 14.

By collecting HepG2-µTPs or HepG2-spheroids supernatants, albumin and urea production were quantified by ELISA and colorimetric assay respectively.

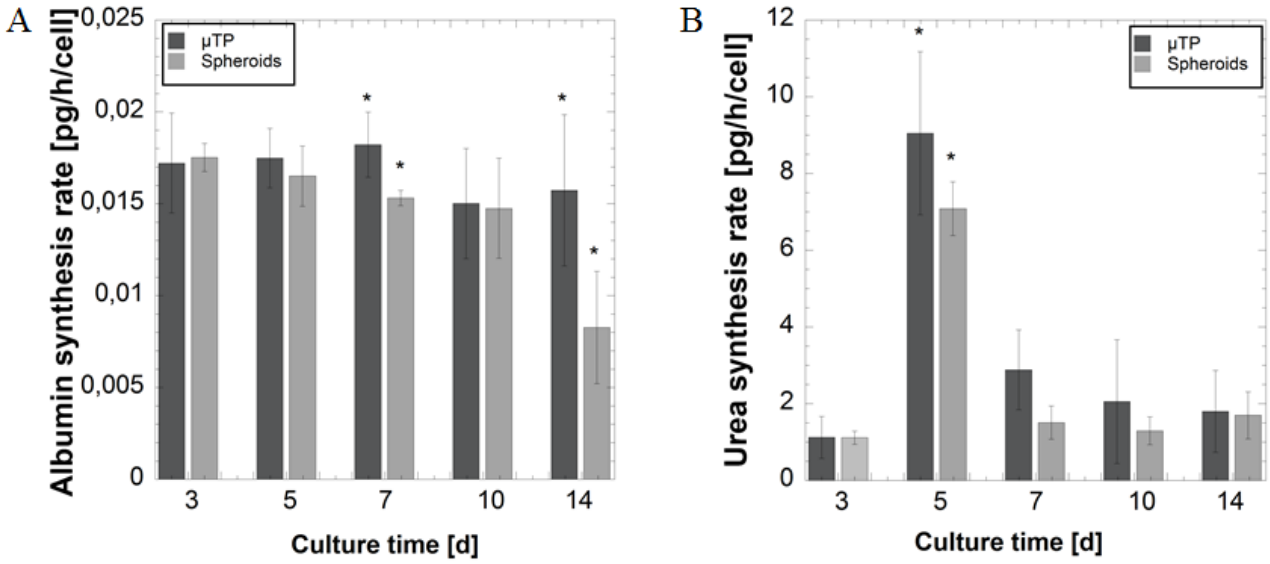

Figure 2.6: Albumin (A) and Urea production rate (B) of µTPs and spheroids during 14 days of culture. Asterisks indicate statistical difference with $p<0.05$

As shown in Figure 2.6 the spinner culture was able to sustain the biomarkers production during culture time better than static spheroid culture. The albumin production (Figure 2.6-A) was 0.0175 ± 0.0027 pg/h/cell at day 3, at day 7 it reached the maximum value of 0.0182 ± 0.0017 pg/h/cell and decrease to 0.0157 ± 0.004 pg/h/cell. For the HepG2-spheroids, albumin production had the same trend but with lower values (Figure 2.6-B).

To assess cell polarization of both 3D model P-gp were analysed via immunofluorescence. The P-gp expression in HepG2-µTPs (Figure 2.7) and HepG2- spheroids (Figure 2.8) detected over 14 days of culture. In Figure 2.7 A-C the immunofluorescence staining shows that the P-gp expression was higher in HepG2-µTPs than in spheroids (Figure 2.8 A-C) where only few pixel were detected. In Figure 2.9 was shown a three dimensional reconstruction of immunofluorescence staining of P-gp in both HepG2-µTPs and HepG2-spheroids. In this images an higher expression of the protein is visible in the microtissues models.

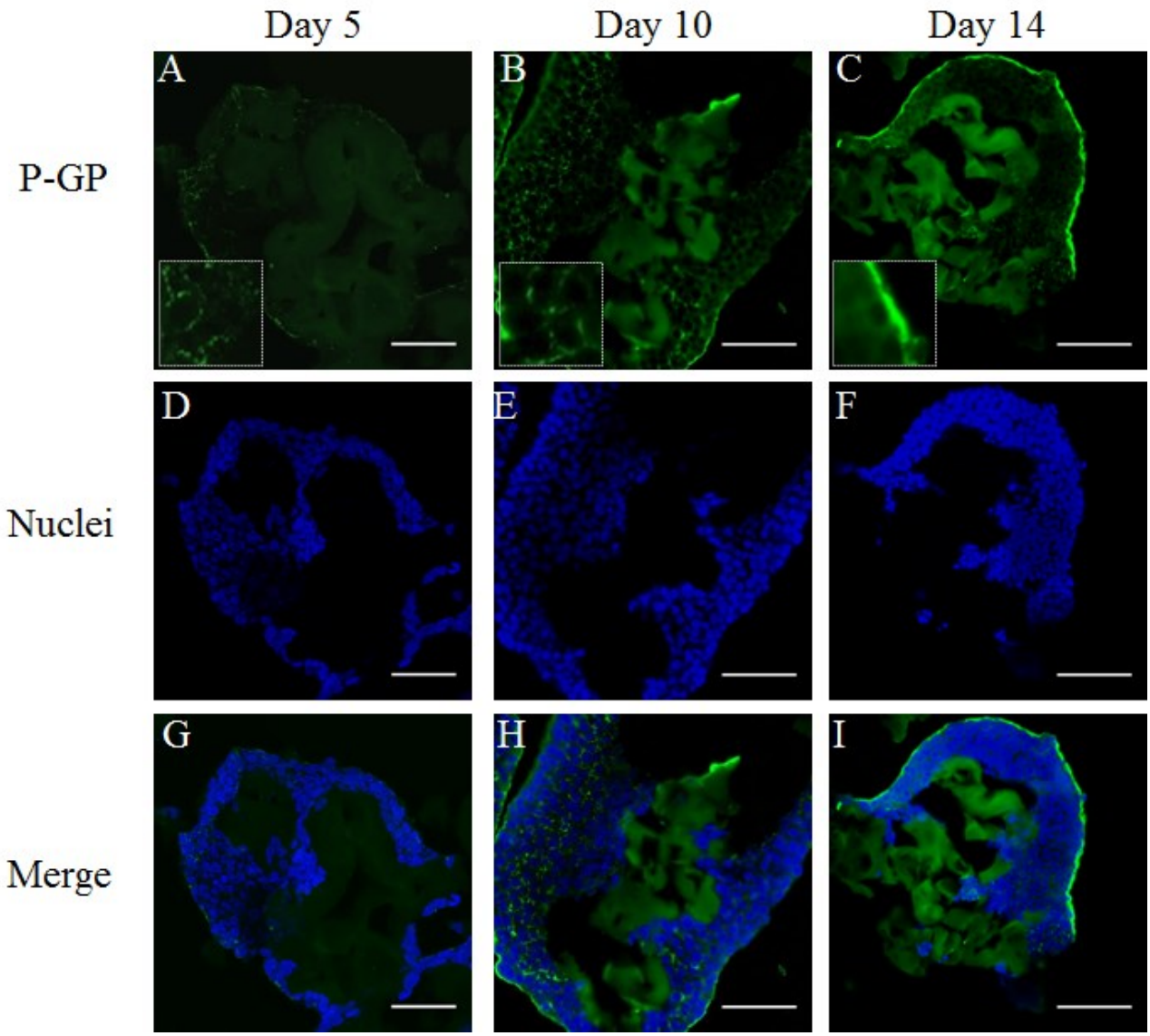

Figure 2.7: Immunofluorescence staining of P-Glycoprotein (green) and nuclei (DAPI, blue) in µTPs at day 5, day 10 and day 14. Scale bar 100 µm.

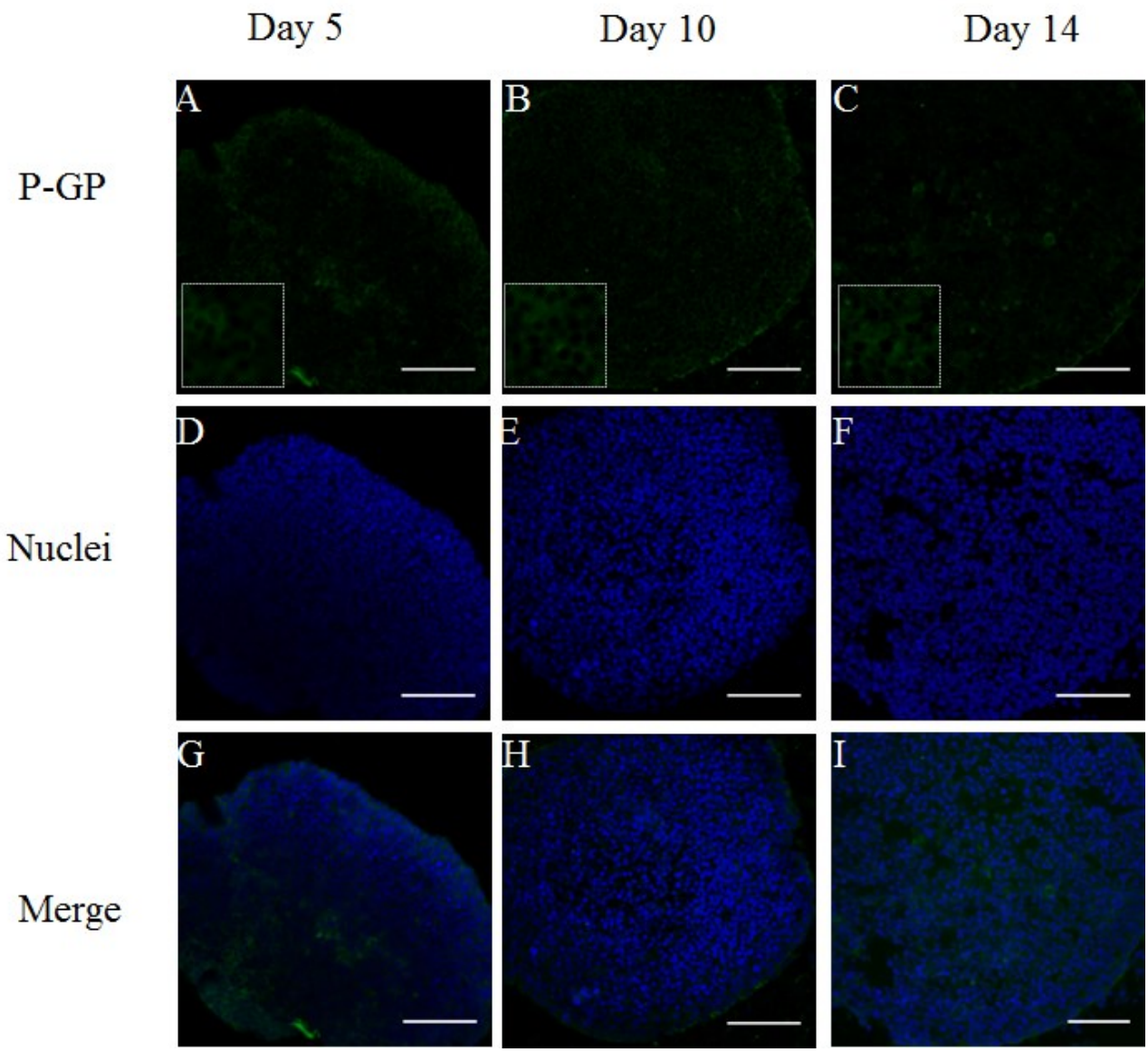

Figure 2.8: Immunofluorescence staining of P-Glycoprotein (green) and nuclei (DAPI, blue) in spheroid at day 5, day 10 and day 14. Scale bar 100 µm.

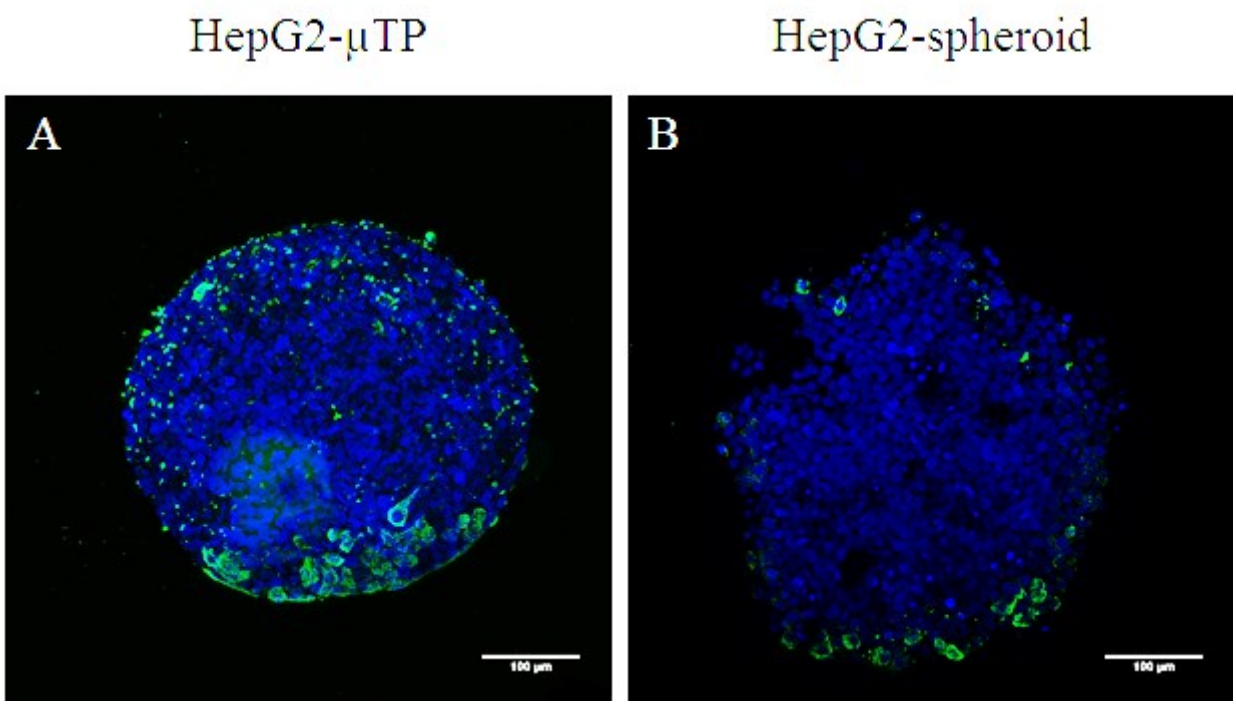

Figure 2.9: 3D reconstruction of immunofluorescence images of P-Glycoprotein (green) and nuclei (DAPI, blue) in HepG2- µTPs (A) and HepG2- spheroid at day 7 (B). Scale bar 100 µm.

2.3.3 Liver-on-chip bioreactor

We developed a microfluidic device to replicate the liver sinusoid structure. The Figure 2.10-A shows the entire experimental set-up connected to a syringe pump and a reservoir in order to have a fluid flow condition and to collect the tissues supernatants respectively. The Figure 2.10 B-C shows the geometrical configuration of the biochip, composed by a central channel that perfuse three parallel compartments which are connected to it by small pillars. The HepG2-µTPs were loaded into the device by pipetting using the three appropriate inlet. The bioreactor system was perfused with a flow rate of 5 µL/min.

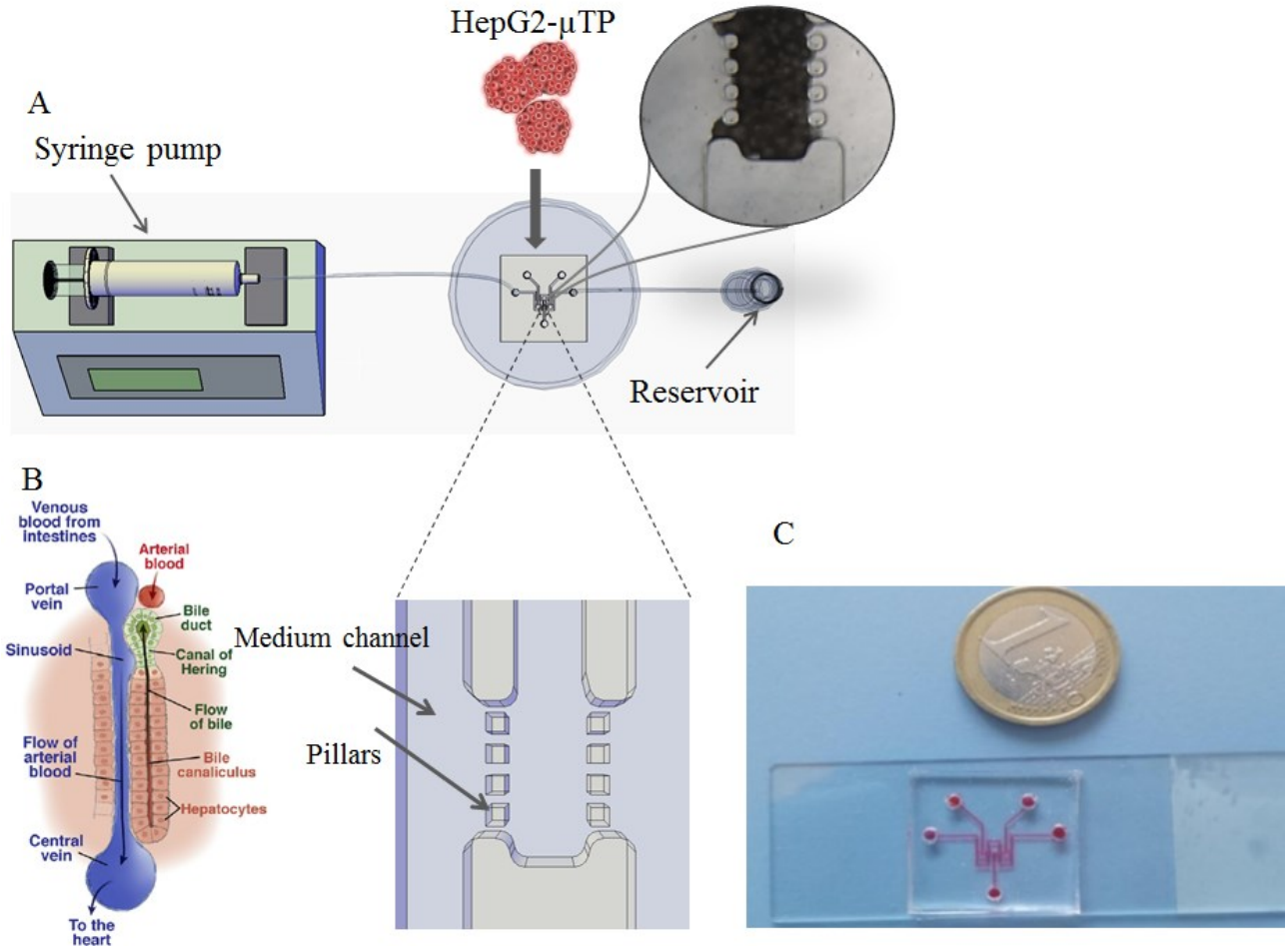

Figure 2.10: Schematic representation of the microfluidic device. (A) Experimental set-up of the biochip connected to a syringe pump and a reservoir. Top view of the design of the biochip (B), three parallel tissues chamber are separated by a medium channel by small pillars. (C) Liver-on-chip device photograph filled with food colouring.

2.3.4 Ethanol cytotoxicity assessment under perfusion culture

Alcoholic injury was investigated by exposing HepG2- µTPs into the biochip to two different ethanol concentrations, 100 mM and 300 mM from 2 to 4 days of culture. To assess the ethanol cytotoxicity a non-invasive method was used, exploiting cell auto-fluorescence coupled with two photon microscopy. The Figure 2.11-A showed the graph of HepG2-µTPs viability into the biochip for the control group and for the treated groups with crescent dose of ethanol for a culture period of 4 days. Control group devices, maintained the same cell viability during culture time, with a value of 66.35 % ± 7.28 % at day 2 and 64.75 % ± 5.08 % at day 4. In contrast, in the treated group there is a decrease of the percentage of viability, for 100mM group it was reduced from 60.62% ± 14.59% at day 2 and 51.58% ± 0.48% at day 4; for the 300 mM group it declined from 41.20% ± 3.68% at day 2 and 19.19% ± 10.45% at day 4. This results were compared with LDH release assay, a typical marker of tissues damage. Measurement of LDH activity in the

eluent showed that cell death in the control group device remained at low levels in the perfusion period (day 2 and day 4) in Figure 2.11-B. Exposure to ethanol levels at 300 mM resulted in an increase in LDH release compared to the untreated tissue, indicative of increased levels of cell death at these concentrations over the time periods assayed. LDH activity at 100 mM showed no marked difference compared with the control.

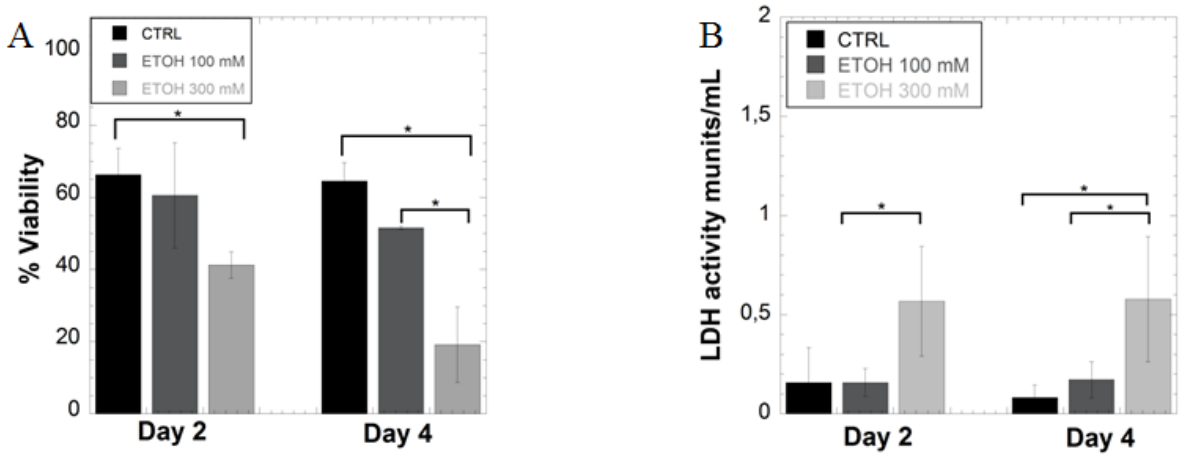

Figure 2.11: Ethanol cytotoxicity assessment. (A) Viability on chip evaluated via cell autofluorescence for control group and traeted groups. (B) Lactate dehydrogenase (LDH) leakage assay present in the µTPs during perfusion culture in biochip. Asterisks indicate statistical difference with $p<0.05$

2.3.5 Assessment of hepatic functions

Ethanol toxicity was also performed by measuring hepatic biomarkers albumin and urea production. As shown in the graphs (Figure 2.12 A-B) albumin and urea synthesis increased in the control group, while the treated group showed a significant decrease of metabolic activity. The albumin production (Figure 2.12-A) of the liver-on-chip device was 56.877 ng ± 9.01 ng at day 2 and 62.723 ng ± 17.418 ad day 4 for the control group. For the ethanol treated groups, albumin decreased in a dose dependent manner and over culture time. In particular for 100 mM group, albumin production decreased from 19.785 ng ± 8.158 ng at day 2, to 12.657 ng ± 9.8552 ng at day 4, for 300 mM group 7.636 ng ± 6.21 ng at day 2 and 0.01985 ng ± 0.0028 ng at day 4. Urea synthesis (Figure 2.12-B) of the biochip had the same reduction during culture time.

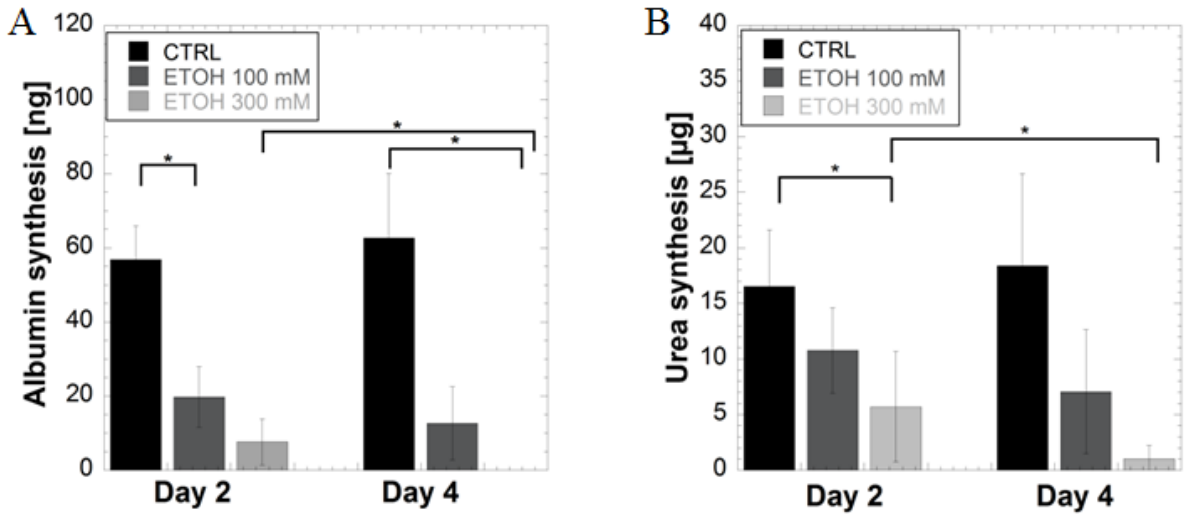

Figure 2.12: Hepatic functions assay: Albumin and urea secretion after 4 days of culture in the perfusion biochip. Asterisks indicate statistical difference with $p<0.05$

2.3.6 Analysis of oxidative stress

With the purpose to investigate the oxidative stress caused by ethanol, we evaluated cellular ROS levels in liver-on-chip device after 2 days and 4 days (Figure 2.13). ROS levels in control group were low after both 2 and 4 days (Figure 2.13 A,D). For 100 mM treated group, at day 2 ROS production is similar to the control but after 4 days it increased (Figure 2.13 B,E). The 300 mM treated group exhibited the highest ROS production after 4 days of ethanol exposition Figure 2.13 C, F). The reported low ROS production is in agreement with previous literature reports [128].

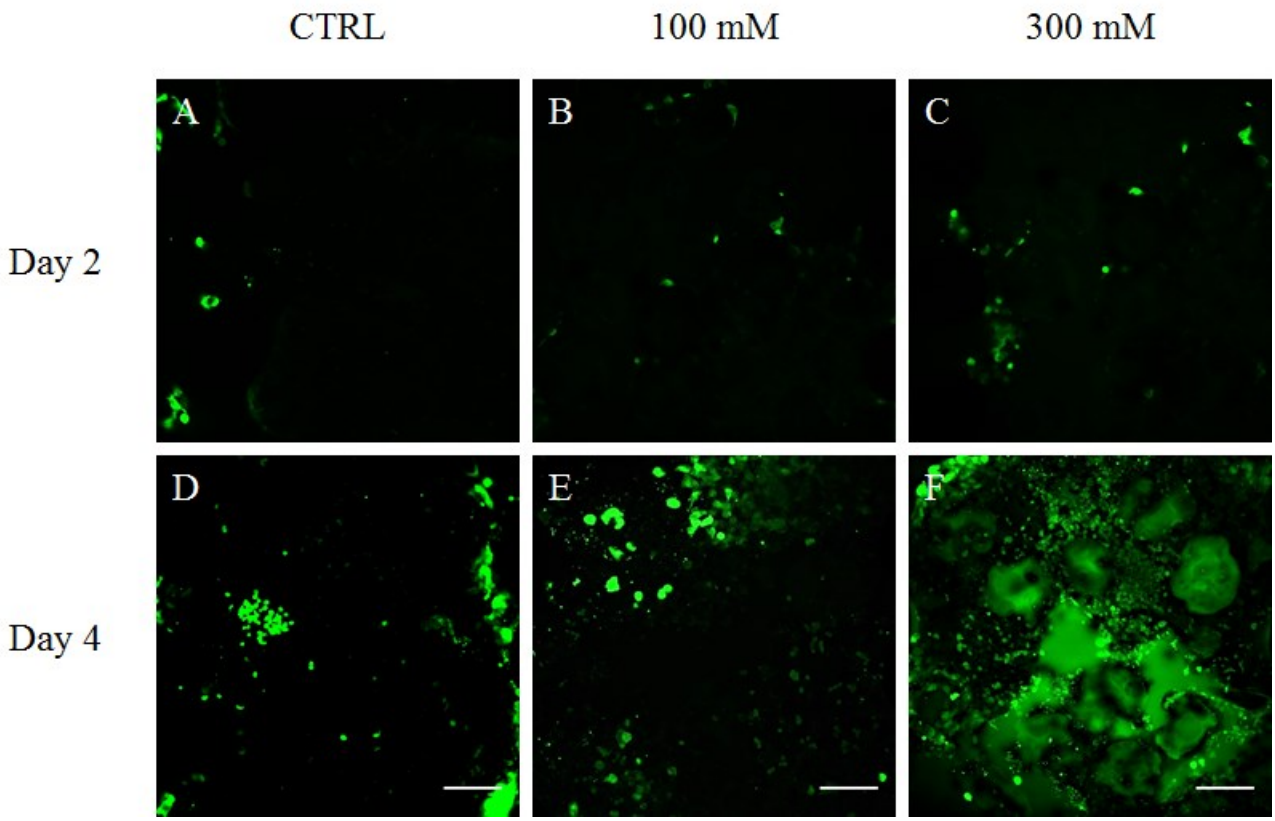

Figure 2.13: ROS detection assay for the analysis of oxidative stress. Representative images of intracellular ROS produced after ethanol treatment at day 2 (A-C) and day 4 (D-F) for control group, 100 mM and 300 mM. Scale bar 100 µm.

2.4 Discussion

In this work HepG2 cells were used to create two different kind of 3D hepatic tissues model: spheroids and microtissues. HepG2-spheroids were obtained by static seeding onto 96 ultra-low attachment well plate, while HepG2- µTPs were obtained in a spinner flask bioreactor by dynamic cell seeding of HepG2 over gelatin porous microbeads. In a previous work, spheroids and microtissues micromodules were compared in order to assess that the µTP model better recapitulate the tumor microenvironment and the important differences between normal and cancer stroma [120]. In another precedent work, it was demonstrated that fibroblasts under microtissues configuration, start to adhere on the microscaffold surface and synthetized extra cellular matrix component like collagen, elastin and so on. The authors studied the interactions among fibroblasts since microscaffolds triggered mechanotrasduction pathways involved in collagen remodelling [126]. In this work we want to compare this two kind of 3D hepatic model in order to prove that the final tissues micromodules showed different physiological properties in terms of cell proliferation, functional and metabolic activity.

Differences between HepG2-µTPs and HepG2-spheroids, were detected during 14 days of culture. In the spheroid model, size remained almost unchanged and it was higher for all the time of the

culture compared to HepG2-μTPs, making spheroids not suitable for the loading into the device. Moreover, spheroids with a size over 250 μm shows lower viability and necrotic core [129]. About the viability, HepG2-spheroids displayed lower viability than HepG2-μTPs during all the time of the culture. In particular still at day 7 they exhibited lower viability then HepG2-μTPs at day 14. This results indicate that the spheroid model is not appropriate for long term culture. In addition, by histological characterization is evident the presence of necrotic core in HepG2-spheroids starting from day 7. This data was in agreement with other literature studies reporting that cell in the outer layer are proliferative instead cells inside the core are apoptotic and so they left the system, in this way the dimension remain constant [130]. We confirm this result by immunohistochemical analysis of Caspase-3 both for HepG2-μTPs and HepG2-spheroids in order to show apoptotic activity of both model. Indeed, the HepG2-spheroids are positive for Caspase-3 still from day 7, unlike HepG2-μTPs which showed only little expression of this protein at day 14. About hepatic functionalities, the maintenance of the metabolic activity of the hepatic 3D tissues model is crucial for their application as drug metabolism studies. However, liver functions of primary hepatocytes are rapidly downregulated during their *in vitro* culture. Although, commercial HepG2 cell line express very low metabolic activity compared to primary hepatocytes, they provide a stable and easy to handle platform for *in vitro* studies of hepatotoxicity and they also are a valid alternative to primary hepatocytes especially for the use in proof-of-concept studies. For this reasons, the developed platform paves the way toward constructs from patient specific hepatocytes derived from stem cells, e.g. iPSCs. To assess the hepatic functionalities, we quantified the albumin and urea secretion during 14 days of culture. The metabolic activity of HepG2-μTPs and HepG2-spheroids had the same decreasing trend during culture time but spheroids shows lower secretion levels of these markers.

The number of cells per HepG2-μTPs and HepG2-spheroids was calculated in order to express the albumin and urea concentration in terms of pg/h/cell, to compare the functionalities of the developed model with the previous existing platforms. The relative albumin secreted by both spheroids and μTPs decreased over time, with a level in a range from 0.2-0.4 pg/cell/day which is the same reported in literature for albumin production of HepG2 [131]. The lower secretion of metabolic marker from spheroids should be attributed to the decreasing oxygen availability within the spheroid core. We further examined the expression pattern of non-secreted proteins by immunostaining in both 3D micromodules. One example is P-gp, a protein transporters known to be expressed and localized to the canalicular membrane of hepatocytes *in vivo*. This protein is involved in the first-pass effect of xenobiotics and endogenous compounds and exports bio-transformed chemicals out of the liver. The expression of this transporter was used to confirm the

cellular polarization and the formation of bile canaliculi for both HepG2-μTPs and HepG2-spheroids. Canalicular structures formed from day 10 in the HepG2-μTPs, while only few pixels are present in the HepG2-spheroids suggesting lack of expression of P-gp, improper polarization or localization, or inactive transporters when cultured in spheroid fashion. Other important aspects are the represent by the handling of both HepG2-μTPs and HepG2-spheroids. μTPs were obtained in a spinner flask bioreactor so cells and microbeads are added together to the spinner and collected from it directly at each time point in a very simple way. This not happened for the spheroids because they are cultured in a 96-well plate where they are accommodated one per well. In this case, it is difficult to change culture media without the risk of aspirate them. Finally, in terms of number of micromodules μTPs have a higher production rate than spheroids using the same cell number. Taking account of these results, we believe the using of HepG2-μTPs as 3D tissue model would better reproduce the *in vivo* hepatic metabolic and physiological activity and represents a more predictive platform for drug testing. Anyway, 3D static culture lack of appropriate mass transport for gas and metabolite waste, which are imperative for drug screening studies. A dynamic microenvironment could be achieved by using organ on chip device, which could allow heterotypic interaction, low shear stress and the diffusion dominated *in vivo* like environment. Once microtissues was identified as the better three dimensional hepatic *in vitro* model, we load the HepG2-μTPs into the biochip in order to obtain a perfusion culture. With the aim to have the better *in vitro* performance of the HepG2-μTPs, we collected them from day 5 to day 7 since they exhibit the higher metabolic activities and viability. In the current report, we devised a 3D tissue based *in vitro* microfluidic model and validate it by applying ethanol-containing media to HepG2-μTPs. Two different ethanol concentrations were selected, 100 mM and 300 mM. Levels over 100 mM ethanol equate to a blood concentration associated with a heavy consumer of alcohol.

Firstly, we investigate the ethanol cytotoxic effect by assess viability. For this purpose, we choose a non-invasive method, using cell auto-fluorescence coupled with two photon microscopy. This technique was based on the acquisition of the emission spectrum of NADH, a cellular fluorophore which plays a central role in cell metabolism. The auto-fluorescence emission of live and dead cells was found to be characterized by distinct spectral differences. Using advanced microscopy methods, the differences of the spectra of dead and live cells may be exploited to accurately differentiate viable from dead cells and assess the cell viability of the HepG2-μTPs.

The use of conventional methods (e.g. Trypan blue) surely represent the most accurate way to assess cell viability but this leads to a discard of the tissue constructs and killing of the cells. Multiphoton microscopy can be employed to detect cell viability without using dye or

disintegrating the constructs in order to continue the culture or to utilize them for other analysis. This method is suitable for those sample that need real time investigation during culture time requiring on-line assessment of viability at different time point. Emission spectra extracted from confocal images of the biochip were post processed using a custom written MATLAB script in order to obtain a percentage of viability of the HepG2-μTPs loaded into the biochip. The viability results were in agreement with the ones of LDH activity where is showed that enzyme production is higher in the treated samples. Exposure to ethanol levels above 100 mM resulted in an increase in LDH release compared to the untreated tissues, indicative of cell death at these concentrations over the time period assay. Alcoholic injury cause accumulation of free radicals inside cells. Although free radicals from stimulated inflammatory cells may play an important role in alcohol-dependent liver toxicity, it seems that enhanced intracellular oxidative stress in hepatocytes during ethanol exposure limits cell viability [132]. The oxidative stress generated by ethanol treatment was assessed by ROS assay. This leads us to prove that acute dose of ethanol causes apoptosis of HepG2 cells within bioreactor leading to a decrease of cell viability, increase of LDH release and accumulation of ROS species into the cells. About metabolic activity, albumin and urea levels steadily increased into the biochip without ethanol treatment, but there is a significant drop in the ethanol treated group. This is supported through finding from a previous study using isolated perfused liver [12].

2.5 Conclusion

In this work two 3D tissue model were compared in order to identify the model that better recapitulate the *in vivo* physiological and metabolic activity of the liver. Compared to the spheroids model, HepG2-μTPs exhibited more viability, higher secretion of biomarker and increased polarization and transport capability. Then we developed a liver-on-chip platform that enabled maintenance of HepG2-μTPs within the culture chambers of the bioreactor. The bioreactor is optical accessible in order to monitor and quantify the cell viability and hepatic functionalities, in real time and without discarding the samples. Our system has been proposed as a new predictive platform to study cytotoxic effects of xenobiotics compounds, like acetaminophen, anti-tumoral drugs, nanoparticles and the hepato-protective effects of nutraceuticals. The characteristic geometrical configuration of the chip is also appropriate to perform co-culture with others cell time in order to assess the tissues cross-talk.

Chapter 3

A microfluidic platform to recreate air-liquid interface of 3D human intestinal equivalent

3.1 Introduction

In our body, drugs and nutrients are effective only when absorbed by the epithelial intestinal cells. Their absorbability, however, changes with the nature of substances involved. To recreate in vitro the model of intestinal absorption and metabolism, often are used Caco-2 cells. These cells derived from human colonic carcinoma and are a well-known system to mimic intestinal epithelial cells. Over two decades ago, several studies of intestinal human in vitro model, were developed by culturing Caco-2 on microporous filters [134]. When forming a monolayer under normal culture conditions, Caco-2 cells spontaneously differentiate into columnar and polarized cells that have similar resistance and permeability as small intestinal enterocytes [134] [135]. Since its development, this 2D model has being widely used for permeability testing of new drug candidates as well as investigating functionality of different intestinal transporters [136],[137]. However, this model lacks physiological relevance in that it fails to capture the 3D microenvironment present on the intestinal *villi*, which has been considered one of the cause for a poor correlation between slowly absorbed drugs *in vitro* and *in vivo* [138]. For this purpose, several studies have been focused on the development of 3D intestinal tissue model. Yu et al. presented a novel method to perform drug permeability test by using 3D scaffold to impart the size and shape of intestinal *villi*. The scaffold was made of collagen and it was seeded with Caco-2 cells, the system was validated by the testing of Anipyrine [92]. However, one of the main factor that is missing in static culture is the shortage of the physiological mechanical microenvironment of the normal gut that is subjected to fluid flow and peristaltic motions [94]. To explore these physical factors, we developed a microfluidic gut-on-chip device in order to establish an air–intestinal interface of Caco-2 cells, which is crucial for maturation and terminal differentiation of 3D human intestinal equivalent (3D-HIE). Bottom-up approach was used to fabricate 3D-ISE based on endogenous ECM, obtained by molding of intestinal microtissues (HI-μTP) in a maturation chamber for a period of 2 weeks. The combination of such innovative 3D-ISE with

microfluidic technology, allowed us to detect the stratification and differentiation of intestinal *epithelium*. Optimized culture conditions were assessed by numerical simulation in order to study how the fluid flown conditions guarantee the right oxygen and nutrients supply.

3.2 Materials and Methods

3.2.1 Microdevice fabrication

The microfluidic gut-on-a-chip device used in this work was fabricated by a rapid prototyping procedure. The upper and lower layers of the microfluidic device were prepared by demolding polydimethylsiloxane (PDMS) (Sylgard 184, Mascherpa), from a Poly(methyl methacrylate) (PMMA, Goodfellow) slab. The PMMA master mold was designed by AutoCAD and carved with micromilling machine (Minithech CNC Mini-Mill) making a relief positive geometry to avoid silanization process of PDMS. The ratio of PDMS prepolymer and curing agent was 10 : 1 (w/w), then the mixture was degassed under vacuum for 20 min to remove air bubbles and then poured on PMMA masters. The set-up was incubated at 80 °C for 60 min, then peeled off from master molds. Inlet and outlet holes were punched with a 2.5 mm biopsy punch (DifaCooper) while gut chamber was punched using a 6.5 mm puncher (Am-Tech).

The lower layer of PDMS with a central microchannel (1.2 mm wide × 40 mm long × 0.6 mm high) and an intestine chamber (6.5 mm diameter × 0.6 mm high) were bonded, facing upwards, to a glass microscope slide (24 mm wide × 60 mm long) for mechanical support by oxygen plasma treatment for 1 min at 50 W in an oxygen plasma oven (Plasma Femto, Diener). Polycarbonate porous membrane (0.4 μm diameter of pores, Merck Millipore) was bonded to the lower layer using revisited method reported by Chueh et al. [139]. Briefly, pre-cured PDMS was spin coated on a glass cover slide for 30s at 750 rpm, PDMS lower layer with recessed microchannel was placed in contact onto the glass slide coated with PDMS pre-cured for 30s. Then polycarbonate membrane was positioned over the gut chamber using a tweezers and let cure at 80 ºC for 30 min. The PDMS upper layer, with a central gut chamber (6.5 mm diameter × 5mm high) was bonded to the lower one by oxygen plasma treatment for 1 min at 50 W. The two layer were overlapped in order to match the upper and lower gut chambers. Then, the whole setup was incubated at 80 ºC overnight to achieve irreversible bonding of the two PDMS layers.

Before tissue culture, gut-on-chip microdevice, tubes and connectors were sterilized by autoclaving. 2-Stop Tygon tubes were inserted into the inlets and outlets of the central channel using male luer lock connectors (Harvard Apparatus), then the whole setup was connected to a

peristaltic pump (Ismatec) in order to obtain a specific flow rate, 40 μL/min or 1000 μL/min. To avoid bacterial contaminations, the intestine chamber was closed laying a 100 μm PDMS membrane fabricated by spin coating of PDMS (750 rpm × 30s).

3.2.2 Perfusion culture optimization

2% Agarose gel (6.5mm diameter, 1 mm high) was punched with a 6.5 mm puncher. The agarose cylinders obtained were used to simulate the solidity of the intestinal equivalent. Then the agarose disk were accommodated into the intestine chamber of the micro-bioreactor device and connected to a peristaltic pump. To simulate medium culture, we used food colouring diluted in PBS and then chose different flow rate (0 μL/min; 40 μL/min; 1000 μL/min) in order to verify at which flow rate the agarose disks were completely perfused. We perfused the agarose disk for two hours and then the disks were collected to take photographs.

3.2.3 Mathematical model CFD simulation

In order to define the experimental setup, the three-dimensional velocity and the oxygen gradients in the microbioreactor before *in vitro* trial, we used the commercial CFD COMSOL Multiphysics vers 5. CDF analysis were performed dividing the entire gut-on-chip bioreactor into two different domains, a fluid domain indicated with *f*, which identified the region filled with culture medium, and a tissue domain, indicated with *t* which identified the region filled with the 3D-HIEs and 3D-ISEs samples. Simulation within the fluid and tissues domain were performed using the steady state Navier–Stokes equation, by means of free and porous media flow physic (1). Moreover, the simulation for O_2 consumption was performed by means of Mass Transport-Convection/Diffusion application mode, using transport of diluted species in porous media physic. Boundary conditions were set to reflect flow configuration. Reference pressure was considered at bioreactor outlet (p = 0 Pa), no slip condition was adopted at the walls, equality for velocity and pressure was imposed at the Navier-Stokes (u, v, w, p)/ Brinkman (u_2, v_2, w_2, p_2) interfaces. Setting for O_2 concentration in the culture medium (0.22 mol/m^3), the diffusion coefficient (D) (10^{-9} m^2/s), cell density (ρ) calculated in a 1 mm^3-dermal equivalent (0.2 1014 cell m3), maximum velocity of O^2 diffusion (V_{max}) (10^{-18} mol/cells/s) and O_2 concentration at $V_{max}/2$ (K_m) (10^3 mol/m^3), the convection-diffusion equation was implemented in the model in order to evaluate the O_2 consumption in the bio-system. All the setting values were previously evaluated experimentally (data not shown). Laminar flow with different flow rates was set at the inlet and zero pressure was set at the outlet.

$$\mu^f \nabla^2 v^f = \nabla P^f \quad (1)$$

Where μ^f is the dynamic viscosity, v^f is the fluid velocity, and P^f is the pressure. Brinkman equation (2) was used to describe the flow through the porous medium:

$$\mu^t \nabla^2 v^t - \frac{K^t}{\mu^t} = \nabla P^t \quad (2)$$

Where K^t is the hydraulic permeability, μ^t is the viscosity of the tissue, and P^t is the pressure.

The oxygen concentration within the system was calculated by means of the following mass balance equation (3):

$$D\nabla^2 C - \nabla(Cv) = -R \quad (3)$$

Where C is the oxygen concentration, v is the fluid is the fluid velocity field that was set equal to v^f in the domain *"f"* and v^t in the domain *"t"* respectively. D is the diffusion coefficient of the oxygen, set as D^f in the domain "f" and D^t in the domain "t" respectively. R is the volumetric oxygen consumption rate expressed by the Michelis–Menten law and according to the following equation (4):

$$R = \rho \frac{V_{max} C}{K_m + C} \quad (4)$$

where V_{max} is the maximum oxygen consumption rate and K_m is the concentration at which the oxygen consumption rate is half of V_{max}, ρ is the cell density in the perfusion chamber obtained by taking into account the number of cells present in the 3D-HIE accommodated into the intestine chamber of the gut-on-chip device. R was set to 0 only in the fluid domain, since cells are present only in the tissue domain. The air-liquid interface was mimicked by an open wall at the bottom of the intestine chamber.

3.2.4 Cell type

Caco-2 cells were provided by American Type Culture Collection (ATCC). Cells were sub-cultured onto 150 mm Petri dishes in Dulbecco Modified E containing 10% fetal bovine serum, 100 μg mL^{-1} L-glutamine, 100 U mL−1 penicillin/streptomycin. Cells were maintained at 37 °C in a humidified atmosphere containing 5% CO2.

3.2.5 Intestinal microtissues precursors: fabrication and characterization

Gelatine microbeads having a diameter of 75-150 μm, stabilized by 4% of glyceraldehyde were fabricated by means of a modified double emulsion technique (O/W/O) as previously reported [85]. Briefly, gelatin (type B Sigma Aldrich Chemical Company, Bloom 225, Mw 176,654 Da)

was dissolved into 10 ml of water containing TWEEN 85 (6% w/v) (Sigma Aldrich Chemical Company) at 60 °C. Toluene containing SPAN 85 (3% w/v) (Sigma Aldrich Chemical Company) was continuously added to the aqueous gelatin solution (8% w/v) to obtain primary oil in water emulsion. Microbeads of gelatin containing droplets of toluene were produced through the addition of excess toluene (30 ml). After cooling below 5 °C, 20 ml of ethanol were added to extract toluene and stabilize gelatin microbeads. The resulting microspheres were filtered and washed with acetone and then dried at room temperature. To make the Intestine-□TP, spinner flask bioreactor (250 ml, CELLSPIN, Integra Biosciences) was inoculated with Human subepithelial myofibroblasts (ISEMFs) extracted ileal biopsy after informed consent at a cell density of 10^5 cell/ml and a gelatin microbeads density of 2 mg/ml (corresponding to $5x10^3$ beads/mg), in order to obtain an initial ratio of 10 cells per microbead. The culture suspension was stirred intermittently at 10 rpm (5 min stirring and 30 min static incubation) for the first 6 h post-inoculation to allow cell adhesion, and then continuously at 30 rpm up to 10 days [126]. All cultures were maintained at 37 °C in a humidified 5% CO2 incubator. Three times per week the media was replaced and 2-O-alpha-D-Glucopyranosyl-L-ascorbic Acid 0.5 mM (TCI Europe) was added. Human intestine microtissues precursors (HI-μTP) were harvested at different time points of spinner cultures to perform the complete characterization.

3.2.6 Organotypic intestinal culture development

Three dimensional intestinal stromal equivalents

3D intestinal stromal equivalents (3D-ISEs) were produced by transferring the HI-μTP into an opportunely designed assembling chamber which contains a silicon mold with disk-shaped spaces (1 mm in thickness, 5 mm in diameter) where the HI-μTP biological assembling takes place. Stainless steel rigid grids are posed directly on the both sides of the system and two polytetrafluoroethylene (PTFE) rings are placed on the grids on both sides of the system and are fastened to each other by means of stainless steel screws, which close the system and ensure that the HI-μTP are retained. The system is autoclavable in each part. Furthermore, the assembling chamber was placed on the bottom of a spinner flask and completely bordered by culture medium. The spinner was operated at 60 rpm and the medium was exchanged every 3 days. After 2 weeks of culture the assembling chamber was opened and the 3D-ISEs were collected. Samples were accommodated in transwell insert (diameter, 6.5 mm; Corning) for static culture with basolateral chamber filled with 600 μL over a period of 5 to 10 days. At the end of the experiment, 3D-ISEs were taken from the insert for further investigation and fixed.

Three-dimensional human intestine equivalent production

In order to produce three-dimensional human intestine equivalents (3D-HIEs), organotypic epithelial cultures were developed. To this aim, 3D-ISEs (0.5 cm diameter) were rinsed with three washes of PBS solution, then the PBS was removed and the 3D-ISEs were accommodate in the transwell inserts and allowed to dry for 5 min under laminar flow. Subsequently, 50 µl of the Caco-2 suspension was seeded to the centre of each 3D-ISE, corresponding to $2x10^5$ cells/3D-ISE. The transwell was incubated for at least 2 hour in incubator at 37°C with 5% CO_2 to allow the cells to adhere onto the 3D-ISE surface. For static culture, 200 µL of DMEM was added into the apical chamber of the transwell insert taking care not to dislodge cells from 3D-ISE and the basolateral chamber was filled with 600 µL of DMEM, in order to perform a submerged culture that promoted Caco-2 horizontal spreading. Submerged culture lasted approximately 7 days. Then, an optimized air-liquid interface culture lasting 2 weeks took place in order to induce the epithelial tissues to differentiate and stratify. The culture medium was replenished on the first day and every 2 days until the end of the experiments. 50 µg/mL of ascorbic acid (l-ascorbic acid, Sigma) were added at each medium change. At day 5 and 10, samples were taken from the transwell and fixed for further investigation.

3.2.7 3D-ISE on a chip and 3D-HIE on a chip

For dynamic culture, 3D-ISE or 3D-HIE (after adhesion of Caco-2) were accommodated into the intestine chamber of the gut-on-chip device and connected to a peristatic pump in order to make a flow rate of Q= 40 µL/min or Q= 1000 µL/min. For 3D-HIE culture, submerged phase lasted approximately 1 day, while air-liquid interface culture lasting from 4 to 9 days for a total culture time of 5 or 10 days respectively. At day 5 and day 10, 3D-ISEs were collected form the biochip and observed for collagen network imaging. At day 5 and day 10, 3D-HIEs samples were collected from the intestine chamber of the biochip and fixed for further analysis. Multiple chips were grown concurrently at 37 ºC in a humidified incubator under 5% CO_2 in air over a period of 5 to 10 days.

3.2.8 ECM microarchitecture of 3D-ISE

Collagen fraction

At the end of the experiment tissue samples 3D-ISEs in static and dynamic conditions were collected and analysed for collagen network imaging. Two-photon excited fluorescence (Leica

TCS SP5 coupled with a Multiphoton Microscope Chamaleon Compact OPO-Vis, Coherent) was used to induce Second Harmonic Generation (SHG) and obtain high resolution images of unstained collagen structures. SHG images from 3D-ISEs in static and dynamic conditions were analysed by using ImageJ software. The collagen fraction in the endogenous ECM space was analysed choosing a ROI in order to exclude the signal rising from the microbeads. We define collagen fraction (CF) as the ratio between bright pixels to total pixels in the selected ROI, as reported in the following the Eq. 1:

$$CF = \frac{N_C}{N_C + N_B} \quad (1)$$

where N_c and N_b represent the number of pixel from the collagen and non collagen portion, respectively.

Degree of collagen assembly (CA) evaluation

The degree of collagen assembly (CAD) network was evaluated by analysing the intensity of the SHG signal from 3D-ISEs in static and dynamic conditions. The analysis was performed within the ECM space where the SHG signal was present. All SHG images were subjected to noise subtraction and the average intensity was evaluated as described by Eq. 2:

$$\mathrm{CAD} \propto \bar{I} = \frac{\sum_{i=1}^{255} I_i p_i}{\sum_{i=1}^{255} p_i} \quad (2)$$

where $\bar{I}$ is the average intensity, Ii is the intensity corresponding to the pixel pi, while the index i = xi, yi runs in the gray value interval from 1 to 255. The intensity $\bar{I}$ of the collagen network is known to be proportional to the degree of assembly of the newly synthesized collagen [124].

Correlation length

At the end of the experiment tissue samples 3D-ISEs in static and dynamic conditions were collected and analysed for collagen network imaging. Two-photon excited fluorescence (Leica TCS SP5 coupled with a Multiphoton Microscope Chamaleon Compact OPO-Vis, Coherent) was used to induce Second Harmonic Generation (SHG) and obtain high resolution images of unstained collagen structures. The samples were observed by using λ_{ex} = 840 nm (two photons) and λ_{em}=415-425 nm. The SHG images have a size of 512 × 512 pixels and were acquired with a resolution of 8 bit using 40X/1.25 objective. To quantify the stroma related changes, we perform Gray-level-Co-occurrence Matrix (GLCM) texture analysis, by using the Image J plug-in "Texture" on SHG images [140]. In this work, we calculated the correlation curve (COR) for

distances ranging from 1 to 100 pixels in the horizontal (0°) and vertical (90°) direction of each optical section that cover a length of interest of 40 μm. In such spatial windows the distance at which the correlation function fall off represents the correlation length of the texture. In particular correlation curve was calculated versus neighbour index and correlation length was obtained by fitting data with an exponential low. The Eq. 3 of Cor is given as below [141]:

$$Cor = \sum_{i,j} \frac{(i-\mu_i)(j-\mu_j)p(i,j)}{\sigma_i \sigma_j}$$

(3)

where μ_i, μ_j, σ_i and σ_j are given by the Eq. (4)-(7):

$$\mu_i = \sum_{i,j} i * p(i,j)$$

(4)

$$\mu_j = \sum_{i,j} j * p(i,j)$$

(5)

$$\sigma_i = \sqrt{\sum_{i,j}(1-\mu_i)^2 p(i,j)}$$

(6)

$$\sigma_j = \sqrt{\sum_{i,j}\left(1-\mu_j\right)^2 p(i,j)}$$

(7)

In particular p(i,j) is the probability of gray level i occurring next to gray level j, μ_i, μ_j, σ_i and σ_j are the means μ and standard deviations σ of column i and line j of the matrix, respectively [141]. All parameters have a maximum value of 1 and a minimum value of 0 or -1 [6]. The Cor curve is an index of the architecture of the network, with a fast decay for fine textures and slow decay for coarse structure. From the Cor curve it is possible to obtain the correlation length λ, defined as the distance at which the Cor decay is equal to 0.5.

Determination of collagen content

At day 5 and 10, 3D-ISEs in static and dynamic conditions were collected in a solution of 10% neutral buffered formalin for 1 h, rinsed in PBS dehydrated in an incremental series of alcohol (75%,85%, 95% and 100% twice, each step 30 min at RT), then treated with xylene (30 min twice) and embedded in paraffin. Tissue sections, 5 μm thick, were stained with Picro Sirius Red (PSR) (Sigma Aldrich) following standard procedure and analysed by an optical microscope (BX53; Olympus). The analysis was performed on Picro Sirius Red stained sections of each type of 3D-ISEs at each time points and about 5 region of interests (ROIs) were examined for each

section excluding the areas occupied by the microscaffold, since the aim of imaging analysis was to investigate the evolution of endogenous ECM composition. Polarized light images of samples stained with PSR alone were acquired with an inverted microscope (BX53; Olympus) with a digital camera (Olympus DP 21). A linear polarizer was placed between the light source and the specimen, while the analyser was installed in the light path between the specimen and the camera. The collagen fibre stained with PSR and viewed with polarized light appear green or red depending upon fibre thickness, as fibre thickness increases, the colour changes from green to red [142]. We used Image J software to quantitatively determine the proportion of different coloured collagen fibres. We resolved each image into its hue, saturation and value (HSV) components by applying the software's "colour threshold" function. Only the hue component was retained and a histogram of hue frequency was obtained from the resolved 8-bit hue images, which contain 256 colours. We used the following hue definitions; red 0-51, green 52-120. The number of pixels within each hue range was determined and expressed as a percentage of the total number of collagen pixels, which in turn was expressed as a percentage of the total number of pixels in the image.

3.2.9 Immunofluorescence and histological analysis

At day 5 and 10, 3D-ISE or 3D-HIEs samples in static and dynamic conditions were fixed in a solution of 10% neutral buffered formalin for 1 h, rinsed in PBS, dehydrated in an incremental series of alcohol (75%,85%, 95% and 100% twice, each step 30 min at RT), then treated with xylene (30 min twice) and embedded in paraffin.

Tissue section, 5 μm thick were stained with haematoxylin and eosin, mounted with Histomount mounting solution (Bioptica) on coverslips and the morphological features of 3D-HIEs were observed with a light microscope.

For immunofluorescence staining of 3D-HIEs deparaffinized and reyhdrated 5 μm thick tissue sections, were heat-induced epitope retrieval in sodium citrate buffer at pH 6.0 for 5 min at 97 °C followed by 10 min at 70 °C in uncloaking chamber, washed with PBS containing 0.2% Triton X-100, blocked in a standard histoblocking for 1h at RT, and incubated with rabbit anti-human Villin (1/250) and ZO-1 (1/50) (Abcam UK) overnight at 4 °C. Then, secondary antibody incubation, goat anti rabbit 568 (Alexa Fluor) (1/500) and goat anti rabbit 488 (Alexa Fluor) (1/1000) for villin and ZO-1 respectively was performed, cell nuclei were detected by DAPI staining (5 μm/mL, Sigma Aldrich).

3.2.10 Alkaline Phosphatase assay (ALP Activity)

In order to evaluate the alkaline phosphatase activity, cell supernatants were collected and were processed by using the colorimetric Alkaline Phosphatase Assay Kit (Abcam, Cambridge Science Park). The kit uses *p*-nitrophenyl phosphate as a phosphatase substrate, which turns yellow when dephosphorylated by alkaline phosphatase. The absorbance was immediately read at 405 nm using a microplate reader (Wallac Victor 3TM; Perkin Elmer), and alkaline phosphatase activity was expressed as Unit (U).

3.2.11 Statistical analysis

Data are expressed, as mean ± standard deviation and show the results from three independent experiments. The differences between two or more groups were evaluated (p value < 0.05) using one-way analysis of variance (ANOVA). A Gaussian distribution for each population was assumed. For pair-wise comparisons within each experimental group, Tukey's post-test was used.

3.3 Results

3.3.1 Microdevice fabrication

In this work, we designed and fabricated a microfluidic device able to remodel the collagen network of the 3D-ISEs samples and to reproduce a dynamic air-liquid interface culture for the 3D-HIE during culture time. Figure 3.1 shows the microfluidic device configuration composed by

a double layer of PDMS with a polycarbonate membrane interposed between the two layers

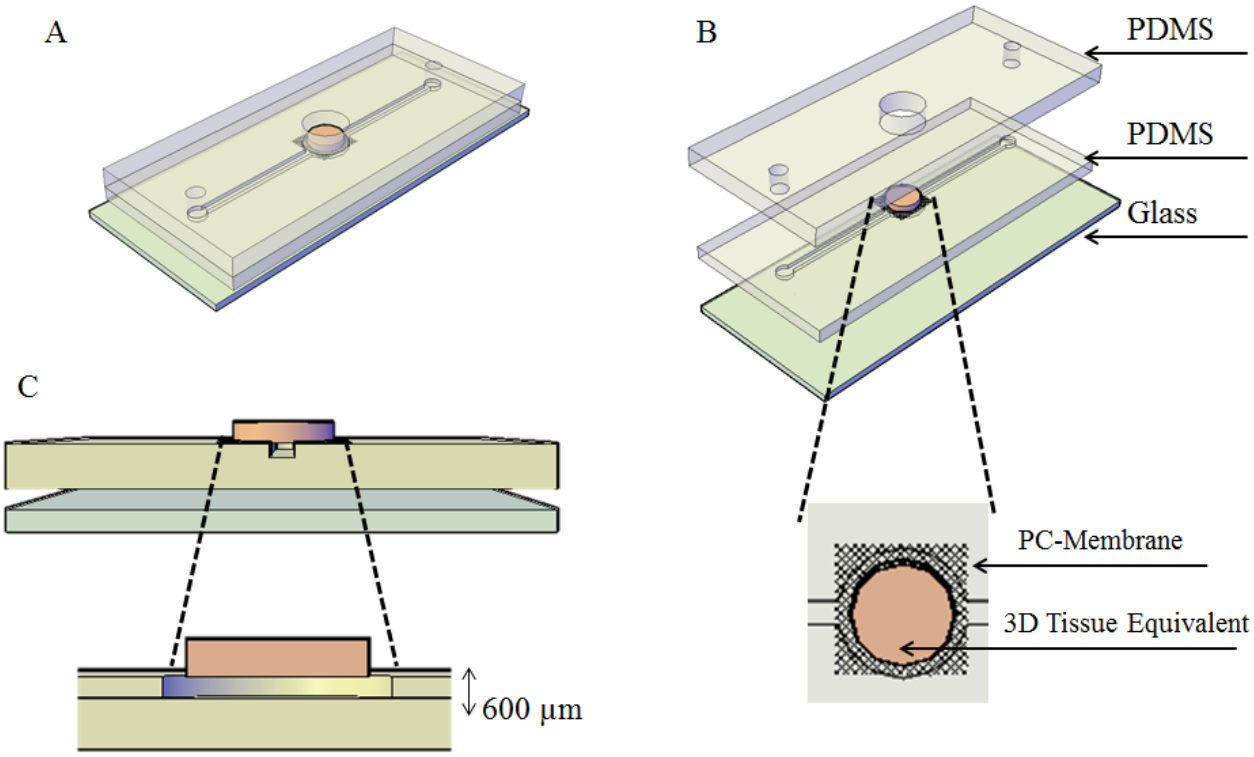

Figure 3.1: Schematic representation of the gut-on-chip device. (A) Top view of the design of the biochip, (B) Two layer of PDMS were bonded on a glass slide, the 3D tissues are accommodated on the polycarbonate membrane between the two layers. (C) Frontal view of the microfluidic device. The microchannel is bonded on the glass facing upwards.

(Figure 3.1 B). Firstly, to assess if the biochip could remodel the collagen network and maintain an air-liquid interface culture, we placed 3D-ISEs into the intestine chamber for 10 days and analysed the ECM remodelling during the culture time. Second, to reproduce ALI culture the 3D-ISEs were placed into the intestine chamber, seeded with intestinal epithelial cells (Caco-2) and cultured for 10 days. The whole setup was connected to a peristaltic pump in order to allow a fluid flow condition. The gut-on-chip device was optically accessible for multiphoton microscope in order to collect real time evolution of collagen network. To maintain the viability of the 3D-ISEs and 3D-HIEs samples the culture conditions were optimized in order to guarantee the correct oxygen and nutrients supply and the collagen network assembly.

3.3.2 Perfusion culture optimization

In order to choose the better flow rate to guarantee the cell viability, nutrient intake, cell differentiation and ECM organization of the both 3D-ISEs and 3D-HIEs, preliminary study were performed on the device. Perfusion preliminary test by using agarose disk to simulate the solidity

and texture of the samples, were firstly conducted with two different flow rate: 40 µL/min and 1000 µL/min and 0 µL/min simulate static condition. After two hours of dynamic culture, the agarose disks were collected and pictured of the samples were taken, with the purpose to evaluate the degree of perfusion of the agarose disk. Figure 3.2-A displayed a gradient of blue starting from the bottom of the agarose disk in static condition (Q=0 µL/min) indicating that the apical part of the tissues were not nourished. In both Q=40 µL/min and Q=1000 µL/min (Figure 3.2 B-C) the agarose disks are completely filled with the blue solution.

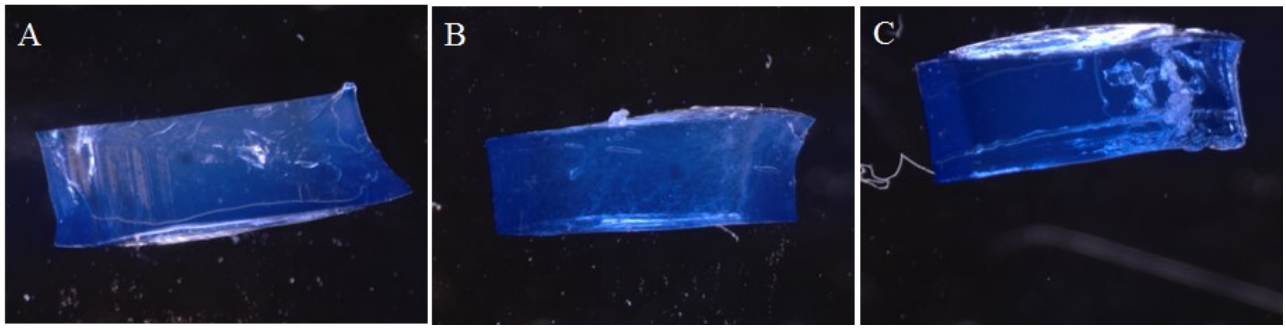

Figure 3.2: Agarose cup perfused with PBS and food colouring . (A) Flow rate of 0 µL/min, (B) 40 µL/min and (C) 1000 µL/min. In A it is possible to see a more intense colour at the bottom part compared to the top part, in comparison B and C exhibited an intense and homogenous colour.

3.3.3 Mathematical model CFD simulation

With the objective to choose the optimal flow rate to perform the dynamic culture, we carried out CFD simulations. We coupled Navier- Stokes equations (1) with Brinkman equation (2), in the fluid compartment and in the tissue compartment respectively. Oxygen consumption, by the cells contained into the 3D equivalent intestinal tissues, was calculated using a Michelis-Menten equation (4), taking into account the diffusive/convective oxygen transport. These numerical simulation were performed equation CFD simulations using different flow rate, 0, 40 and 1000 µL/min. In Figure 3.3 are were reported the colour map of the oxygen profile with black arrows to represents the convective (Figure 3.3 A,D,G) and diffusive transport (Figure 3.3 B,E,H), the light blue line represents showed the stream line of velocity field (Figure 3.3 C,F,I). The simulations show that at flow rate Q=1000 µL/min, the oxygen concentration was higher in all the part of the sample due to the increased contribution of convective transport, since the velocity field was higher. Operating in static conditions, flow rate of 0 µL/min, the convective contribution was the lowest but the diffusive contribution is not adequate to perfuse and feed all the part of the sample. The same situation was presented in the simulation at flow rate of 40 µL/min. A little convective contribution was obtained but it is still too low for guarantee the optimal culture conditions.

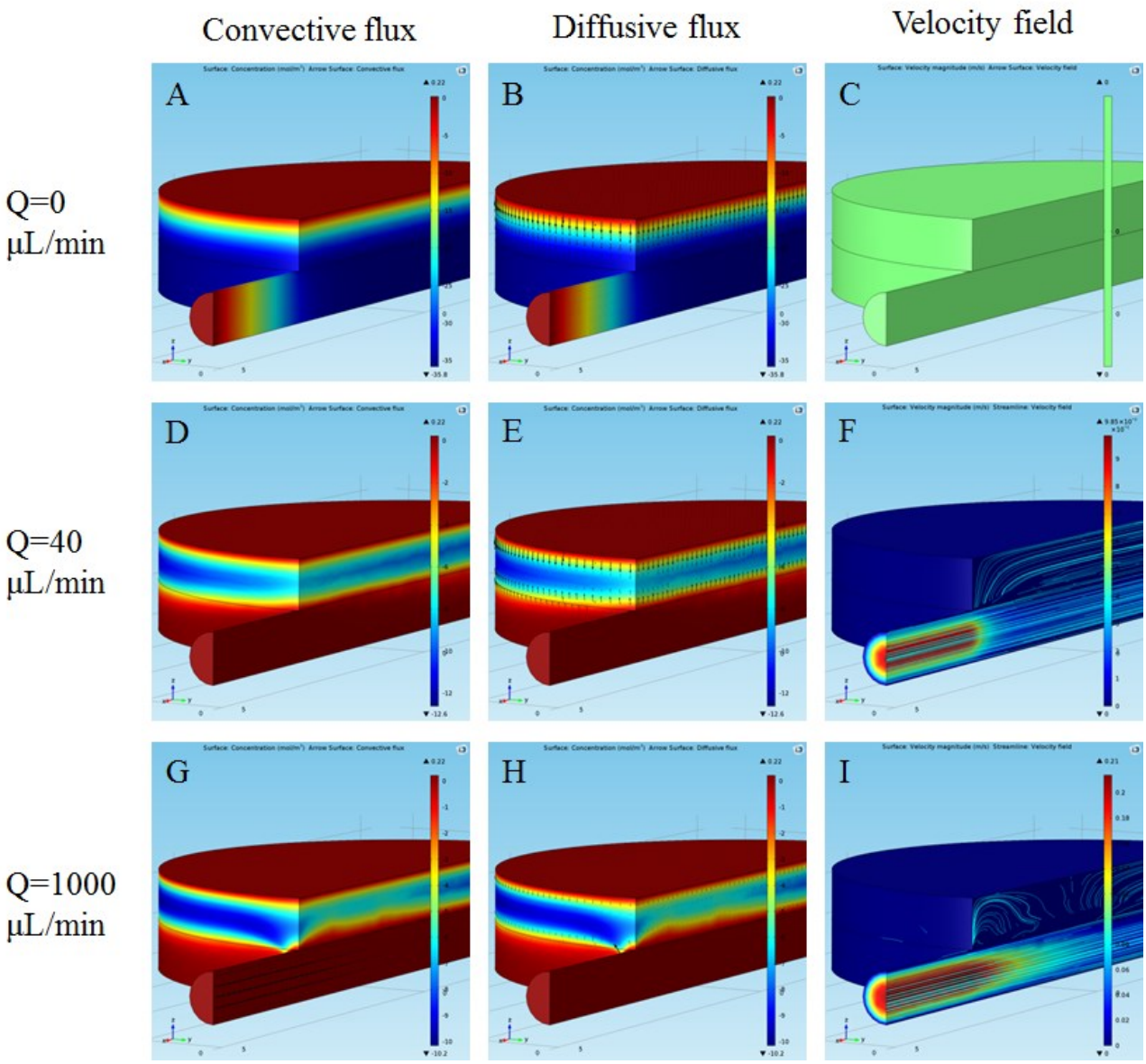

Figure 3.3: CFD simulations using COMSOL Multiphysics. In A-C are reported simulations for convective, diffusive flux and the stream line of the velocity field for the static culture (Q= 0 µL/min), D-F for 40 µL/min and 1000 µL/min

3.3.4 Collagen organization

For 3D-ISE on-chip, four samples were cultured in parallel, two in static condition, in a transwell insert, and two in dynamic condition, into the microfluidic device, both for a culture time from 5 to 10 days. The analysis of the architecture of the ECM was performed at day 5 and 10, for both static and dynamic culture, by using MPM that allow to visualize unstained collagen structure. Figure 3.4 shows SHG images rising collagen signal of 3D-ISEs in static (Figure 3.4 A-B) and dynamic (Figure 3.4 C-D) conditions during all the culture time. The collagen assembly degree (CAD) were extrapolated by SHG images (Figure 3.4 E), in particular, according to the above-mentioned Eq. (2), the measured CAD was higher for 3D-ISEs in dynamic culture where it reaches the value of 16,57% $\pm$ 4,87% at day 5, and 43.99% $\pm$ 9.84% at day 10.

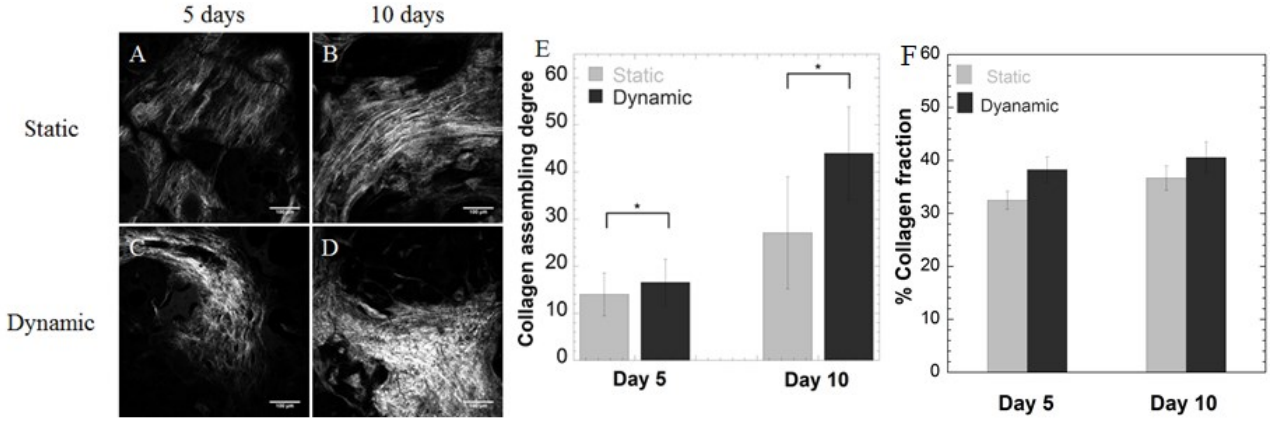

Figure 3.4: SHG signal (gray scale) from fibrillar collagen in (A,C) 3D-ISE in static and dynamic condition at day 5 and in (B,D) in 3D-ISE at day 10. Scale bar 100 µm. (E) Collagen assembly degree (CAD) in static and dynamic culture during culture time. (F) Collagen fraction (CF) in static and dynamic conditions. Statistical difference was determined using ANOVA. Asterisks indicate statistical difference with $p<0.05$

In order to quantify the collagen amount SHG image were analysed by image j software. Collagen fraction (Figure 3.4 F) graph, showed how the collagen content increase for the samples in dynamic conditions with culture time increasing.

Picro Sirius Red staining allowed monitoring collagen maturation with time. In the Figure 3.5 A-D representative images of Picro Sirius Red stained 3D-ISE's section are reported for static and dynamic culture at days 5 and 10. Figure 3.5 E-F shows the results from imaging elaboration of Picro Sirius Red images indicating that collagen was present at each time point for all the 3D-ISE type. The graph showed that the percentage of immature collagen content decrease as culture time increase, in particular for the 3D-ISEs in dynamic conditions. On the other hand, percentage of mature collagen content increase as culture time increase and for 3D-ISE in dynamic conditions, reaching $3.90\% \pm 1.39\%$ for 3D-ISE at day 10.

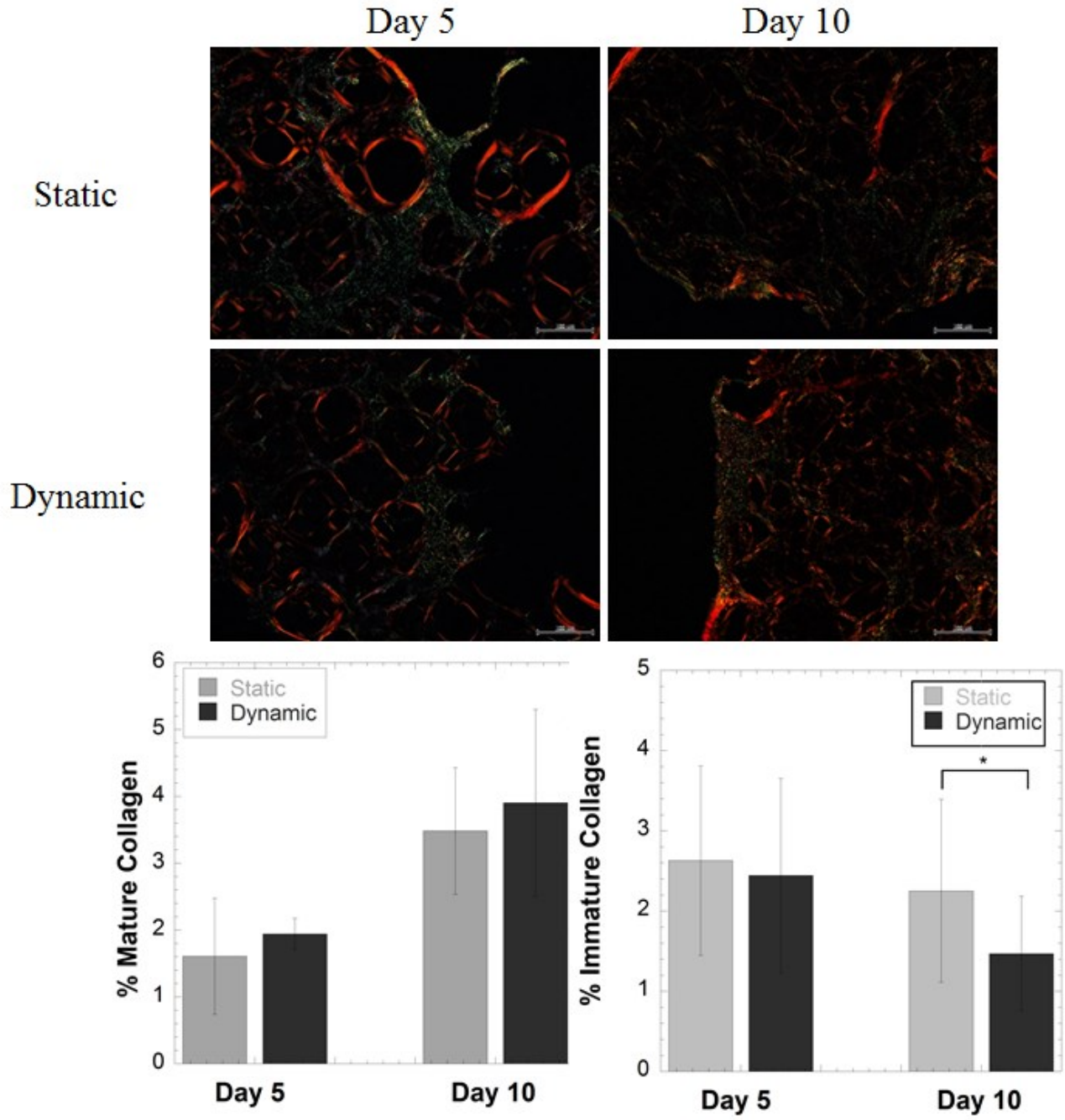

Figure 3.5: Morphological and compositional features of 3D-ISEs. Picro sirius stained sections (A-D) for 3D-ISE in static and in dynamic culture at day 5 and day 10. Quantification of immature and mature collagen fraction (E-F). Asterisks indicate statistical difference with $p<0.05$

To quantitatively assess the collagen-related changes, we applied GLCM texture analysis to the SHG images (Figure 3.6 A). The correlation feature extracted from the GLCM provided an estimate of collagen fibres organization and structure. By using Gray-Level-co-occurrence-matrix (GLCM) we evaluated the correlation (*Cor*) of the collagen network in order to detect the transition of the network from a fine to a wavy architecture (Figure 3.6 B).

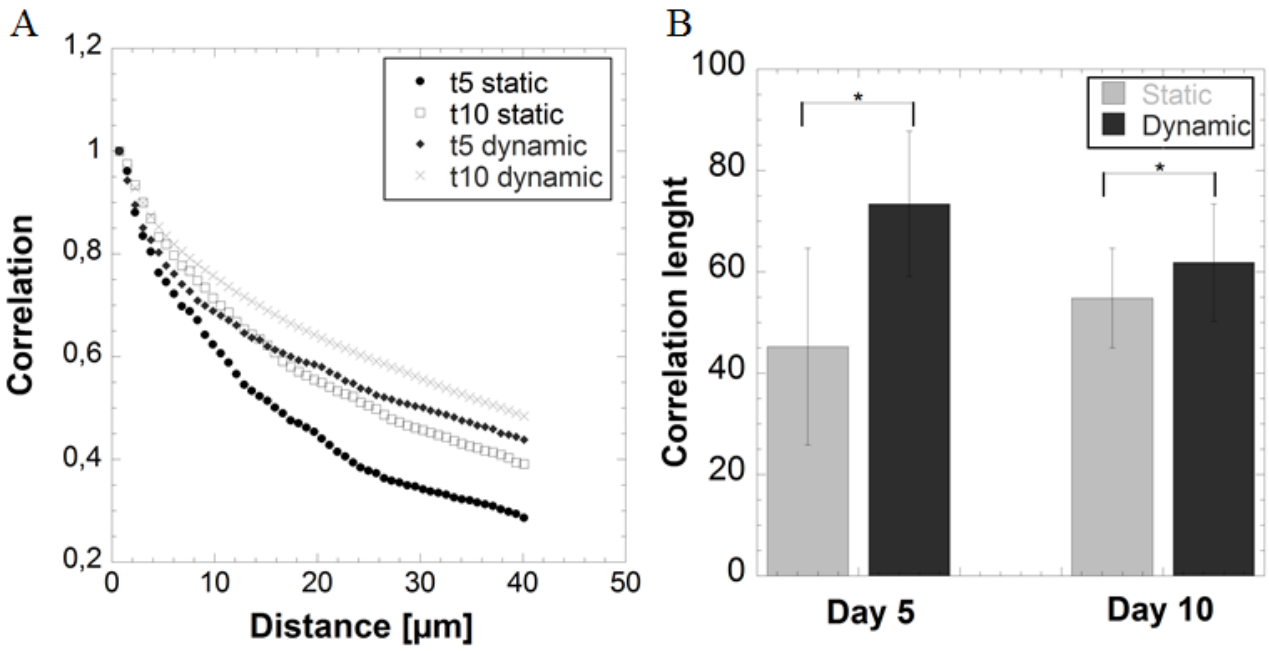

Figure 3.6: Correlation curve as function of distance in of 3D-ISEs in static and dynamic condition at day 5 and 10 (A). Correlation length obtained by fitting parameters from normalized correlation curves (B). Asterisks indicate statistical difference with $p<0.05$.

3.3.5 Organotypic intestinal culture development

Intestinal microtissues were transferred in a maturation chamber into a spinner flask in order to obtain their moulding in a disk shaped construct (1mm high, 6.4 mm diameter). After two weeks the 3D-ISE were collected from the spinner flask and used to perform static and dynamic culture, or they were seeded with Caco-2 cells in order to obtain 3D-HIEs samples which are cultured in the same static and dynamic conditions. In Figure 3.7 A is the reported the phase of the µTPs loading in the maturation chamber. Figure 3.7-B,C shows how 3D-ISEs looked after two weeks of maturation in a spinner flask. The 3D-ISEs removed from the mould disc-shaped, has a completely smooth surface, remains intact and shows a certain elasticity and firmness.

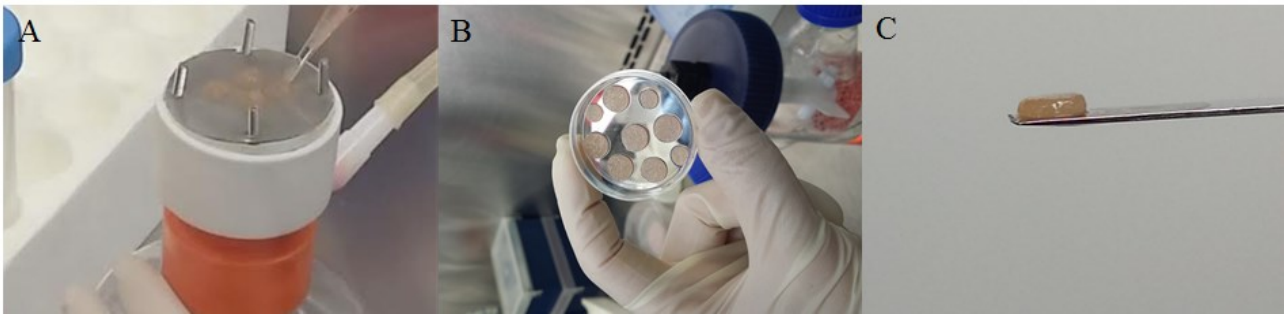

Figure 3.7: HD-µTPs moulding in the maturation chamber (A); Two pictures(B,C) of the 3D-ISE obtained. The organotypic intestinal tissues are smooth and disk shaped after 2 weeks of maturation

3.3.6 Histological analysis

To evaluate the morphological features of the 3D-HIEs, histological analysis were performed. The 3D-HIEs were stained with Haematoxylin and Eosin at day 5 and 10 in static and dynamic conditions, as shown in Figure 3.8. The H&E staining of 3D-HIEs showed the epithelial stratification and organization of the samples. For samples in static conditions (Figure 3.8 A,B), the epithelial thickness is lower compared to samples in dynamic conditions (Figure 3.8 C,D).

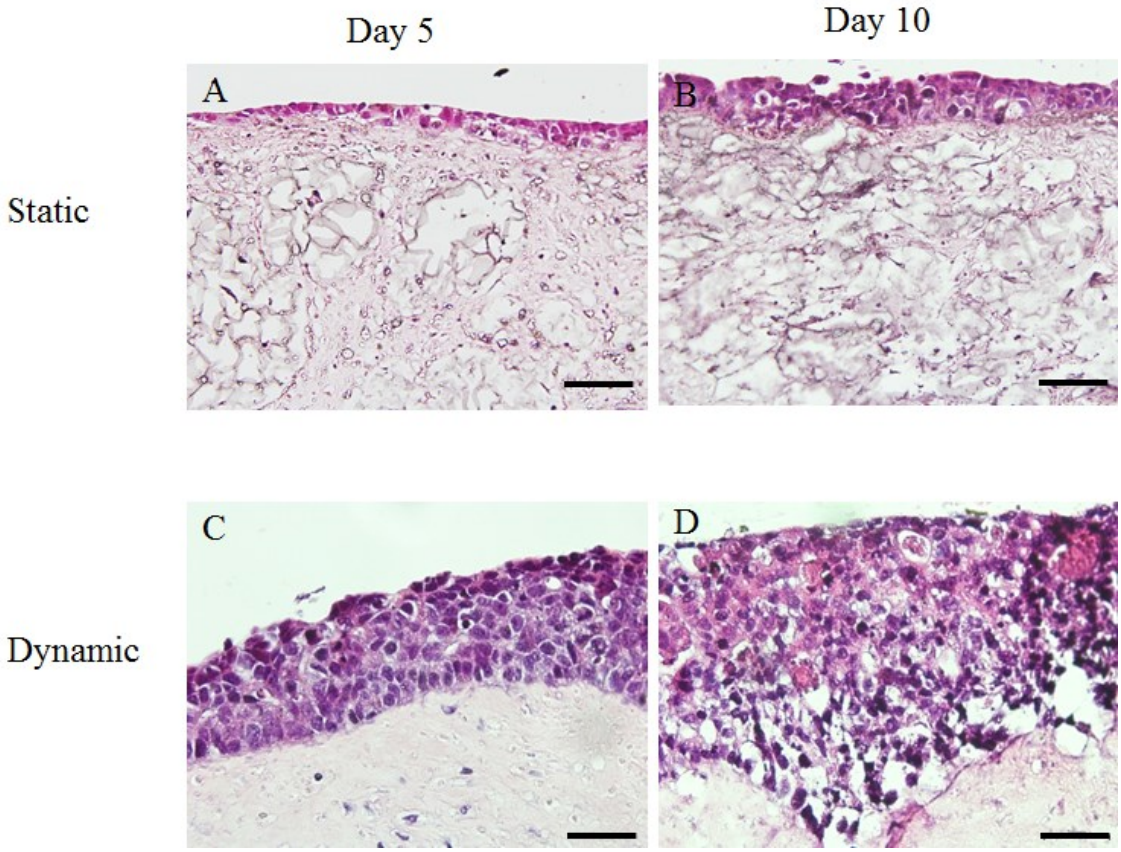

Figure 3.8: Histological images of Haematoxylin and Eosin of 3D-HIEs under static (A-B) and dynamic culture (C-D) compared at different time point. 3D-HIEs in both static and dynamic condition at day 5 (C) and day 10 (D). Scale bar 50 µm.

3.3.7 Immunofluorescence analysis

In order to study the epithelial differentiation in static and dynamic air liquid interface conditions, we perform immunofluorescence of ZO-1 and villin. In Figure 3.9 and Figure 3.10 are reported immunofluorescence images of these markers. As shown in the pictures Figure 3.9, for 3D-HIEs in static conditions lower fluorescent of signal is present than samples in dynamic conditions.

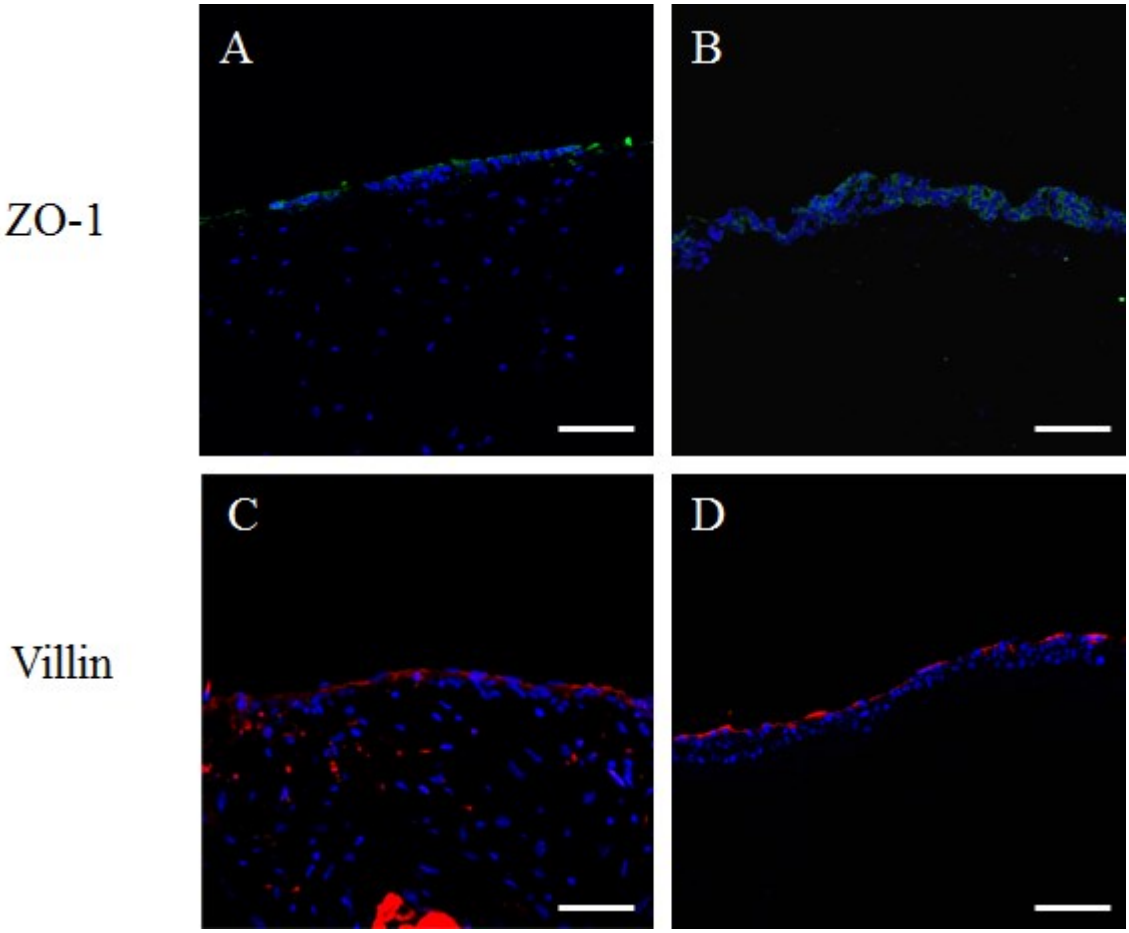

Figure 3.9: Immunofluorescence staining of ZO-1 (A-B) and villin (C-D) in static culture conditions. Scale bar 100 μm.

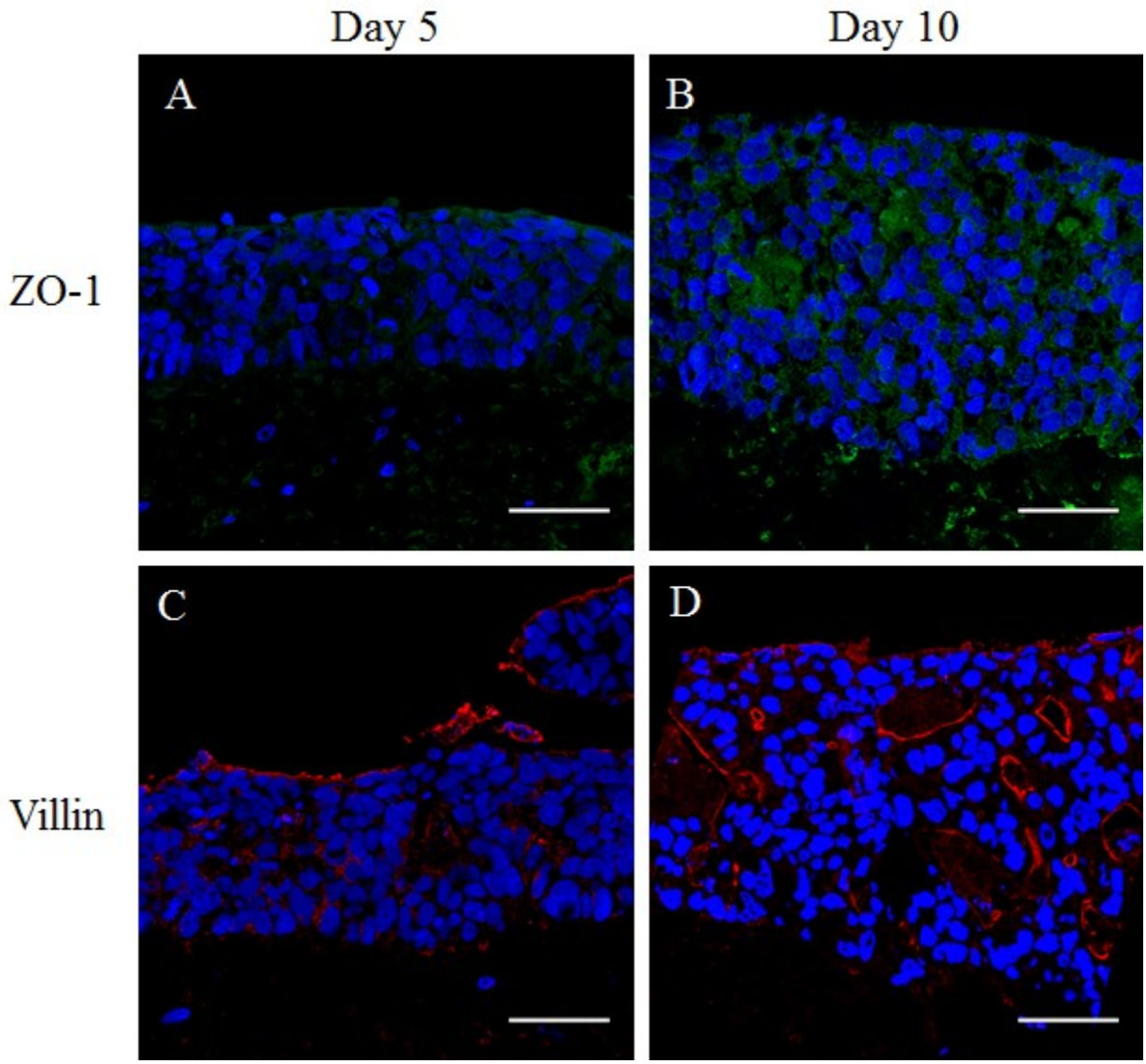

Figure 3.10: Immunofluorescence staining of ZO-1 (A-B) and villin (C-D) dynamic culture conditions. Scale bar 50 μm.

As reported in Figure 3.9 and Figure 3.10, ZO-1 staining is presents for all the samples but at day 5 the signal its low and not form a grid, instead visible in the 3D-HIEs section at day 10 (Figure 3.10 B) . In Figure 3.9 C-D and Figure 3.10 C-D, are represented the immunofluorescence images of villin a marker of differentiation expressed in the intestinal micro *villi*. At day 5 in static (Figure 3.9 C) and dynamic conditions (Figure 3.10 C), villin is expressed only in the apical part of the epithelium indicating a principle of differentiation, anyway it was not organized as well as in the 3D-HIEs at day 10 in dynamic conditions, where it forms a well-oriented epithelium.

3.3.8 Alkaline Phosphatase assay (ALP Activity)

With the aim to study the epithelial differentiation, alkaline phosphatase assay was carried out in both static and dynamic conditions. In Figure 3.11 the graphs showed the ALP released in the

culture media for air liquid interface culture in static and dynamic conditions. ALP activity is higher as time of the culture goes up and in dynamic air liquid interface conditions, indicating major cells differentiation.

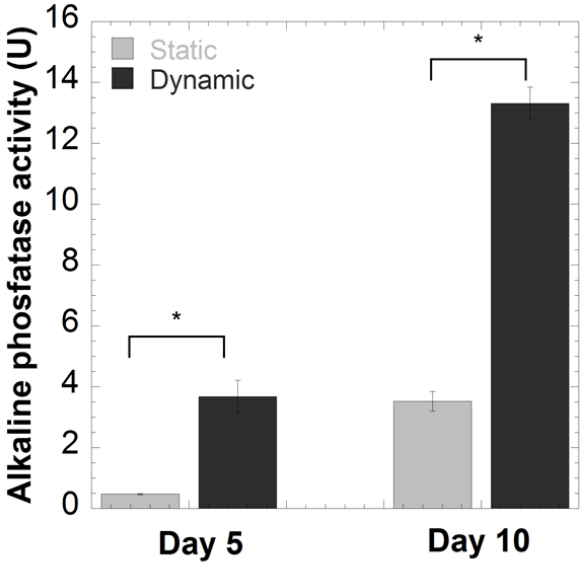

Figure 3.11: Effect of culture conditions on the epithelial differentiation. Alkaline phosphatase activity in both static and dynamic conditions at day 5 and day 10. Asterisks indicate statistical difference with $p<0.05$.

3.4 Discussion

In this work we have designed and fabricated a microfluidic bioreactor able to perform an air-liquid interface culture of 3D human intestinal equivalent and to maintain viability and cells differentiation for the culture time. In the preliminary experiment we tried different flow rate in order to choose the better dynamic culture conditions for the 3D-HIEs. In the first part of the study we perfused agarose disks to simulate the intestinal tissue equivalent in the gut-on-chip device. For the static condition (Q=0 µL/min), there was a non-uniform permeation of the food colouring solution, indicating that the apical part of the tissues were not nourished. In both Q=40 µL/min and Q=1000 µL/min the agarose disks are completely filled with the blue solution. With the aim to assess the optimal dynamic culture conditions, numerical simulation were carried out. The CFD simulations showed that at flow rate Q=1000 µL/min, the oxygen concentration was higher in all the part of the sample due to the increased contribution of convective transport, since the velocity field was higher. Operating in static conditions, the convective contribution was the lowest but the diffusive contribution is not adequate to perfuse and feed all the part of the sample. The same situation was presented in the simulation at flow rate of 40 µL/min. A little convective contribution was obtained but it is still too low to guarantee the optimal culture conditions.

Taking into account these results, experimental session were carried out for the two culture conditions, 0 and 1000 µL/min on 3D-HIE and 3D-ISE. To obtain 3D intestinal stromal

equivalent, intestinal μTPs were molded into a maturation chamber in spinner flask, in a tangential flow conditions that provide nutrient supply and waste removal during maturation time. 3D human intestinal equivalent were obtained by Caco-2 seeding on the 3D-ISE in a transwell insert.

The maintenance of the 3D-HIEs was assessed by the formation of desired intestinal epithelial layers, the integrity of each layer, as well as the differentiation of the epithelium. The H&E staining of 3D-HIEs histology sections from day 5 to day 10 demonstrated the integrity of intestinal epithelial layers in static and dynamic conditions. Stratification of Caco-2 was observed 5 days after raising the culture to the air-liquid interface in both static and dynamic culture. Maximum stratification was observed at day 10 for samples in dynamic conditions. The epithelium appeared well organized and differentiated. For the static culture, the epithelial thickness is lower than tissues in dynamic conditions, indicating a lower provision of oxygen and nutrients [143]. The dynamic culture into the gut-on-chip device of the 3D-HIEs, mimic the in vivo flow of small intestine, leads to an improved gas and nutrients transport. These results are confirmed by the numerical CFD simulations.

To evaluate the formation of a continuous and pluri-stratified cell layer, the tight junctions of the Caco-2 cells were stained by immunofluorescence assay of ZO-1. This protein contributes to cell-cell bonds between cells. A network of ZO-1 was expressed on the tissue section of 3D-HIEs samples in both static and dynamic culture conditions. Anyway a more dense grid of this tight junction protein is expressed in the 3D-HIEs in dynamic conditions indicating that the fluid flown conditions increase the tightness of the intestinal epithelium [144]. Moreover the morphological differentiation of Caco-2 cells was investigated by staining villin. Villin is an actin binding protein present in the brush border membrane, expressed in particular in *villi* than in the crypts. This differentiation marker was performed on both static and dynamic 3D-HIEs sample. The villin signal is higher in the gut-on-chip device indicating that cell differentiation occurs faster in the dynamic culture conditions. Higher cells differentiation under dynamic conditions was confirmed by ALP assay which shows increased production of this enzyme for 3D-HIEs in gut-on-chip device. Our results are in agreement with literature studies, indeed other researchers compared dynamic conditions to the static one. Cells cultured on the device exhibited accelerated intestinal epithelial cell differentiation, formation of *villi*-like structures and increased intestinal barrier functions [111].

In order to estimate the interaction between stroma and epithelium regulate the gut homeostasis and disease, we observed ECM organization and remodelling of 3D-ISE in dynamic conditions. To achieve that, 3D intestinal stromal equivalents were collected from the spinner flask and accommodated into the intestine chamber of the gut-on-chip device.

We performed several specific analysis about samples' ECM remodelling during culture time in both static and in microfluidic conditions, using SHG imaging. SHG is becoming an intrinsic biomarker to evaluate ECM changes and remodelling, since it leads the visualization and quantification of collagen matrix change also *in vivo*. SHG imaging has been performed on static and dynamic 3D-ISEs in order to highlight responsiveness and structural difference in collagen organization in fluid flown conditions. In SHG images of 3D-ISEs, in static conditions, the fibres appear short, thin, loosely packed. On the contrary in dynamic conditions in the 3D-ISEs image is possible to observe an intense SHG signal that displays a denser matrix with collagen bundles much tighter more organized.

Furthermore, we assessed the collagen fibre morphology revealed by SHG in a quantitative manner by using texture analysis. One of the most important statistical texture method is the grey level co-occurrence matrix (GLCM). In combination with SHG, GLCM is used to quantify the collagen fibre size, arrangement and distribution of the collagen fibrillary bundles [145].

The GLCM characteristic curves calculated, provide information for detailed morphological characterization of the collagen fibres, allowing to further sights into various physiological and pathological processes, such as the structural modification of the extracellular matrix during the migration and invasion of tumour cells.

We quantified the collagen structure by using GLCM texture analysis and evaluating the difference between the more dense fibre then fine fibrils. To achieve this, we performed GLCM analysis on 3D-ISEs at day 5 and day 10 in static and dynamic culture condition, the correlation curves of all the sample exhibited a decrease of the correlation as pixel distance increase, indicating that the collagen matrix is distinct [146]. According to the literature, the correlations curves give information about the fibre size of collagen bundles. In particular as reported by Hu et al. [147], the collagen fibres size may be estimated by the distance between the y-axis and the first valley of the curves. As reported in our correlations curve the 3D-ISEs in dynamic conditions at day 10 exhibited the higher correlation curves, followed by the sample at day 5. The lowest correlation curves was obtained for the 3D-ISEs at day 5 in static conditions, indicating smaller and thin collagen fibre. These results indicates that the endogenous ECM of the 3D-ISE is subjected to a faster remodelling in dynamic conditions. This data is also confirmed by the CAD analysis which shows higher assembly degree of collagen in dynamic conditions.

About the quality of the collagen fibre, we performed Picro Sirius Red staining, leading us to evaluate the level of maturation of collagen fibre. The colour of collagen fibres stained with Picro Sirius Red and viewed with polarized light depends upon fibre thickness; as fibre thickness increases, the colour changes from green to red [140]. In our experiments, mature collagen content

increased in dynamic conditions and as culture time rose. On the contrary, immature fibre content goes down for sample in microfluidic flown conditions. This results are in agreement with previous studies in which it was assessed that Caco-2 cells exhibit higher proliferation, increased production of phosphatase alkaline when cultured in presence of ECM protein like collagen and laminin, despite of plastic surfaces [148].

3.5 Conclusion

In this study, we demonstrated a microfluidic platform that allows long term maintenance of 3D-HIEs and 3D-ISE in an air-liquid interface culture in micro-scale setting, for the purpose of drug testing and intestinal absorption evaluation. The dynamic fluid flown conditions allows more stratified and differentiated epithelium in less time compared to the conventional transwell culture. Since the interaction between cells and ECM are fundamental to maintain the homeostasis of the tissues, we assessed ECM organization in our gut-on-chip device concluding that the gut-on-chip is valid to speed up the remodelling processes.

The gut-on-a-chip, along with the mathematical model described here, can be used to estimate intrinsic intestinal transport properties and the effects of ingested nanoparticles. Overall, the gut-on-a-chip is a user-friendly and cost-effective in vitro platform for drug testing of candidate molecules for intestinal first-pass evaluation.

Chapter 4

Human first-pass metabolism on a chip

4.1 Introduction

The two organ that play a major role in the process of absorption, distribution, metabolism and excretion of xenobiotics (ADME) are the liver and the intestine. Oral administration of drugs is the most preferred route of administration because it is easy and comfortable for the patients.

After oral absorption, xenobiotics are eventually absorbed from the small intestine, thanks to its particular physiological properties with folds, *villi* and micro *villi*. Xenobiotics may further be metabolized by intestine, through an intestinal first-pass effect. Then and other metabolites are directed to the liver where they are further metabolized, excreted and more generally detoxified.

The intestinal and the hepatic first-pass effects is involved mainly in the reduction of bioavailability of drugs and xenobiotics, which is important for the study of this two organs, both in terms of the development of new therapeutic substances, but also for toxicity testing [149]. For this reason, it is fundamental to study their functionalities with experiment performed *in vivo* and *in vitro*. However, conventional *in vitro* and *in vivo* testing are really expensive, rise ethical problems and are unable to reproduce accurately the cellular response of the intestine and liver [150]. Typical methods consist in static cell culture of human cell line in Petri dish or in transwell insert. 2D cultures are really easy to handle and are commonly used to monitor the metabolism and toxicity of xenobiotics on a short term, but they have the disadvantages of not recapitulating the in vivo cellular microenvironment. In this culture conditions, primary cells dedifferentiate quickly and exhibit low metabolic activity, implying low predictability of those models [151]. New *in vitro* platform have been established in recent years to overcome these problems. One of these models consists of using microfluidic devices, which exhibit many advantages like the better control of the microenvironment, the state of differentiation of the cells and the perfusion new medium continuously [152]. Using microfluidic device it is possible to recreate organ to organ interaction in order to mimic first-pass metabolism between intestine and liver. Several model have been proposed in the last years. For example, Prot et al. developed polycarbonate bioreactor where the Caco-2 cells were cultivated on a conventional cell culture insert. The insert was then incorporated into a dedicated fluidic platform that could be coupled with a microfluidic biochip which is cultivated with HepG2/C3a, freshly isolated rat primary hepatocytes and human cryopreserved hepatocytes, for comparative purposes. First-pass intestinal absorption and liver

metabolism were studied using phenacetin. In addition, a mathematical model was built based on the experimental data. The corresponding PK model was used to estimate the kinetic parameters describing the transfer of the molecule across the intestinal barrier, as well as intestinal and hepatic clearances. Finally organ mathematical models were used to predict situations in humans [116]. However, this kind of model lack of the three dimensional architecture and also the experimental set-up is quite bulky. Since 3D culture replicate better the hepatic and intestinal *in vivo* physiologic environment, Midwoud et al. designed a microfluidic system for the purpose of investigating inter-organ effects, made by coupling two micro-chambers, one containing an intestinal tissue slice, the other a liver slice, which can be sequentially perfused. In this way, metabolites formed by the intestine in the first chamber can be directed to the liver in the second chamber for further metabolism, thereby mimicking *in vivo*, first-pass metabolism [117]. Nevertheless, tissues slices have poor availability, especially for human tissues, lose viability in few days of culture, and are difficult to use in high-throughput studies, making this model not so convenient. In perspective, in order to combine 3D tissues and microfluidic devices, we design and developed a microfluidic device which interconnect 3D human intestinal equivalent (3D-HIE) and HepG2-microtissues in a perfusion microdevice. 3D-HIE were obtained by bottom up approach, using intestinal microtissues moulded into a maturation chamber. The biochip recapitulate the intestinal and hepatic first-pass mechanism of ethanol using a selective transport from the upper to the lower part of the device.

4.2 Materials and Methods

4.2.1 Cell type

HepG2 were provided by American Type Culture Collection (ATCC). Cells were sub-cultured onto 150 mm Petri dishes in Minimum Essential Medium Earle's Salt (Microtech) containing 10% fetal bovine serum, 100 μg mL^{-1} L-glutamine, 100 U mL−1 penicillin/streptomycin, 0.1 mM Non Essential Amino Acid and 0.1 mM Sodium pyruvate. Caco-2 cells were provided by American Type Culture Collection (ATCC). Cells were subcultured onto T-flask in Dulbecco Modified Eagle Medium with 10% of fetal bovine serum, 100 μg mL^{-1} L-glutamine, 100 U mL−1 penicillin/streptomycin. Cells were maintained at 37 °C in a humidified atmosphere containing 5% CO2. Culture medium for fist-pass metabolism on chip was obtained using HepG2 and Caco-2 medium in 1:1 ratio.

4.2.2 Intestinal microtissue precursors: fabrication and characterization

Gelatine microbeads having a diameter of 75-150 μm, stabilized by 4% of glyceraldehyde were fabricated by means of a modified double emulsion technique (O/W/O) as previously reported [85], [126]. Briefly, gelatine (type B Sigma Aldrich Chemical Company, Bloom 225, Mw 176,654 Da) was dissolved into 10 ml of water containing TWEEN 85 (6% w/v) (Sigma Aldrich Chemical Company) at 60 °C. Toluene containing SPAN 85 (3% w/v) (Sigma Aldrich Chemical Company) was continuously added to the aqueous gelatine solution (8% w/v) to obtain primary oil in water emulsion. Microbeads of gelatine containing droplets of toluene were produced through the addition of excess toluene (30 ml). After cooling below 5 °C, 20 ml of ethanol were added to extract toluene and stabilize gelatine microbeads. The resulting microspheres were filtered and washed with acetone and then dried at room temperature. To make the intestine-μTP, spinner flask bioreactor (250 ml, CELLSPIN, Integra Biosciences) was inoculated with Human sub-epithelial myofibroblasts (ISEMFs) extracted ileal biopsy after informed consent at a cell density of 10^5 cell/ml and a gelatin microbeads density of 2 mg/ml (corresponding to $5*10^3$ beads/mg), in order to obtain an initial ratio of 10 cells per microbeads. The culture suspension was stirred intermittently at 10 rpm (5 min stirring and 30 min static incubation) for the first 6 h post-inoculation to allow cell adhesion, and then continuously at 30 rpm up to 10 days [126]. All cultures were maintained at 37 °C in a humidified 5% CO2 incubator. Three times per week the media was replaced and 2-O-alpha-D-Glucopyranosyl-L-ascorbic Acid 0.5 mM (TCI Europe) was added. Human intestine microtissue precursors (HI-μTP) were harvested at different time points of spinner cultures to perform the complete characterization.

4.2.3 Three-dimensional human intestine equivalent production

3D intestinal stromal equivalents (3D-ISEs) were produced by transferring the HI-μTP into an opportunely designed assembling chamber which contains a silicon mold with disc-shaped spaces (1 mm in thickness, 5 mm in diameter) where the HI-μTP biological assembling takes place. Stainless steel rigid grids are posed directly on the both sides of the system and two polytetrafluoroethylene (PTFE) rings are placed on the grids on both sides of the system and are fastened to each other by means of stainless steel screws, which close the system and ensure that the HI-μTP are retained. The system is autoclavable in each part. Furthermore, the assembling chamber was placed on the bottom of a spinner flask and completely bordered by culture medium.

The spinner was operated at 60 rpm and the medium was exchanged every 3 days. After 2 weeks of culture the assembling chamber was opened and the 3D-ISEs were collected. Samples were accommodated in transwell insert (diameter, 6.5 mm; Corning) for static culture with basolateral chamber filled with 600 μL over a period of 5 to 10 days. At the end of the experiment, 3D-ISEs were taken from the insert for further investigation and fixed.

In order to produce three-dimensional human intestine equivalents (3D-HIEs), organotypic epithelial cultures were developed. To this aim, 3D-ISEs we obtained as reported in Par. 3.2.5(0.5 cm diameter) were rinsed with three washes of PBS solution, then the PBS was removed and the 3D-ISEs were accommodate in the transwell inserts and allowed to dry for 5 min under laminar flow. Subsequently, 50 μL of the Caco-2 suspension was seeded to the center of each 3D-ISE, corresponding to $2x10^5$ cells/3D-ISE. The transwell insert was incubated for at least 2 hours in incubator at 37°C with 5% CO_2 to allow the cells to adhere onto the 3D-ISE surface. Then 200 μL of DMEM was added into the apical chamber of the transwell insert taking care not to dislodge cells from 3D-ISEs and the basolateral chamber was filled with 600 μL of DMEM, in order to perform a submerged culture that promoted Caco-2 horizontal spreading. Submerged culture lasted approximately 7 days. Then, an optimized air-liquid interface culture lasting 2 weeks took place in order to induce the epithelial tissues to differentiate and stratify. The culture medium was replenished on the first day and every 2 days until the end of the experiments.

4.2.4 HepG2-Microtissues production

All cell cultures on microscaffolds were performed in spinner flask (Integra). Briefly, 35 mg of GPMs were loaded with $5{,}25 \times 10^6$cells (30 cell/GMP ratio). To promote cell seeding on GMPs an intermittent stirring regime (30 min at 0 rpm, 5 min at 30 rpm) for 24 h. After seeding, the stirring speed was kept at a continuous 30 rpm for up to 14 days. Culture medium were changed every two days. All cultures were maintained at 37 °C in a humidified 5% CO_2 incubator. The HepG2 microtissues precursors obtained (HepG2-μTPs) samples were taken for further investigations at days 3, 5, 7, 10 and 14 and fixed for further investigations.

4.2.5 Microfluidic device fabrication

The microfluidic first pass-on-a-chip device used in this work was fabricated by a rapid prototyping procedure. The PMMA master mold was designed by AutoCAD and carved with micromilling machine (Minithech CNC Mini-Mill) making a relief positive geometry to avoid silanization process of PDMS. The ratio of PDMS pre-polymer and curing agent was 10 : 1 (w/w), then the mixture was degassed under vacuum for 20 min to remove air bubbles and then poured on

PMMA masters. The set-up was incubated at 80 °C for 60 min, then peeled off from master molds. Inlet, outlet and μTPs holes were punched with a 2.5 mm biopsy punch (DifaCooper) while gut chamber was punched using a 9.5 mm puncher (Am-Tech). Then the PDMS device was bonded to a glass microscope slide (24 mm wide × 60 mm long) by oxygen plasma treatment for 1 min at 50 W in an oxygen plasma oven (Plasma Femto, Diener).

The devices is divided into two parts, the gut and the liver part which are connected by a central channel. The gut part was designed with a central microchannel (1.2 mm wide × 40 mm long × 0.6 mm high) which transported the medium into a gut chamber (9.5 mm diameter × 5mm high).

The liver part, communicate with the central gut microchannel which was separated from three parallels tissue chamber (0.5 mm wide ×0.3 mm high × 1 mm long) by small pillars (0.100 mm diameter × 0.09 mm pillar interspace). A middle collection channel (0.5mm wide × 0.3 high) was used to collect tissue supernatants.

Finally the PDMS layer was bonded to glass coverslip by oxygen plasma treatment for 1 min at 50 W. Then, the whole setup was incubated at 80 ºC overnight to achieve irreversible bonding of the two PDMS layers. Then a transwell insert was placed into the 9.5 mm holes of the biochip. To obtain the selective transport of fluid from the apical part of the epithelium to the basal part, then to the liver compartment, sealing gasket were fabricated. In particular, PDMS gasket was fabricated by punching of 1 mm thick PDMS layer, first with a 4 mm puncher (for the inner hole) and then with a 6.5 mm puncher (for the outer hole). PMMA hollow cylinder (5 mm high, 1 mm thick) was fabricated with Micromilling machine. Once transwell insert with 3D-HIE was inserted into the biochip, PDMS gasket was placed over the surface of the 3D-HIE. Then PMMA cylinder was put in the transwell insert. To avoid bacterial contaminations, the intestine chamber was closed laying a 100 μm PDMS membrane fabricated by spin coating of PDMS (750 rpm × 30s). The PDMS biochip was sterilized by autoclave, while PDMS gasket and PMMA cylinder were sterilized by UV light.

4.2.6 First-pass on a chip culture conditions

The perfusion culture of first-pass device was structured into different phases. The first phase was devoted to the Caco-2 differentiation over 3D-HIEs surface for a period of 21 days. The second phase was focused on the fabrication of the HepG2-μTP in a spinner flask bioreactor 4.2.4, then the third phase consists in the accommodation of transwell insert, gasket and PMMA cylinder into the first pass device, at the same time HepG2-μTPs from day 5 to 7 were collected from the spinner flask and loaded into the first-pass device. The final phase consists into the connection of all the experimental set-up to a syringe pump. Since the gut epithelium was already stratified we

didn't have to use the flow rate used for gut-on-chip device (Q= 1000 µL/min) (as reported in 3.2.7), moreover this flow rate could carry away the HepG2-µTPs loaded into the biochip. Whereby, the final flow rate of the first-pass-on-chip device was set to 5 µL/min. Culture medium was a combination of half HepG2 medium and half Caco-2 medium. To simulate oral ingestion of compounds, 300 µL of culture media diluted with 400 mM of 100% ethanol were diluted in culture medium and added in the PMMA cylinder over the 3D-HIE. In each experiment three parallel device were carried out, one without ethanol treatment, two treated with ethanol 400 mM, one stopped after 24h and the second after 48h of culture.

4.2.7 Measurement of selective permeation properties

To simulate oral drug ingestion and selective permeation of compounds, 5 µg/ml of 3KDa FITC-Dextran solution were dissolved in HepG2-Caco-2 medium and flew in the first pass device for 24h and 48h. At each time point Dextran permeation measurements were conducted with a laser scanning microscope (TCS SP5, Leica). Samples were illuminated with a 25X (NA 0.95) objective and 488 nm excitation line from Argon laser operating with 5% output power.

4.2.8 Immunofluorescence assay

At 24h and 48 h, 3D-HIEs samples were withdrawn from the first-pass device and fixed with 4% paraformaldehyde for 20 min and then rinsed in PBS. For immunofluorescence staining of 3D-HIEs, samples were incubated inti permeabilizing solution (0.2% Triton X-100 + 3%BSA + PBS) for 10 min. After blocked for 1h at RT, primary antibody (anti-human Claudin-1, 1/40, Abcam) was incubated for 1h at RT. Then, secondary antibody incubation, goat AlexaFluor 546-conjugated anti-rabbit IgG antibodies was incubated for 1h. Cells nuclei were detected by DAPI staining (5 µm/mL, Sigma Aldrich).

4.2.9 Alcohol dehydrogenase release assay

The culture media supernatant from first-pass on chip device each devices was collected for the evaluation of alcohol dehydrogenase (ADH) release. Culture media supernatants accumulated in the reservoir and in the PMMA well, were collected and stored at -20 °C before being analysed. ADH activity was performed, using Alcohol Dehydrogenase Activity Detection Kit (Abcam) according to the manufacturer's protocol. Briefly, 50 µL of sample or NADH standard were added to a well of a 96-well microtiter. Then reaction mix was added to each well and after 2-5 min the absorbance at 450 nm was measured using a microplate reader, in this way a $T_{initial}$ was fixed.

Subsequent measurement were lead every 5 min until the value of the most active sample is greater than the value of the highest standard, the time of the penultimate reading is T_{final}. The ADH activity was evaluated by the following equation:

$$ADH = \frac{B \times Sample\ diluition\ factor}{Reaction\ time\ \times V}$$

Where B is the amount (nmole) of NADH generated between $T_{initial}$ and T_{final}, reaction time is the difference between T_{final} and $T_{initial}$, and V is the sample volume. ADH was expressed as mUnit/mL.

4.2.10 Statistical analysis

The differences between two or more groups were evaluated (p value < 0.05) using one-way analysis of variance (ANOVA). A Gaussian distribution for each population was assumed. For pair-wise comparisons within each experimental group, Tukey's post-test was used.

4.3 Results

4.3.1 Microfluidic device fabrication

We developed a microfluidic device to replicate first pass metabolism mechanism. The Figure 4.1 A shows the geometrical configuration of the biochip, composed by an intestine compartments filled where a transwell insert accommodated inside filled with the 3D-HIE, after 21 days of air-liquid culture. PDMS gasket and PMMA cylinder were used to avoid that non selective passage of the compound, form the apical side to the basolateral part. The liver's part is designed as previously described in par. 2.10. The HepG2-μTPs were collected from the spinner flask form day 5 to 7 because the exhibit the best performance in terms of viability and hepatic functionality, as reported in Chapter 2. They loaded into the liver compartment by pipetting via the three appropriate inlet. The entire set-up was connected to a syringe pump (flow rate 5 μL/min) and a reservoir in order to have a dynamic fluid flow condition and to collect the tissues supernatants respectively. Figure 4.1 B shows the top view of the first pass bioreactor.

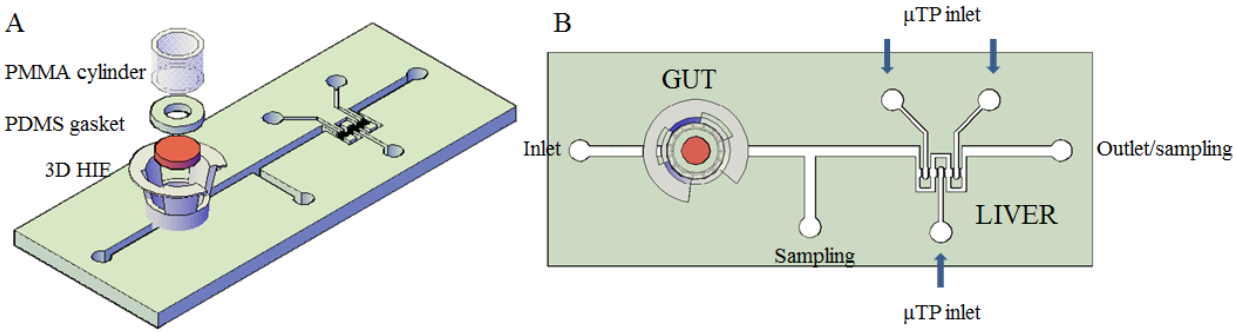

Figure 4.1: (A) Lateral view of the first pass bioreactor with details of each sealing part in order to have selective permeation of the drug. (B) Top view of the first pass device that shows inlet, outlet and HepG2-µTPs port. Whole set-up was connected to a syringe pump.

4.3.2 Measurement of selective permeation properties

In order to study the selective transport of drugs from the bottom part of the device, we simulate it by using 3kDa FITC-Dextran. Dextran was diluted in the perfusion culture media and added to the apical part of the gut compartment, using PMMA cylinder as a well. After 24h, confocal images of the 3D-HIE and HepG2-µTPs were taken in order to evaluate if dextran solution crossed and permeated 3D-HIE (Figure 4.2) .

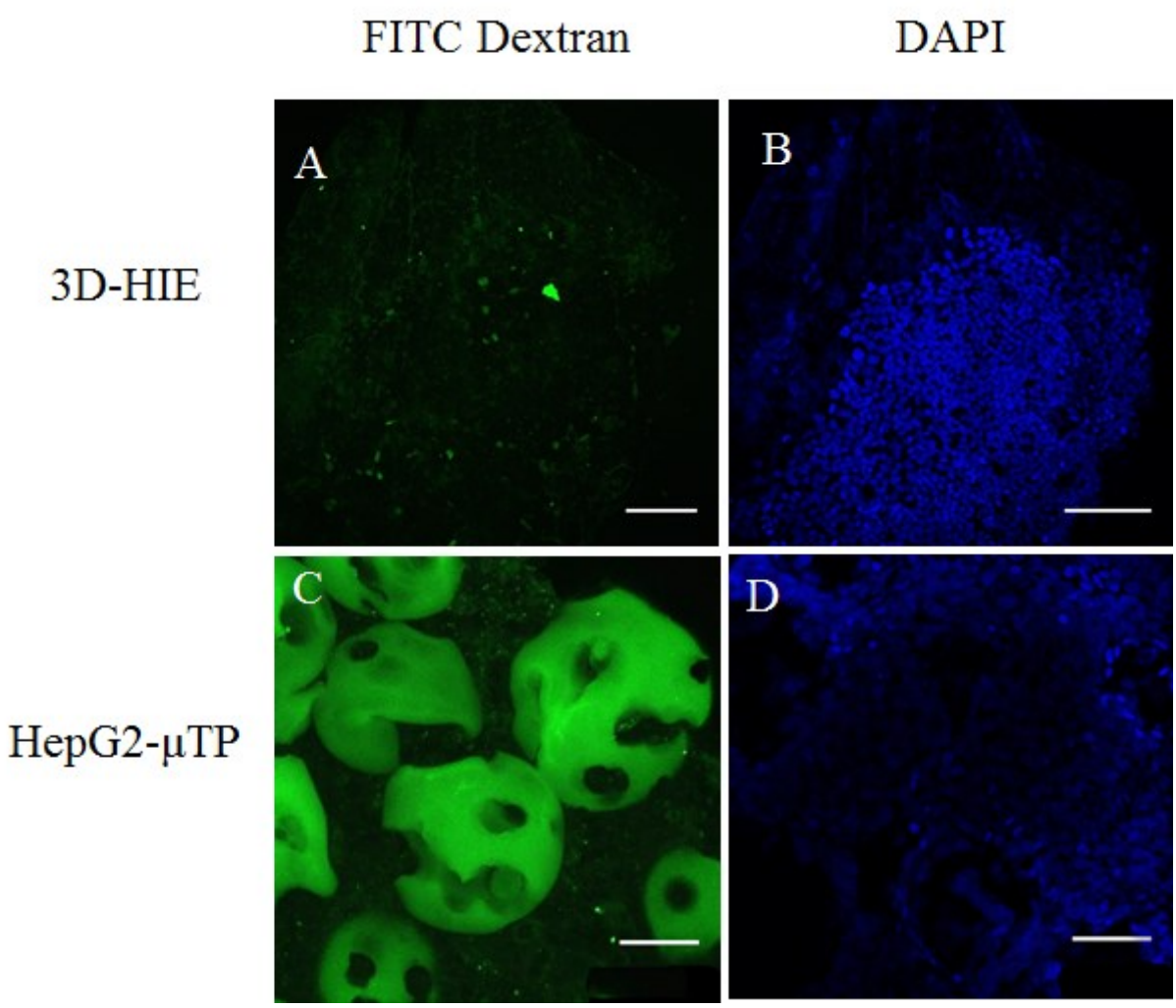

Figure 4.2: FITC Dextran 3kDa and DAPI cells staining images of 3D-HIE(A,B) and HepG2-µTPs (C,D) after 24h of perfusion culture into the microfluidic first-pass device. Scale bar 75 µm.

4.3.3 Immunofluorescence assay

To determine the effect of ethanol on the integrity of the tight junctions, 3D samples were stained for claudin-1. In Figure 4.3 were reported the images of this tight junction marker. Higher expression intensity of claudin-1 was observed for control group 3D-HIE compared to the ethanol treated group at 24h (Figure 4.3 B) and 48h (Figure 4.3 C).

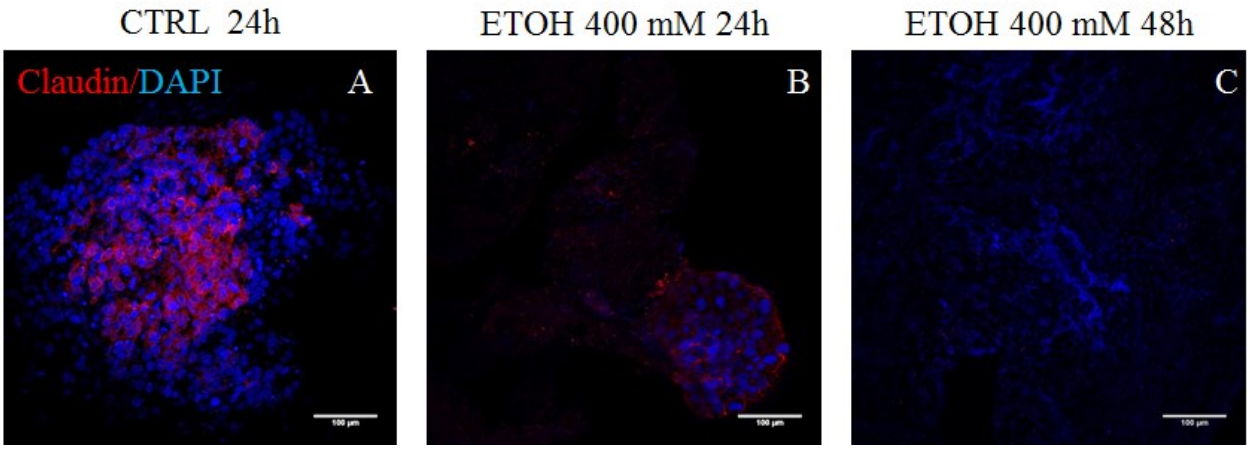

Figure 4.3: Imunofluorescence of 3D-HIE for claudin-1 for control (A) at 24h and ethanol treated group at 24h (B) and 48h (C). Scale bar 100 μm.

4.3.4 Alcohol dehydrogenase release assay

In order to evaluate the metabolic activity of the gut and liver tissues equivalent we measured the release of alcohol dehydrogenase, an enzyme which plays a crucial role in ethanol metabolism. Measurement of ADH activity in the eluent showed that both hepatic and intestinal cells produced this enzyme during culture time, in response to ethanol treatment. Exposure to ethanol levels at 400 mM resulted in an higher ADH released in tissues supernatant of both gut and liver tissues equivalent, compared to the only gut contribution (Figure 4.4).

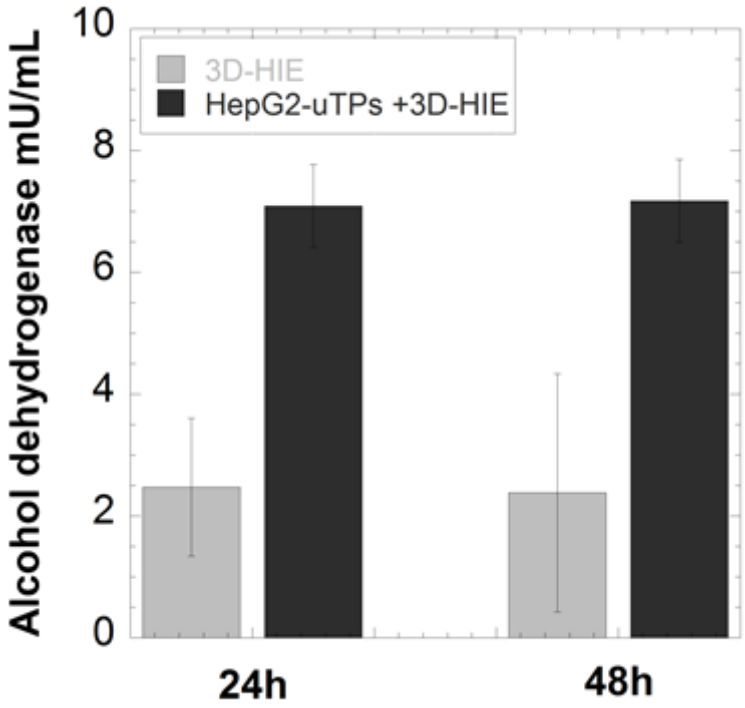

Figure 4.4: Alcohol dehydrogenase release assay after 24h and 48h of 400 mM ethanol treatment. Tissues supernatants were collected from the PMMA cylinder, for the contribution only of 3D-HIE, and from the reservoir for the contribution of both HepG2-µTP and 3D-HIE.

4.4 Discussion

Intestinal and hepatic first-pass metabolism may depress extensively the bioavailability of drugs and xenobiotics compounds. Routinely classical *in vitro* studies consist of drug exposure of hepatocytes cultivated in suspension or in monolayer and in a monolayer in Petri dishes. Moreover, *in vitro* and *in vivo* oral bioavailability extrapolations are calculated using separate in vitro data obtained from cultures of Caco-2 (mainly permeability data) and of hepatocytes [153].

In this chapter we want to recreate and study the first-pass metabolism mechanism into a microfluidic device. Through the microfluidic device it was possible to simulate the *in vivo* route of orally ingested compound. To mimic such complex mechanism, we integrated on a chip the two mainly involved organs: gut and liver. For both gut and liver model we used 3D tissues engineered *in vitro*. In particular we recreate human intestinal equivalent by bottom up approach using fibroblast intestinal microtissues molded into a maturation chamber. We also developed HepG2-µTP obtained by dynamic cells seeding in a spinner flask bioreactor. In the chapter 2 and 3 we showed the dynamic culture in a microfluidic device for liver and gut model respectively. The connection between this two organ allows us to mimic the intestinal and hepatic first-pass metabolism on a chip. In the first part of the work we designed a microfluidic device, which it was constituted of the combination of the liver and gut on chip device. The main problem of the

recreation of first-pass metabolism is the maintenance of a selective transport route from gut to the liver part. To achieve this, we fabricated a kind of sealing chamber using a PDMS gasket accommodated over the 3D-HIE and a PMMA cylinder, acting as a well. To assess the permeation properties of the entire set up, we used FITC dextran. Dextran was diluted into the culture medium and added to PMMA cylinder, on the apical part of the 3D-HIE. Dextran solution perfuse the 3D-HIE space and reach the liver compartment, as demonstrated by confocal images after 24h of culture. Ethanol was selected as a model molecule to test if the gut-liver chip can reproduce first-pass metabolism of orally taken drugs. The staining of the nucleus and the claudin-1 of Caco-2 was performed to characterize the cell layer on the 3D-ISE after 24h of integration in the first-pass on chip device. Claudin is a transmembrane protein of tight junction. Tight junctions are fundamental in the studies of absorption and permeation of compounds, because they form a physical barrier to the diffusion of macromolecules. Loss of the tight junctions barrier leads to an higher absorption of toxin and xenobiotic compounds. Previous studies demonstrated that acetaldehyde rather than ethanol can cause the disruption of tight junctions in Caco-2 monolayer [154]. About this, the major pathway of oxidative metabolism of ethanol in the liver, involves alcohol dehydrogenase (ADH). Acetaldehyde is the metabolism product of the ADH. This compound is highly reactive and toxic so its accumulation cause the destabilization of the tight junctions and incremented permeation of endotoxin which play a crucial role in alcoholic liver disease[155],[156]. With the aim to assess the metabolic activity of ADH in our model we performed ADH release assay, collecting tissues supernatants. ADH measurement assessed that the contribution of 3D-HIE only leads to a lower contribution of the release of this enzyme.

4.5 Conclusion

In this study, we developed a microfluidic gut-liver with an aim of reproducing the first pass metabolism. 3D hepatic and intestinal equivalent were accommodated inside the chip and co-cultured in successful way verified by the dextran permeation assay. Changes in the metabolic and absorptive properties of both gut and liver cells were observed. Using ethanol as a model xenobiotics, we have shown that this device can be used as a tool to reproduce the first pass metabolism of drugs and xenobiotics. Although several improvements are still needed for more accurate reproduction of a PK profile, we think that our proposed model is a more predictive platform than cell culture in monolayer and resembles the physiological way route of the *in vivo* first-pass metabolism.

Chapter 5

Future perspectives

In this thesis we want to propose a platform to reproduce in vitro the first-pass metabolism's mechanisms. We focused on the two mainly involved organs in this mechanism , the liver and the gut. About liver, we firstly started to identify the 3D tissues that better reproduce the liver microarchitecture and functionality. We carried out a detailed comparison between two 3D model, spheroids, the most used three dimensional *in vitro* model, and the microtissues, our proposed 3D model. We demonstrated that the microtissues were more viable and functional during all the time of the culture then the spheroids, moreover the microtissues shows higher yield, are more easy to handle and are more suitable for long term culture. Since microtissues are a more predictive model of the liver physiology, we loaded them into a microfluidic device, which mimic the functional unit of the liver, the hepatic lobule. This biochip allowed the dynamic culture of the HepG2-μTPs, ensuring the maintenance of viability and it has been validated using ethanol, one of the major hepatotoxic compounds. However, this proposed model need to be optimized for several reasons. First of all, we used HepG2 cells that is an immortalized cell line, really easy to handle but with low expression of the specific hepatic markers. For this reason, the next step is to consider the possibility to use primary hepatocytes, in order to make this novel platform more similar to the human hepatic *in vivo* microenvironment. One other possibility to address is to consider the use of iPSC-derived human liver cells. Ultimately, personalized drug screening on mature iPSC-derived human liver cells could potentially allow custom drug therapies for different patients. Our liver-on-chip device allows the possible co-culture with non-parenchymal cells serving as a functional platform for understanding functional maintenance, cell–cell communication, cytotoxic metabolism, and inflammatory cascade in a liver sinusoid.

About gut-on-chip device, presented in the third chapter, we developed first a three dimensional intestinal tissue equivalent, obtained by bottom-up approach. The biohybrid is obtained by molding of intestinal fibroblasts microtissues into a maturation chamber. Once a 3D disk-shaped tissue was obtained, it was seeded with an intestinal epithelium using Caco-2 cell line. In this study, our aim was to compare the conventional static air-liquid culture, obtained in transwell insert, with a dynamic one using a microfluidic device. We proved that the shear stress imposed by the perfusion culture, allows the faster organization of the extracellular matrix secreted by the intestinal fibroblasts and assembled during the maturation step, compared to the static culture. Other important advantage of the dynamic culture, was expressed by the faster stratification and

differentiation of the gut epithelium, already after 5 days. The over mentioned model paves the way to new developed platform to assess the intestinal absorption of drugs, nutraceuticals and nanoparticles. The device can be adapted to reproduce human gut microbiome to provide a versatile platform for other host-microbiome ecosystems that can be found in various human organs, which may facilitate *in vitro* study of the role of human microbiome in orchestrating health and disease. About the biochip itself, it can be useable for the air-liquid culture of other epithelium like dermal or pulmonary ones.

In last part of the thesis we conclude the study of first-pass metabolism by introducing a simple microfluidic device which interconnect gut and liver, with the aim to simulate the anatomic and physiological connection. The proposed biochip, allowed the selective communication and passage of compound from the intestinal lumen to the liver tissues. Although other experiments needs to be performed, the biochip open the way to reproduce the first-pass metabolism of drugs and to resemble the *in vivo* condition in a more predictive way compared to conventional gut/ liver monoculture. With this new tool, it should be possible to gain a better insight into inter-organ interactions and elucidate unknown mechanisms involved in toxicity, gene regulation and drug–drug interactions. Accordingly, this microflow system will help minimize the gap between the in vitro and in vivo situation, and will moreover contribute to the reduction of the use of experimental animals.

Bibliography

[1] G. Liu, E. Franssen, M. I. Fitch, and E. Warner, "Patient preferences for oral versus intravenous palliative chemotherapy," *J. Clin. Oncol. Off. J. Am. Soc. Clin. Oncol.*, vol. 15, no. 1, pp. 110–115, Jan. 1997.

[2] G. R. Wilkinson, "Drug Metabolism and Variability among Patients in Drug Response," *N. Engl. J. Med.*, vol. 352, no. 21, pp. 2211–2221, May 2005.

[3] S. Hurst, C.-M. Loi, J. Brodfuehrer, and A. El-Kattan, "Impact of physiological, physicochemical and biopharmaceutical factors in absorption and metabolism mechanisms on the drug oral bioavailability of rats and humans," *Expert Opin. Drug Metab. Toxicol.*, vol. 3, no. 4, pp. 469–489, Aug. 2007.

[4] E. T. Hellriegel, T. D. Bjornsson, and W. W. Hauck, "Interpatient variability in bioavailability is related to the extent of absorption: implications for bioavailability and bioequivalence studies," *Clin. Pharmacol. Ther.*, vol. 60, no. 6, pp. 601–607, Dec. 1996.

[5] D. J. Greenblatt, "Presystemic Extraction: Mechanisms and Consequences," *J. Clin. Pharmacol.*, vol. 33, no. 7, pp. 650–656, Jul. 1993.

[6] L. C. Wienkers and T. G. Heath, "Predicting in vivo drug interactions from in vitro drug discovery data," *Nat. Rev. Drug Discov.*, vol. 4, no. 10, pp. 825–833, Oct. 2005.

[7] I. Arias, *The Liver Biology and Pathobiology*, Lippincott Williams & Wilkins. 2001.

[8] H. Tsutsui and S. Nishiguchi, "Importance of Kupffer Cells in the Development of Acute Liver Injuries in Mice," *Int. J. Mol. Sci.*, vol. 15, no. 5, pp. 7711–7730, May 2014.

[9] M. N. Martinez and G. L. Amidon, "A mechanistic approach to understanding the factors affecting drug absorption: a review of fundamentals," *J. Clin. Pharmacol.*, vol. 42, no. 6, pp. 620–643, Jun. 2002.

[10] M. F. Paine, H. L. Hart, S. S. Ludington, R. L. Haining, A. E. Rettie, and D. C. Zeldin, "The human intestinal cytochrome P450 'pie,'" *Drug Metab. Dispos. Biol. Fate Chem.*, vol. 34, no. 5, pp. 880–886, May 2006.

[11] B. Achour, J. Barber, and A. Rostami-Hodjegan, "Expression of Hepatic Drug-Metabolizing Cytochrome P450 Enzymes and Their Intercorrelations: A Meta-Analysis," *Drug Metab. Dispos.*, vol. 42, no. 8, pp. 1349–1356, Jul. 2014.

[12] W. G. Levine, "Biliary excretion of drugs and other xenobiotics," *Annu. Rev. Pharmacol. Toxicol.*, vol. 18, pp. 81–96, 1978.

[13] G. Ghibellini, E. M. Leslie, and K. L. R. Brouwer, "Methods to evaluate biliary excretion of drugs in humans: an updated review," *Mol. Pharm.*, vol. 3, no. 3, pp. 198–211, Jun. 2006.

[14] International Transporter Consortium *et al.*, "Membrane transporters in drug development," *Nat. Rev. Drug Discov.*, vol. 9, no. 3, pp. 215–236, Mar. 2010.

[15] P. Lundquist *et al.*, "Prediction of In Vivo Rat Biliary Drug Clearance from an In Vitro Hepatocyte Efflux Model," *Drug Metab. Dispos.*, vol. 42, no. 3, pp. 459–468, Feb. 2014.

[16] "Basic anatomical and physiological data for use in radiological protection: reference values. A report of age- and gender-related differences in the anatomical and physiological characteristics of reference individuals. ICRP Publication 89," *Ann. ICRP*, vol. 32, no. 3–4, pp. 5–265, 2002.

[17] J. M. DeSesso and C. F. Jacobson, "Anatomical and physiological parameters affecting gastrointestinal absorption in humans and rats," *Food Chem. Toxicol. Int. J. Publ. Br. Ind. Biol. Res. Assoc.*, vol. 39, no. 3, pp. 209–228, Mar. 2001.

[18] G. J. Tortora and M. T. Nielsen, *Principles of human anatomy*, Wiley., vol. 257. 1999.

[19] L. Z. Benet, T. Izumi, Y. Zhang, J. A. Silverman, and V. J. Wacher, "Intestinal MDR transport proteins and P-450 enzymes as barriers to oral drug delivery," *J. Control. Release Off. J. Control. Release Soc.*, vol. 62, no. 1–2, pp. 25–31, Nov. 1999.

[20] J. H. Lin, M. Chiba, and T. A. Baillie, “Is the role of the small intestine in first-pass metabolism overemphasized?,” *Pharmacol. Rev.*, vol. 51, no. 2, pp. 135–158, Jun. 1999.
[21] A. Bruyère *et al.*, “Effect of variations in the amounts of P-glycoprotein (ABCB1), BCRP (ABCG2) and CYP3A4 along the human small intestine on PBPK models for predicting intestinal first pass,” *Mol. Pharm.*, vol. 7, no. 5, pp. 1596–1607, Oct. 2010.
[22] S. K. Gupta and G. Sathyan, “Pharmacokinetics of an oral once-a-day controlled-release oxybutynin formulation compared with immediate-release oxybutynin,” *J. Clin. Pharmacol.*, vol. 39, no. 3, pp. 289–296, Mar. 1999.
[23] J. Yang, G. T. Tucker, and A. Rostami-Hodjegan, “Cytochrome P450 3A expression and activity in the human small intestine,” *Clin. Pharmacol. Ther.*, vol. 76, no. 4, p. 391, Oct. 2004.
[24] Paine, M. F., Shen, D. D., Kunze, K. L., Perkins, J. D., Marsh, C. L., McVicar, J. P., Barr, D. M., Gillies, B. S. and Thummel, K. E., “First-pass metabolism of midazolam by the human intestine,” *Clinical Pharmacology & Therapeutics*, pp. 14–24, 1996.
[25] L. Z. Benet, “The drug transporter-metabolism alliance: uncovering and defining the interplay,” *Mol. Pharm.*, vol. 6, no. 6, pp. 1631–1643, Dec. 2009.
[26] null Watkins, “The barrier function of CYP3A4 and P-glycoprotein in the small bowel,” *Adv. Drug Deliv. Rev.*, vol. 27, no. 2–3, pp. 161–170, Sep. 1997.
[27] M. Gertz, A. Harrison, J. B. Houston, and A. Galetin, “Prediction of Human Intestinal First-Pass Metabolism of 25 CYP3A Substrates from In Vitro Clearance and Permeability Data,” *Drug Metab. Dispos.*, vol. 38, no. 7, pp. 1147–1158, Jul. 2010.
[28] M. Jamei, G. L. Dickinson, and A. Rostami-Hodjegan, “A framework for assessing inter-individual variability in pharmacokinetics using virtual human populations and integrating general knowledge of physical chemistry, biology, anatomy, physiology and genetics: A tale of ‘bottom-up’ vs ‘top-down’ recognition of covariates,” *Drug Metab. Pharmacokinet.*, vol. 24, no. 1, pp. 53–75, 2009.
[29] I. Kola and J. Landis, “Opinion: Can the pharmaceutical industry reduce attrition rates?,” *Nat. Rev. Drug Discov.*, vol. 3, no. 8, pp. 711–716, Aug. 2004.
[30] C. Logan, “Use of Animals for the Determination of Absorption and Bioavailability,” in *Methods and Principles in Medicinal Chemistry*, vol. 40, H. van de Waterbeemd and B. Testa, Eds. Weinheim, Germany: Wiley-VCH Verlag GmbH & Co. KGaA, 2008, pp. 161–184.
[31] R. S. Obach *et al.*, “The prediction of human pharmacokinetic parameters from preclinical and in vitro metabolism data,” *J. Pharmacol. Exp. Ther.*, vol. 283, no. 1, pp. 46–58, Oct. 1997.
[32] H. Boxenbaum, “Interspecies scaling, allometry, physiological time, and the ground plan of pharmacokinetics,” *J. Pharmacokinet. Biopharm.*, vol. 10, no. 2, pp. 201–227, Apr. 1982.
[33] I. Mahmood, “Prospective Allometric Scaling: Does the Emperor Have Clothes?,” *J. Clin. Pharmacol.*, vol. 40, no. 4, pp. 341–344, Apr. 2000.
[34] V. H. Thomas *et al.*, “The road map to oral bioavailability: an industrial perspective,” *Expert Opin. Drug Metab. Toxicol.*, vol. 2, no. 4, pp. 591–608, Aug. 2006.
[35] X. Cao *et al.*, “Why is it challenging to predict intestinal drug absorption and oral bioavailability in human using rat model,” *Pharm. Res.*, vol. 23, no. 8, pp. 1675–1686, Aug. 2006.
[36] W. L. Chiou, H. Y. Jeong, S. M. Chung, and T. C. Wu, “Evaluation of using dog as an animal model to study the fraction of oral dose absorbed of 43 drugs in humans,” *Pharm. Res.*, vol. 17, no. 2, pp. 135–140, Feb. 2000.
[37] W. K. Sietsema, “The absolute oral bioavailability of selected drugs,” *Int. J. Clin. Pharmacol.*, vol. 27, no. 4, pp. 179–211, Apr. 1989.

[38] I. Mahmood, “Can absolute oral bioavailability in humans be predicted from animals? A comparison of allometry and different indirect methods,” *Drug Metabol. Drug Interact.*, vol. 16, no. 2, pp. 143–155, 2000.
[39] T. Akabane, K. Tabata, K. Kadono, S. Sakuda, S. Terashita, and T. Teramura, “A comparison of pharmacokinetics between humans and monkeys,” *Drug Metab. Dispos. Biol. Fate Chem.*, vol. 38, no. 2, pp. 308–316, Feb. 2010.
[40] W. L. Chiou and P. W. Buehler, “Comparison of oral absorption and bioavailablity of drugs between monkey and human,” *Pharm. Res.*, vol. 19, no. 6, pp. 868–874, Jun. 2002.
[41] G. M. Grass and P. J. Sinko, “Physiologically-based pharmacokinetic simulation modelling,” *Adv. Drug Deliv. Rev.*, vol. 54, no. 3, pp. 433–451, Mar. 2002.
[42] M. N. Berry, “High-yield preparation of isolated rat liver parenchymal cells: A Biochemical and Fine Structural Study,” *J. Cell Biol.*, vol. 43, no. 3, pp. 506–520, Dec. 1969.
[43] C. Guguenguillouzo *et al.*, “High yield preparation of isolated human adult hepatocytes by enzymatic perfusion of the liver,” *Cell Biol. Int. Rep.*, vol. 6, no. 6, pp. 625–628, Jun. 1982.
[44] K. P. Kanebratt and T. B. Andersson, “HepaRG Cells as an in Vitro Model for Evaluation of Cytochrome P450 Induction in Humans,” *Drug Metab. Dispos.*, vol. 36, no. 1, pp. 137–145, Oct. 2007.
[45] D. P. Aden, A. Fogel, S. Plotkin, I. Damjanov, and B. B. Knowles, “Controlled synthesis of HBsAg in a differentiated human liver carcinoma-derived cell line,” *Nature*, vol. 282, no. 5739, pp. 615–616, Dec. 1979.
[46] P. J. Sinko, G. D. Leesman, and G. L. Amidon, “Predicting fraction dose absorbed in humans using a macroscopic mass balance approach,” *Pharm. Res.*, vol. 8, no. 8, pp. 979–988, Aug. 1991.
[47] W. M. A. Westerink and W. G. E. J. Schoonen, “Cytochrome P450 enzyme levels in HepG2 cells and cryopreserved primary human hepatocytes and their induction in HepG2 cells,” *Toxicol. Vitro Int. J. Publ. Assoc. BIBRA*, vol. 21, no. 8, pp. 1581–1591, Dec. 2007.
[48] S.-I. Horiuchi *et al.*, “Global gene expression changes including drug metabolism and disposition induced by three-dimensional culture of HepG2 cells-Involvement of microtubules,” *Biochem. Biophys. Res. Commun.*, vol. 378, no. 3, pp. 558–562, Jan. 2009.
[49] P. Gripon *et al.*, “Infection of a human hepatoma cell line by hepatitis B virus,” *Proc. Natl. Acad. Sci.*, vol. 99, no. 24, pp. 15655–15660, Nov. 2002.
[50] C. Aninat *et al.*, “Expression of cytochromes P450, conjugating enzymes and nuclear receptors in human hepatoma HepaRG cells,” *Drug Metab. Dispos. Biol. Fate Chem.*, vol. 34, no. 1, pp. 75–83, Jan. 2006.
[51] M. Lübberstedt *et al.*, “HepaRG human hepatic cell line utility as a surrogate for primary human hepatocytes in drug metabolism assessment in vitro,” *J. Pharmacol. Toxicol. Methods*, vol. 63, no. 1, pp. 59–68, Feb. 2011.
[52] M. Le Vee, E. Jigorel, D. Glaise, P. Gripon, C. Guguen-Guillouzo, and O. Fardel, “Functional expression of sinusoidal and canalicular hepatic drug transporters in the differentiated human hepatoma HepaRG cell line,” *Eur. J. Pharm. Sci. Off. J. Eur. Fed. Pharm. Sci.*, vol. 28, no. 1–2, pp. 109–117, May 2006.
[53] S. Antherieu *et al.*, “Stable Expression, Activity, and Inducibility of Cytochromes P450 in Differentiated HepaRG Cells,” *Drug Metab. Dispos.*, vol. 38, no. 3, pp. 516–525, Mar. 2010.
[54] R. Jossé *et al.*, “Long-term functional stability of human HepaRG hepatocytes and use for chronic toxicity and genotoxicity studies,” *Drug Metab. Dispos. Biol. Fate Chem.*, vol. 36, no. 6, pp. 1111–1118, Jun. 2008.
[55] V. Cerec *et al.*, “Transdifferentiation of hepatocyte-like cells from the human hepatoma HepaRG cell line through bipotent progenitor,” *Hepatol. Baltim. Md*, vol. 45, no. 4, pp. 957–967, Apr. 2007.

[56] C. Guguen-Guillouzo *et al.*, “Maintenance and reversibility of active albumin secretion by adult rat hepatocytes co-cultured with another liver epithelial cell type,” *Exp. Cell Res.*, vol. 143, no. 1, pp. 47–54, Jan. 1983.
[57] P. Krause, F. Saghatolislam, S. Koenig, K. Unthan-Fechner, and I. Probst, “Maintaining hepatocyte differentiation in vitro through co-culture with hepatic stellate cells,” *Vitro Cell. Dev. Biol. - Anim.*, vol. 45, no. 5–6, pp. 205–212, May 2009.
[58] L. Riccalton-Banks, C. Liew, R. Bhandari, J. Fry, and K. Shakesheff, “Long-term culture of functional liver tissue: three-dimensional coculture of primary hepatocytes and stellate cells,” *Tissue Eng.*, vol. 9, no. 3, pp. 401–410, Jun. 2003.
[59] Y. S. Zinchenko, L. W. Schrum, M. Clemens, and R. N. Coger, “Hepatocyte and Kupffer Cells Co-cultured on Micropatterned Surfaces to Optimize Hepatocyte Function,” *Tissue Eng.*, vol. 12, no. 4, pp. 751–761, Apr. 2006.
[60] Y. Edling, L. K. Sivertsson, A. Butura, M. Ingelman-Sundberg, and M. Ek, “Increased sensitivity for troglitazone-induced cytotoxicity using a human in vitro co-culture model,” *Toxicol. Vitro Int. J. Publ. Assoc. BIBRA*, vol. 23, no. 7, pp. 1387–1395, Oct. 2009.
[61] M. A. West, G. A. Keller, B. J. Hyland, F. B. Cerra, and R. L. Simmons, “Hepatocyte function in sepsis: Kupffer cells mediate a biphasic protein synthesis response in hepatocytes after exposure to endotoxin or killed Escherichia coli,” *Surgery*, vol. 98, no. 3, pp. 388–395, Sep. 1985.
[62] A. Bader *et al.*, “3-D coculture of hepatic sinusoidal cells with primary hepatocytes-design of an organotypical model,” *Exp. Cell Res.*, vol. 226, no. 1, pp. 223–233, Jul. 1996.
[63] Y. B. A. Kang, S. Rawat, J. Cirillo, M. Bouchard, and H. M. Noh, “Layered long-term co-culture of hepatocytes and endothelial cells on a transwell membrane: toward engineering the liver sinusoid,” *Biofabrication*, vol. 5, no. 4, p. 045008, Dec. 2013.
[64] K. Ohashi *et al.*, “Engineering functional two- and three-dimensional liver systems in vivo using hepatic tissue sheets,” *Nat. Med.*, vol. 13, no. 7, pp. 880–885, Jul. 2007.
[65] S. N. Bhatia, U. J. Balis, M. L. Yarmush, and M. Toner, “Effect of cell-cell interactions in preservation of cellular phenotype: cocultivation of hepatocytes and nonparenchymal cells,” *FASEB J. Off. Publ. Fed. Am. Soc. Exp. Biol.*, vol. 13, no. 14, pp. 1883–1900, Nov. 1999.
[66] S. N. Bhatia, M. L. Yarmush, and M. Toner, “Controlling cell interactions by micropatterning in co-cultures: hepatocytes and 3T3 fibroblasts,” *J. Biomed. Mater. Res.*, vol. 34, no. 2, pp. 189–199, Feb. 1997.
[67] P. Godoy *et al.*, “Recent advances in 2D and 3D in vitro systems using primary hepatocytes, alternative hepatocyte sources and non-parenchymal liver cells and their use in investigating mechanisms of hepatotoxicity, cell signaling and ADME,” *Arch. Toxicol.*, vol. 87, no. 8, pp. 1315–1530, Aug. 2013.
[68] J. Landry, D. Bernier, C. Ouellet, R. Goyette, and N. Marceau, “Spheroidal aggregate culture of rat liver cells: histotypic reorganization, biomatrix deposition, and maintenance of functional activities,” *J. Cell Biol.*, vol. 101, no. 3, pp. 914–923, Sep. 1985.
[69] R. M. Tostões *et al.*, “Human liver cell spheroids in extended perfusion bioreactor culture for repeated-dose drug testing,” *Hepatol. Baltim. Md*, vol. 55, no. 4, pp. 1227–1236, Apr. 2012.
[70] T. M. Walker and A. J. Woodrooffe, “Cytochrome P450 activity in control and induced long-term cultures of rat hepatocyte spheroids,” *Toxicol. Vitro Int. J. Publ. Assoc. BIBRA*, vol. 15, no. 6, pp. 713–719, Dec. 2001.
[71] J. Yang, M. Goto, H. Ise, C.-S. Cho, and T. Akaike, “Galactosylated alginate as a scaffold for hepatocytes entrapment,” *Biomaterials*, vol. 23, no. 2, pp. 471–479, Jan. 2002.
[72] J. L. Luebke-Wheeler, G. Nedredal, L. Yee, B. P. Amiot, and S. L. Nyberg, “E-Cadherin Protects Primary Hepatocyte Spheroids From Cell Death by a Caspase-Independent Mechanism,” *Cell Transplant.*, vol. 18, no. 12, pp. 1281–1287, Dec. 2009.

[73] Y. Sakai, S. Yamagami, and K. Nakazawa, “Comparative Analysis of Gene Expression in Rat Liver Tissue and Monolayer- and Spheroid-Cultured Hepatocytes,” *Cells Tissues Organs*, vol. 191, no. 4, pp. 281–288, 2010.
[74] M. Bhattacharya *et al.*, “Nanofibrillar cellulose hydrogel promotes three-dimensional liver cell culture,” *J. Controlled Release*, vol. 164, no. 3, pp. 291–298, Dec. 2012.
[75] J. D. Baranski *et al.*, “Geometric control of vascular networks to enhance engineered tissue integration and function,” *Proc. Natl. Acad. Sci.*, vol. 110, no. 19, pp. 7586–7591, May 2013.
[76] T. Takebe *et al.*, “Vascularized and functional human liver from an iPSC-derived organ bud transplant,” *Nature*, vol. 499, no. 7459, pp. 481–484, Jul. 2013.
[77] L. G. Griffith, B. Wu, M. J. Cima, M. J. Powers, B. Chaignaud, and J. P. Vacanti, “In vitro organogenesis of liver tissue,” *Ann. N. Y. Acad. Sci.*, vol. 831, pp. 382–397, Dec. 1997.
[78] V. Hasirci *et al.*, “Expression of liver-specific functions by rat hepatocytes seeded in treated poly(lactic-co-glycolic) acid biodegradable foams,” *Tissue Eng.*, vol. 7, no. 4, pp. 385–394, Aug. 2001.
[79] M. Schutte *et al.*, “Rat primary hepatocytes show enhanced performance and sensitivity to acetaminophen during three-dimensional culture on a polystyrene scaffold designed for routine use,” *Assay Drug Dev. Technol.*, vol. 9, no. 5, pp. 475–486, Oct. 2011.
[80] R. Glicklis, L. Shapiro, R. Agbaria, J. C. Merchuk, and S. Cohen, “Hepatocyte behavior within three-dimensional porous alginate scaffolds,” *Biotechnol. Bioeng.*, vol. 67, no. 3, pp. 344–353, Feb. 2000.
[81] J. A. Rowley, G. Madlambayan, and D. J. Mooney, “Alginate hydrogels as synthetic extracellular matrix materials,” *Biomaterials*, vol. 20, no. 1, pp. 45–53, Jan. 1999.
[82] Y. Du, E. Lo, S. Ali, and A. Khademhosseini, “Directed assembly of cell-laden microgels for fabrication of 3D tissue constructs,” *Proc. Natl. Acad. Sci.*, vol. 105, no. 28, pp. 9522–9527, Jul. 2008.
[83] A. P. McGuigan and M. V. Sefton, “Vascularized organoid engineered by modular assembly enables blood perfusion,” *Proc. Natl. Acad. Sci.*, vol. 103, no. 31, pp. 11461–11466, Aug. 2006.
[84] R. Chang, K. Emami, H. Wu, and W. Sun, “Biofabrication of a three-dimensional liver micro-organ as an *in vitro* drug metabolism model,” *Biofabrication*, vol. 2, no. 4, p. 045004, Dec. 2010.
[85] C. Palmiero, G. Imparato, F. Urciuolo, and P. Netti, “Engineered dermal equivalent tissue in vitro by assembly of microtissue precursors,” *Acta Biomater.*, vol. 6, no. 7, pp. 2548–2553, Jul. 2010.
[86] P. Artursson and R. T. Borchardt, “Intestinal drug absorption and metabolism in cell cultures: Caco-2 and beyond,” *Pharm. Res.*, vol. 14, no. 12, pp. 1655–1658, Dec. 1997.
[87] Y. Sambuy, I. De Angelis, G. Ranaldi, M. L. Scarino, A. Stammati, and F. Zucco, “The Caco-2 cell line as a model of the intestinal barrier: influence of cell and culture-related factors on Caco-2 cell functional characteristics,” *Cell Biol. Toxicol.*, vol. 21, no. 1, pp. 1–26, Jan. 2005.
[88] X.-M. Chen, I. Elisia, and D. D. Kitts, “Defining conditions for the co-culture of Caco-2 and HT29-MTX cells using Taguchi design,” *J. Pharmacol. Toxicol. Methods*, vol. 61, no. 3, pp. 334–342, May 2010.
[89] L. Wang, S. K. Murthy, W. H. Fowle, G. A. Barabino, and R. L. Carrier, “Influence of micro-well biomimetic topography on intestinal epithelial Caco-2 cell phenotype,” *Biomaterials*, vol. 30, no. 36, pp. 6825–6834, Dec. 2009.
[90] L. Wang, S. K. Murthy, G. A. Barabino, and R. L. Carrier, “Synergic effects of crypt-like topography and ECM proteins on intestinal cell behavior in collagen based membranes,” *Biomaterials*, vol. 31, no. 29, pp. 7586–7598, Oct. 2010.

[91] J. H. Sung, J. Yu, D. Luo, M. L. Shuler, and J. C. March, “Microscale 3-D hydrogel scaffold for biomimetic gastrointestinal (GI) tract model,” *Lab Chip*, vol. 11, no. 3, pp. 389–392, 2011.
[92] J. Yu, S. Peng, D. Luo, and J. C. March, “In vitro 3D human small intestinal villous model for drug permeability determination,” *Biotechnol. Bioeng.*, vol. 109, no. 9, pp. 2173–2178, Sep. 2012.
[93] M. Schweinlin *et al.*, “Development of an Advanced Primary Human In Vitro Model of the Small Intestine,” *Tissue Eng. Part C Methods*, vol. 22, no. 9, pp. 873–883, Sep. 2016.
[94] D. Huh, G. A. Hamilton, and D. E. Ingber, “From 3D cell culture to organs-on-chips,” *Trends Cell Biol.*, vol. 21, no. 12, pp. 745–754, Dec. 2011.
[95] N. K. Inamdar and J. T. Borenstein, “Microfluidic cell culture models for tissue engineering,” *Curr. Opin. Biotechnol.*, vol. 22, no. 5, pp. 681–689, Oct. 2011.
[96] M. P. Hughes and K. F. Hoettges, Eds., *Microengineering in biotechnology*. New York: Humana, 2010.
[97] M. D. Rawlins, “Cutting the cost of drug development?,” *Nat. Rev. Drug Discov.*, vol. 3, no. 4, pp. 360–364, Apr. 2004.
[98] J. W. Allen, S. R. Khetani, and S. N. Bhatia, “In vitro zonation and toxicity in a hepatocyte bioreactor,” *Toxicol. Sci. Off. J. Soc. Toxicol.*, vol. 84, no. 1, pp. 110–119, Mar. 2005.
[99] P. J. Lee, P. J. Hung, and L. P. Lee, “An artificial liver sinusoid with a microfluidic endothelial-like barrier for primary hepatocyte culture,” *Biotechnol. Bioeng.*, vol. 97, no. 5, pp. 1340–1346, Aug. 2007.
[100] Y.-C. Toh, T. C. Lim, D. Tai, G. Xiao, D. van Noort, and H. Yu, “A microfluidic 3D hepatocyte chip for drug toxicity testing,” *Lab. Chip*, vol. 9, no. 14, p. 2026, 2009.
[101] Y. Nakao, H. Kimura, Y. Sakai, and T. Fujii, “Bile canaliculi formation by aligning rat primary hepatocytes in a microfluidic device,” *Biomicrofluidics*, vol. 5, no. 2, p. 022212, Jun. 2011.
[102] J. Lee, S. H. Kim, Y.-C. Kim, I. Choi, and J. H. Sung, “Fabrication and characterization of microfluidic liver-on-a-chip using microsomal enzymes,” *Enzyme Microb. Technol.*, vol. 53, no. 3, pp. 159–164, Aug. 2013.
[103] D. Yoon No, K.-H. Lee, J. Lee, and S.-H. Lee, “3D liver models on a microplatform: well-defined culture, engineering of liver tissue and liver-on-a-chip,” *Lab Chip*, vol. 15, no. 19, pp. 3822–3837, 2015.
[104] P. Chao, T. Maguire, E. Novik, K.-C. Cheng, and M. L. Yarmush, “Evaluation of a microfluidic based cell culture platform with primary human hepatocytes for the prediction of hepatic clearance in human,” *Biochem. Pharmacol.*, vol. 78, no. 6, pp. 625–632, Sep. 2009.
[105] J. Schütte *et al.*, “‘Artificial micro organs’—a microfluidic device for dielectrophoretic assembly of liver sinusoids,” *Biomed. Microdevices*, vol. 13, no. 3, pp. 493–501, Jun. 2011.
[106] J. Lee *et al.*, “A 3D alcoholic liver disease model on a chip,” *Integr Biol*, vol. 8, no. 3, pp. 302–308, 2016.
[107] S.-A. Lee, D. Y. No, E. Kang, J. Ju, D.-S. Kim, and S.-H. Lee, “Spheroid-based three-dimensional liver-on-a-chip to investigate hepatocyte–hepatic stellate cell interactions and flow effects,” *Lab. Chip*, vol. 13, no. 18, p. 3529, 2013.
[108] I. Wagner *et al.*, “A dynamic multi-organ-chip for long-term cultivation and substance testing proven by 3D human liver and skin tissue co-culture,” *Lab. Chip*, vol. 13, no. 18, p. 3538, 2013.
[109] M. B. Esch *et al.*, “On chip porous polymer membranes for integration of gastrointestinal tract epithelium with microfluidic ‘body-on-a-chip’ devices,” *Biomed. Microdevices*, vol. 14, no. 5, pp. 895–906, Oct. 2012.

[110] H. Kimura, T. Yamamoto, H. Sakai, Y. Sakai, and T. Fujii, “An integrated microfluidic system for long-term perfusion culture and on-line monitoring of intestinal tissue models,” *Lab. Chip*, vol. 8, no. 5, pp. 741–746, May 2008.
[111] H. J. Kim, D. Huh, G. Hamilton, and D. E. Ingber, “Human gut-on-a-chip inhabited by microbial flora that experiences intestinal peristalsis-like motions and flow,” *Lab. Chip*, vol. 12, no. 12, pp. 2165–2174, Jun. 2012.
[112] N. Barker *et al.*, “Identification of stem cells in small intestine and colon by marker gene Lgr5,” *Nature*, vol. 449, no. 7165, pp. 1003–1007, Oct. 2007.
[113] S. H. Choi, O. Fukuda, A. Sakoda, and Y. Sakai, “Enhanced cytochrome P450 capacities of Caco-2 and Hep G2 cells in new coculture system under the static and perfused conditions: evidence for possible organ-to-organ interactions against exogenous stimuli,” *Mater. Sci. Eng. C*, vol. 24, no. 3, pp. 333–339, Apr. 2004.
[114] G. J. Mahler, M. B. Esch, R. P. Glahn, and M. L. Shuler, “Characterization of a gastrointestinal tract microscale cell culture analog used to predict drug toxicity,” *Biotechnol. Bioeng.*, vol. 104, no. 1, pp. 193–205, Sep. 2009.
[115] J. S. Gujral, T. R. Knight, A. Farhood, M. L. Bajt, and H. Jaeschke, “Mode of cell death after acetaminophen overdose in mice: apoptosis or oncotic necrosis?,” *Toxicol. Sci. Off. J. Soc. Toxicol.*, vol. 67, no. 2, pp. 322–328, Jun. 2002.
[116] J. M. Prot *et al.*, “First pass intestinal and liver metabolism of paracetamol in a microfluidic platform coupled with a mathematical modeling as a means of evaluating ADME processes in humans: Human Intestine Liver coculture bioreactor,” *Biotechnol. Bioeng.*, vol. 111, no. 10, pp. 2027–2040, Oct. 2014.
[117] P. M. van Midwoud, M. T. Merema, E. Verpoorte, and G. M. M. Groothuis, “A microfluidic approach for in vitro assessment of interorgan interactions in drug metabolism using intestinal and liver slices,” *Lab. Chip*, vol. 10, no. 20, p. 2778, 2010.
[118] R. Glicklis, J. C. Merchuk, and S. Cohen, “Modeling mass transfer in hepatocyte spheroids via cell viability, spheroid size, and hepatocellular functions,” *Biotechnol. Bioeng.*, vol. 86, no. 6, pp. 672–680, Jun. 2004.
[119] Y. T. Matsunaga, Y. Morimoto, and S. Takeuchi, “Molding Cell Beads for Rapid Construction of Macroscopic 3D Tissue Architecture,” *Adv. Mater.*, vol. 23, no. 12, pp. H90–H94, Mar. 2011.
[120] V. Brancato *et al.*, “3D is not enough: Building up a cell instructive microenvironment for tumoral stroma microtissues,” *Acta Biomater.*, vol. 47, pp. 1–13, Jan. 2017.
[121] C.-T. Ho *et al.*, “Liver-cell patterning Lab Chip: mimicking the morphology of liver lobule tissue,” *Lab. Chip*, vol. 13, no. 18, p. 3578, 2013.
[122] G. G. Giobbe *et al.*, “Functional differentiation of human pluripotent stem cells on a chip,” *Nat. Methods*, vol. 12, no. 7, pp. 637–640, Jun. 2015.
[123] P. M. van Midwoud, G. M. M. Groothuis, M. T. Merema, and E. Verpoorte, “Microfluidic biochip for the perifusion of precision-cut rat liver slices for metabolism and toxicology studies,” *Biotechnol. Bioeng.*, vol. 105, no. 1, pp. 184–194, Jan. 2010.
[124] A. Garziano, F. Urciuolo, G. Imparato, F. Martorina, B. Corrado, and P. Netti, “A micro-perfusion bioreactor for on line investigation of ECM remodeling under hydrodynamic and biochemical stimulation,” *Lab Chip*, vol. 16, no. 5, pp. 855–867, 2016.
[125] F. Gioiella, F. Urciuolo, G. Imparato, V. Brancato, and P. A. Netti, “An Engineered Breast Cancer Model on a Chip to Replicate ECM-Activation In Vitro during Tumor Progression,” *Adv. Healthc. Mater.*, vol. 5, no. 23, pp. 3074–3084, Dec. 2016.
[126] G. Imparato, F. Urciuolo, C. Casale, and P. A. Netti, “The role of microscaffold properties in controlling the collagen assembly in 3D dermis equivalent using modular tissue engineering,” *Biomaterials*, vol. 34, no. 32, pp. 7851–7861, Oct. 2013.

[127] R. Dittmar, E. Potier, M. van Zandvoort, and K. Ito, “Assessment of Cell Viability in Three-Dimensional Scaffolds Using Cellular Auto-Fluorescence,” *Tissue Eng. Part C Methods*, vol. 18, no. 3, pp. 198–204, Mar. 2012.
[128] M. Gori, M. C. Simonelli, S. M. Giannitelli, L. Businaro, M. Trombetta, and A. Rainer, “Investigating Nonalcoholic Fatty Liver Disease in a Liver-on-a-Chip Microfluidic Device,” *PLOS ONE*, vol. 11, no. 7, p. e0159729, Jul. 2016.
[129] G. Hamilton, “Multicellular spheroids as an in vitro tumor model,” *Cancer Lett.*, vol. 131, no. 1, pp. 29–34, Sep. 1998.
[130] R.-Z. Lin and H.-Y. Chang, “Recent advances in three-dimensional multicellular spheroid culture for biomedical research,” *Biotechnol. J.*, vol. 3, no. 9–10, pp. 1172–1184, Oct. 2008.
[131] Y. Torisawa, A. Takagi, Y. Nashimoto, T. Yasukawa, H. Shiku, and T. Matsue, “A multicellular spheroid array to realize spheroid formation, culture, and viability assay on a chip,” *Biomaterials*, vol. 28, no. 3, pp. 559–566, Jan. 2007.
[132] D. Wu, X. Wang, R. Zhou, and A. Cederbaum, “CYP2E1 enhances ethanol-induced lipid accumulation but impairs autophaghy in HepG2 E47 cells,” *Biochem. Biophys. Res. Commun.*, vol. 402, no. 1, pp. 116–122, Nov. 2010.
[133] M. A. Rothschild, M. Oratz, and S. S. Schreiber, “Effects of Nutrition and Alcohol on Albumin Synthesis,” *Alcohol. Clin. Exp. Res.*, vol. 7, no. 1, pp. 28–30, Dec. 1983.
[134] I. J. Hidalgo, T. J. Raub, and R. T. Borchardt, “Characterization of the human colon carcinoma cell line (Caco-2) as a model system for intestinal epithelial permeability,” *Gastroenterology*, vol. 96, no. 3, pp. 736–749, Mar. 1989.
[135] M. Rousset *et al.*, “Enterocytic differentiation and glucose utilization in the human colon tumor cell line Caco-2: Modulation by forskolin,” *J. Cell. Physiol.*, vol. 123, no. 3, pp. 377–385, Jun. 1985.
[136] P. Artursson, “Epithelial Transport Of Drugs In Cell Culture. I: A Model For Studying The Passive Diffusion Of Drugs Over Intestinal Absorbtive (Caco-2) Cells,” *J. Pharm. Sci.*, vol. 79, no. 6, pp. 476–482, Jun. 1990.
[137] P. Artursson and J. Karlsson, “Correlation between oral drug absorption in humans and apparent drug permeability coefficients in human intestinal epithelial (Caco-2) cells,” *Biochem. Biophys. Res. Commun.*, vol. 175, no. 3, pp. 880–885, Mar. 1991.
[138] P. Artursson, K. Palm, and K. Luthman, “Caco-2 monolayers in experimental and theoretical predictions of drug transport1PII of original article: S0169-409X(96)00415-2. The article was originally published in Advanced Drug Delivery Reviews 22 (1996) 67–84.1,” *Adv. Drug Deliv. Rev.*, vol. 46, no. 1–3, pp. 27–43, Mar. 2001.
[139] B. Chueh, D. Huh, C. R. Kyrtsos, T. Houssin, N. Futai, and S. Takayama, “Leakage-Free Bonding of Porous Membranes into Layered Microfluidic Array Systems,” *Anal. Chem.*, vol. 79, no. 9, pp. 3504–3508, May 2007.
[140] G. Imparato *et al.*, “A novel engineered dermis for *in vitro* photodamage research: A dermis equivalent for investigating UVA damage *in vitro*,” *J. Tissue Eng. Regen. Med.*, p. n/a-n/a, 2016.
[141] P.-C. Wu, T.-Y. Hsieh, Z.-U. Tsai, and T.-M. Liu, “In vivo Quantification of the Structural Changes of Collagens in a Melanoma Microenvironment with Second and Third Harmonic Generation Microscopy,” *Sci. Rep.*, vol. 5, p. 8879, Mar. 2015.
[142] L. Rich and P. Whittaker, “Collagen and picrosirius red staining: a polarized light assessment of fibrillar hue and spatial distribution,” *Braz J Morphol Sci*, vol. 22, no. 2, pp. 97–104, 2005.
[143] H. Kato, C. L. Marcelo, J. B. Washington, E. L. Bingham, and S. E. Feinberg, “Fabrication of Large Size *Ex Vivo*- Produced Oral Mucosal Equivalents for Clinical Application,” *Tissue Eng. Part C Methods*, vol. 21, no. 9, pp. 872–880, Sep. 2015.

[144] L. M. Griep *et al.*, “BBB ON CHIP: microfluidic platform to mechanically and biochemically modulate blood-brain barrier function,” *Biomed. Microdevices*, vol. 15, no. 1, pp. 145–150, Feb. 2013.
[145] N. D. Kirkpatrick, M. A. Brewer, and U. Utzinger, “Endogenous Optical Biomarkers of Ovarian Cancer Evaluated with Multiphoton Microscopy,” *Cancer Epidemiol. Biomark. Amp Prev.*, vol. 16, no. 10, pp. 2048–2057, Oct. 2007.
[146] S. Wu, Y. Peng, L. Hu, X. Zhang, and H. Li, “Classification and recognition of texture collagen obtaining by multiphoton microscope with neural network analysis,” *J. Phys. Conf. Ser.*, vol. 680, p. 012014, Jan. 2016.
[147] W. Hu, H. Li, C. Wang, S. Gou, and L. Fu, “Characterization of collagen fibers by means of texture analysis of second harmonic generation images using orientation-dependent gray level co-occurrence matrix method,” *J. Biomed. Opt.*, vol. 17, no. 2, p. 026007, 2012.
[148] M. D. Basson, G. Turowski, and N. J. Emenaker, “Regulation of Human (Caco-2) Intestinal Epithelial Cell Differentiation by Extracellular Matrix Proteins,” *Exp. Cell Res.*, vol. 225, no. 2, pp. 301–305, Jun. 1996.
[149] V. Carrière, J. Chambaz, and M. Rousset, “Intestinal responses to xenobiotics,” *Toxicol. In Vitro*, vol. 15, no. 4–5, pp. 373–378, Aug. 2001.
[150] F. Antunes, F. Andrade, D. Ferreira, H. Morck Nielsen, and B. Sarmento, “Models to Predict Intestinal Absorption of Therapeutic Peptides and Proteins,” *Curr. Drug Metab.*, vol. 14, no. 1, pp. 4–20, Jan. 2013.
[151] C. Guguen-Guillouzo and A. Guillouzo, “General Review on In Vitro Hepatocyte Models and Their Applications,” in *Hepatocytes*, vol. 640, P. Maurel, Ed. Totowa, NJ: Humana Press, 2010, pp. 1–40.
[152] A. M. Ghaemmaghami, M. J. Hancock, H. Harrington, H. Kaji, and A. Khademhosseini, “Biomimetic tissues on a chip for drug discovery,” *Drug Discov. Today*, vol. 17, no. 3–4, pp. 173–181, Feb. 2012.
[153] Y. N. Gavhane and A. V. Yadav, “Loss of orally administered drugs in GI tract,” *Saudi Pharm. J. SPJ Off. Publ. Saudi Pharm. Soc.*, vol. 20, no. 4, pp. 331–344, Oct. 2012.
[154] K. J. Atkinson and R. K. Rao, “Role of protein tyrosine phosphorylation in acetaldehyde-induced disruption of epithelial tight junctions,” *Am. J. Physiol. Gastrointest. Liver Physiol.*, vol. 280, no. 6, pp. G1280-1288, Jun. 2001.
[155] R. Rao, “Endotoxemia and gut barrier dysfunction in alcoholic liver disease,” *Hepatol. Baltim. Md*, vol. 50, no. 2, pp. 638–644, Aug. 2009.
[156] M. Dunagan, K. Chaudhry, G. Samak, and R. K. Rao, “Acetaldehyde disrupts tight junctions in Caco-2 cell monolayers by a protein phosphatase 2A-dependent mechanism,” *AJP Gastrointest. Liver Physiol.*, vol. 303, no. 12, pp. G1356–G1364, Dec. 2012.